CHALMERS
UNIVERSITY OF TECHNOLOGY

Investigation on Working Platforms for Tracked Plant

A full scale field study to evaluate the performance of different working platform reinforcements

Master's thesis in Infrastructure and Environmental Engineering

ELLINOR MALMROS
MATHILDA RINGDAHL

DEPARTMENT OF ARCHITECTURE AND CIVIL ENGINEERING
CHALMERS UNIVERSITY OF TECHNOLOGY
Gothenburg, Sweden 2022
www.chalmers.se

Master's thesis ACEX30

Investigation on Working Platforms for Tracked Plant

A full scale field study to evaluate the performance of different working platform reinforcements

ELLINOR MALMROS
MATHILDA RINGDAHL

CHALMERS
UNIVERSITY OF TECHNOLOGY

Department of Architecture and Civil Engineering
Division of Geology and Geotechnics
Chalmers University of Technology
Gothenburg, Sweden 2022

Investigation on Working Platforms for Tracked Plant
A full scale field study to evaluate the performance of different working platform reinforcements

ELLINOR MALMROS
MATHILDA RINGDAHL

Supervisor: Mats Karlsson, Department of Architecture and Civil Engineering
Industry Supervisor: Jimmie Andersson, Peab
Industry Supervisor: Nils Gustafsson, Peab
Industry Supervisor: Michael Sabattini, Peab
Examiner: Mats Karlsson, Department of Architecture and Civil Engineering

Department of Architecture and Civil Engineering
Division of Geology and Geotechnics
Chalmers University of Technology
SE-412 96 Gothenburg
Telephone +46 31 772 1000

Cover: Picture from field trial with a working platform reinforced with log mats.

Department of Architecture and Civil Engineering
Gothenburg, Sweden 2022

Investigation on Working Platforms for Tracked Plant
A full scale field study to evaluate the performance of different working platform reinforcements
ELLINOR MALMROS
MATHILDA RINGDAHL
Department of Architecture and Civil Engineering
Chalmers University of Technology

Abstract

Working platforms are often used on construction sites where the ground conditions needs to be improved to carry tracked plant such as pile rigs. There are risks concerning the economy and safety on site if the working platform is not sufficiently designed to withstand the pressure from the tracks. Reinforcements can be used to increase the bearing capacity of the working platform. This Master's thesis studies the influence of two different types of working platform reinforcements. The types of reinforcements studied are geogrids and log mats. This was mainly done through a field trial, although, numerical models and analytical calculations were conducted to validate and further analyse the behaviour of a reinforced working platform. The results show that the load spread efficiency is improved when using reinforcements, however, it could not be positively concluded which type of reinforcement was most efficient. It was found that the efficiency of the log mat was largely dependent on the contact surface of the log mat with the working platform hence affecting the effective load spread area of the log mat. The influence of the geogrid was thought to be due to mechanical stabilisation of the soil as the load spread efficiency was improved even for small strains of the geogrid.

Keywords: working platform, load spread, reinforcement, geogrid, log mat, field trial.

Studie om arbetsplattformar för tunga larvburna maskiner
En fullskalig fältstudie för utvärderande av olika förstärkningsmetoder i arbetsplattformar
ELLINOR MALMROS
MATHILDA RINGDAHL
Institutionen för Arkitektur och Samhällsbyggnadsteknik
Chalmers Tekniska Högskola

Sammanfattning

Arbetsplatformar används ofta på byggarbetsplatser när den befintliga jordens bärighet inte är tillräcklig för att bära larvburna maskiner så som exempelvis pålkranar. En arbetsplattform med otillräcklig bärighet är förenad med risker då ett jordbrott kan leda till att maskinen välter. Konsekvenserna kan vara väldigt kostsamma men också påverka miljön eller i värsta fall äventyra säkerheten för de som arbetar på platsen. I fall då arbetsplatformen inte kan uppnå tillräcklig bärighetskapacitet kan förstärkningar tillämpas. Det här examensarbetet kommer studera två förstärkningsmetoder, geonät och stockmattor. Det gjordes genom att utföra ett fältförsök och kompleterande numeriska och analytiska studier för att vidare analysera beteendet av de olika förstärkningarna. Resultaten visar att försärkningarna bidrar till en effektivare lastspridning, däremot kunde inget entydigt svar ges angående vilken av de två förstärkningsmetoderna som gav bäst lastspridande effekt. De huvudsakliga fynden visade dock att stockmattans lastspridande effekt var starkt beroende av kontaktytan med platformen och därmed den effektiva lastspridande arean. Resultaten för en arbetsplattform förstärkt med geonät visade att en det fanns en effekt av mekanisk stabilisering även vid små töjningar av geonätet.

Keywords: arbetsplattform, lastspridning, förstärkning, geonät, stockmatta, fältförsök.

Acknowledgements

This master's thesis has been our final project of the Civil engineering program and the master Infrastructure and Environmental Engineering at Chalmers Technical University. The thesis has been made as a collaboration with Peab and was partly funded by The Development Fund of the Swedish Construction Industry (SBUF). We want to give a thank you to SBUF for giving us the opportunity to perform this project.

We want to give a big thank you to Peab for believing in us and letting us do this project with you. Thank you Jimmie Andersson and Nils Gustafsson for the guidance during the project and especially for helping us during all parts of the field trial. We want to give a thank you to Michael Sabattini for your overall support during the project. We also want to thank the project manager David Eriksson, the site manager Patrik Hedlund, Ronny the excavator operator, the crane truck driver and everyone else that helped us with the field trial and at the site in Erikssund.

At Chalmers we want to give our supervisor and examiner, Mats Karlsson a thank you for your support and guidance through the project. Thank you for calming us down in stressful situations.

To all our friends that we have meet during our five years of studies together, we want to give a big thank you. Without you, those years would never have been as much fun. Clara, Linnea, Julia, Rebecca, Maria and Sofia, thank you for all the laughs, fun nights and for all the fika's. We also want to thank our families for always being there for us and for never stopped believing in us.

Finally we want to thank each other for enduring each other's company during this project!

Ellinor Malmros, Gothenburg, June 2022

Mathilda Ringdahl, Gothenburg, June 2022

Table of Contents

List of Figures

List of Tables

Notations

Roman upper case letters

		Unit
A_{ef}	effective area	m^2
B	width of loaded area	m
B_{ef}	effective width	m
C_a	total adhesion	kPa
D	depth from ground surface to foundation bottom	m
E_{oed}	Oedometer elasticity modulus	MPa
F	Load	kN
H	thickness of non-cohesive layer	m
K_0	ratio of effective vertical and horizontal stress	-
K_p	coefficient of passive earth pressure	-
K_s	coefficient of punching shear resistance	-
L	length of loaded area	m
L_{ef}	effective length	m
M_0	compressibility modulus	MPa
$N_{c,q,\gamma}$	bearing capacity factors	-
T	load transfer efficiency coefficient	-
T_{corr}	corrected load transfer efficiency coefficient	-
T_{ult}	geogrid tensile strength	kPa

Roman lower case letters

c	cohesion	kPa
c_a	unit cohesion	kPa
c_u	undrained cohesion	kPa
c'	effective cohesion	kPa
c'_{max}	additional effective cohesion	kPa
$e_{x,y,b,l}$	eccentricities	m
q	pressure	kPa
q_b	ultimate bearing capacity of subgrade	kPa
q_{bv}	vertical component of ultimate bearing capacity of subgrade	kPa
q_g	component of bearing resistance from geogrid	kPa
q_p	component of bearing resistance from punching shear	kPa
q_u	ultimate bearing capacity	kPa
$q_u v$	vertical component of ultimate bearing capacity	kPa
s	track spacing	kPa
$s_{c,q,\gamma,p}$	shape correction factors	-
s_u	undrained shear strength	kPa
u	pore water pressure	kPa

Greek letters

α	angle	$^\circ$
β	load spread angle	$^\circ$
Γ	shear strain	-
γ	unit weight	kN/m^3
γ'	effective unit weight	kN/m^3
δ	inclination of passive earth pressure	$^\circ$
ε	normal strain	-
θ	resulting force angle	$^\circ$
$\xi_{c,q,\gamma}$	correction factors	-
σ	total stress	kPa
$\sigma_{1,2,3}$	principal stresses	kPa
σ_h	horizontal stress	kPa
σ_v	vertical stress	kPa
σ'	effective stress	kPa
σ'_b	effective stress at bottom of foundation	kPa
σ'_h	horizontal effective stress	kPa
σ'_p	pre-consolidation pressure	kPa
σ'_0	effective vertical stress at the base of granular layer	kPa
σ'_v	vertical effective stress	kPa
τ	shear stress	kPa
τ_f	failure shear stress	kPa
ϕ	friction angle	$^\circ$
ϕ_u	undrained friction angle	$^\circ$
ϕ'	effective friction angle	$^\circ$
ψ	dilatancy	$^\circ$

1 Introduction

Heavy machines, such as pile rigs, are used and operated at construction sites. Assessments are made to determine the pressures that are exerted on the ground by the tracks of the plant (Topolnicki et al., 2021). This is done to assure that the ground can withstand the pressures (Rankka, Liedberg, Rudebeck, & Dehlbom, 2022). Therefore the subgrade must be investigated such that the ground conditions are known.

Working platforms to support the pile rig are necessary at almost all construction sites to improve the ground (Temporary Works forum, 2019). But the design and construction of them are seldom ensured to meet the requirement at site, as they are frequently derived from experience. Current methods for a technical design have proved to be reliable but there is a lack of consistency for how and when they are applied.

If the pile rig imposes ground bearing pressures that are higher than what the ground conditions and working platform can withstand, deformations can occur (Topolnicki et al., 2021). This can cause the plant to overturn, and further cause damages on the environment and lead to economical consequences (Rankka et al., 2022). Most importantly, it can endanger the safety of people on site. The design and construction of a sufficient working platform, in relation to its subgrade, is therefore of great importance.

1.1 Background

A working platform is by the Swedish Association for Foundation Engineering (2020) (SAFE) defined as a temporary construction with the aim of creating bearing capacity for a tracked plant. They are usually constructed with a layer of granular soil and with the purpose of spreading the load and improve bearing capacity of the weaker subgrade (Lees & Matthias, 2019). If the bearing capacity needed can not be achieved by the platform it can be improved by using reinforcement (Swedish Association for Foundation Engineering, 2020).

One type of reinforcement is load-distributing elements, such as log mats. Log mats are used to reinforce soil and enable tracked plants to access areas where the soil conditions are poor (Markskydd, n.d.). The log mats spread the pressure from the tracks of the rig to a larger surface. Another type of reinforcement is geosynthetics. Geogrids are a type of geosynthetics and are used within the platform to stabilize soil (Swedish Association for Foundation Engineering, 2020). Geogrid uses either its tensile strength or lateral restraint via confinement or a combination of the mechanisms to improve the platform (Temporary Works forum, 2019).

When designing working platforms common practice is to use methods normally used for shallow foundations (Temporary Works forum, 2019). A foundation is a structure that transmits load to an underlying soil (Knappet & Craig, 1974). It is built such that bearing capacity is sufficient to resist applied load and to avoid deformations which would lead to a loss of function for the supported structure. A foundation that is wider compared to its depth is often refereed to as a shallow foundation. There are various methods to calculate the bearing capacity and stress distribution of a shallow foundation (Temporary Works forum, 2019). Additionally there are several uncertainties concerning bearing capacity of multiple soil layers as well as reinforced working platforms. As analytical methods are not always applicable when calculating bearing capacity of platforms with multiple soil layers (Swedish Standards Institute, 2005). Instead numerical methods can be used for design of geotechnical structures such as working platforms.

SAFE released guidelines for design of working platforms. The aim of it was to show how a safe working environment can be achieved while working with tracked plants and it should work as guidance for the contractor during design, use and maintenance of the working platform. The guidelines includes methods for how geogrids contributes to bearing capacity of the platform while load-distributing elements are not mentioned.

A publication by Rankka et al. (2022) was released with the aim to create a guide that can be used in industry for design and use of working platforms for heavy tracked machines. In the publication working platforms reinforced with geogrids and/or load-distrubuting elements are discussed. Though, methods for design are only included for load-distributing elements.

When a wider stress distribution is seen in a working platform a better load spread and load spread angle is achieved. This results in an increasing effective bearing area and also the overall bearing resistance (Temporary Works forum, 2019). Therefore this master's thesis studies the stress distribution, caused by a tracked plant, in a working platform reinforced with log mats or geogrid. This is done to analyse and compare the behaviour of these reinforcements as there still are large uncertainties concerning their influence. A field trial is performed where the total stress is measured at different locations in the working platforms to analyse the stress distribution. One platform reinforced with a geogrid and another with log mats are tested. A third test is performed on a working platform without reinforcements to enable analyses of the influence of the reinforcements individually. The platforms are loaded step wise until a total load corresponding to the pressure imposed by one track of a pile rig is reached. Further this thesis studies the bearing capacity and behaviour of the working platforms using analytical methods and numerical models. The thesis is done in collaboration with Peab and the field trial is partly funded by The Development Fund of the Swedish Construction Industry.

1.2 Aim

The aim of this master's thesis project is to study the load spread efficiency of working platforms to answer questions concerning design. Furthermore, comparing the load spread efficiency of working platforms reinforced with log mats or geogrid to conclude which of the reinforcements are superior in a bearing capacity perspective.

This will be done by;

- performing a field trial to study the stress distribution, settlements and behaviour of the reinforcements,
- performing a numerical analysis to compare and validate the field trial results with as well as studying the bearing capacity,
- performing analytical calculations to make assumptions about the bearing capacity.

1.3 Limitations

The definition for working platforms, provided by SAFE, states that the aim is to provide bearing capacity for tracked plant. This thesis will also use that definition. However, as design methods of shallow foundations are used for calculation of bearing capacity and stress distribution it is applicable for any type of footing and therefore any type of heavy machine. The focus of this thesis lies within the geotechnical part of working platforms and will only briefly discuss different load-cases from tracked plant. Other effects, such as dynamic loads will not be studied. The field trial will be performed with a granular fill on a soft soil subgrade, hence all analyses will be restricted to these conditions.

2 Theory

This chapter will present the theory needed to understand the mechanism of soil failure, stress distribution and design of working platforms. It will also provide information on the measurement instrumentation used to collect data during the field trial as well as the ground investigation methods used to evaluate the conditions on the site of the field trial.

2.1 Introduction to soil mechanics

Soils are materials consisting of mineral particles of different fractions as well as water and air that fills the voids between the particles (Knappet & Craig, 1974). There are fine grained soils such as clay and silt where the grain fractions are smaller than 0.06 mm and there are more coarse grained fractions such as gravel and sand. Soils can consist of only one fraction but is more often a mixture of different fractions. The voids between the particles called pores are filled with water and/or air. Water is considered incompressible while air compressible. In a fully saturated soil beneath the ground water table, the pores are completely filled with water. The pressure of the water filling the pores are called pore water pressure (u).

For fine grained soils, such as clay, the void sizes are very small. This results in a negative pore pressure due to capillary tension (Knappet & Craig, 1974). This is called cohesion (c) and describes the strength of the fine grained soil. Soils, where its strength is described by cohesion, are therefore called cohesive soils. Subsequently more coarse grained soils, where there is no cohesion, are called non-cohesive soils.

When a soil is exposed to compression, due to self weight or external loading, stress is built up and transmitted by the solid particles and pore water as a system (Knappet & Craig, 1974). The stress transmitted by the soil system is called total stress (σ) while the stress transmitted by the solid mineral particles only is called effective stress (σ'). The relationship can be seen in Equation 2.1.

$$\sigma = \sigma' + u \tag{2.1}$$

For a soil where the ground level is horizontal the principal stresses, σ_1 and σ_3, are the vertical (σ_v) and horizontal stresses (σ_h) respectively (Sällfors, 2013). Under these conditions the stress state on a three dimensional soil element can be seen in Figure 2.1.

σ_v is often larger than σ_h and can easily be calculated according to Equation 2.2.

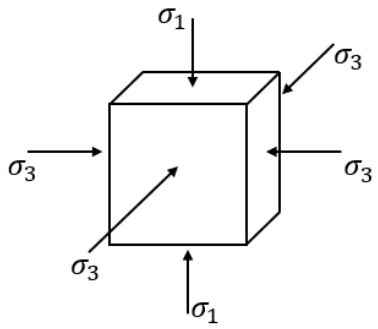

Figure 2.1: *Principal stresses. Figure modified from Sällfors (2013).*

$$\sigma_v = \gamma z \tag{2.2}$$

where;
γ = unit weight of soil
z = depth.

The σ_h is more complicated to calculate as empirical values have to be used. The ratio ($K0$) between the effective vertical (σ'_v) and effective horizontal stress (σ'_h) can be written as in Equation 2.3.

$$K_0 = \frac{\sigma'_h}{\sigma'_v} \tag{2.3}$$

For a soil element where the vertical stress is larger than the horizontal stress the element is compressed vertically, this is called active earth pressure (P_a) (Knappet & Craig, 1974). Consequently, when the horizontal stress is larger than the vertical stress and the soil is experiencing horizontal compression it is called passive earth pressure (P_p).

While both the mineral particles and the pore water pressure can resist normal stresses, only the mineral particles can resist shear stress (Knappet & Craig, 1974). Shear stress is built up due to loading of the soil and consequently shear strain occurs as points in the soil mass are displaced relative to the axes and one another. The stress and strain state for a two dimensional soil element in shear can be seen in Figure 2.2 where τ is the shear stress, Γ is the shear strain and ε is the normal strain.

The relationship between the normal and shear strain in two dimensions, known as the requirement of compatibility can be shown in Equation 2.4. It is independent of material properties. However, since soil is not a homogeneous material the stress-strain relationship is not linear but very dependent on the stress history of the soil. To be able to predict the soil behaviour the stress-strain relationship can be idealised in different ways, for example elastic perfectly plastic.

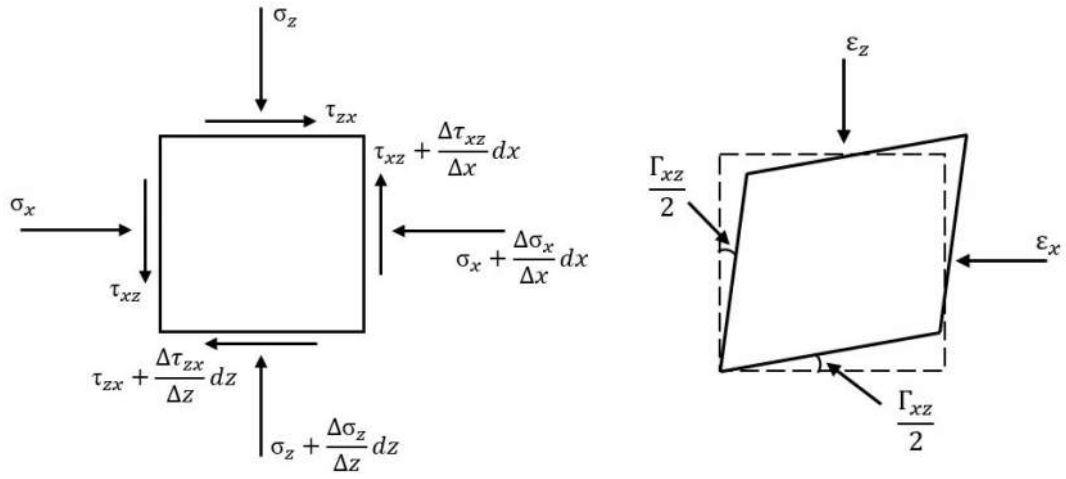

(a) *state of stress* ***(b)*** *state of strain*

Figure 2.2: *State of stress and strain in a two-dimensional soil element. Figure modified from Knappet and Craig (1974).*

$$\frac{\Delta^2 \varepsilon_x}{\Delta z^2} + \frac{\Delta^2 \varepsilon_z}{\Delta x^2} - \frac{\Delta \Gamma_{xz}}{\Delta x \Delta z} \tag{2.4}$$

If the the idealisation of a perfectly plastic behaviour can be expected the Mohr-Coulomb failure criterion can be utilized. The failure envelope of Mohr-Coulomb can be illustrated by a straight line according to Equation 2.5.

$$\tau_f = c' + \sigma' tan\phi' \tag{2.5}$$

where;
τ_f = fauilure shear stress
c' = effective cohesion
ϕ' = effective friction angle.

The stress state can be illustrated as a circle where the principal stresses make out the diameter of the Mohr circle as shown in Figure 2.3. If the circle, at any point, touches the failure envelope shear failure will occur.

The shear strength in a soil differs depending on the drainage conditions (Knappet & Craig, 1974). For drained conditions the shear strength parameters are defined as effective parameters (c' and ϕ') while the parameters for undrained conditions are defined in terms of total stress (c_u and ϕ_u). For coarse-grained soils the shear strength is usually defined in terms of effective parameters as the characteristics of such soil are often the same dry or saturated as long as excess pore pressures are not built up. The shear resistance of coarse-grained soil is dependent on the interlocking effect of the particles which can be expressed through ϕ' and the dilatancy angle (ψ).

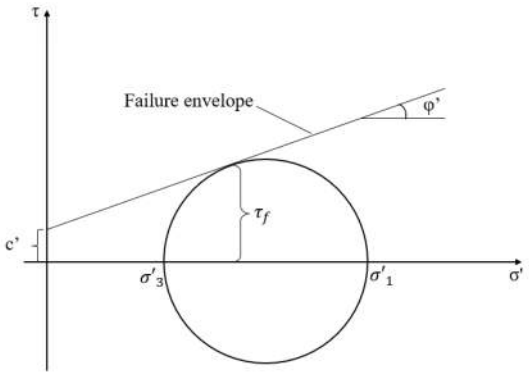

Figure 2.3: *Mohr-Coulomb failure criterion. Figure modified from Knappet and Craig (1974).*

The dilatancy angle is the average angle of shearing on a particle plane. As coarse-grained soils do not have cohesion bonds between it's particles the c' is usually equal to zero. The failure envelope of such drained soil conditions can be seen in Figure 2.4a. For undrained behaviour however, the conditions can be considered to be the opposite. Undrained shear strengths are usually used to describe the strength of fine-grained soils since the in-situ conditions for such soils often are undrained. For these kind of soils it is the cohesion that resists the shearing, therefore the undrained shear strength is only expressed through c_u as can be seen in Figure 2.4b.

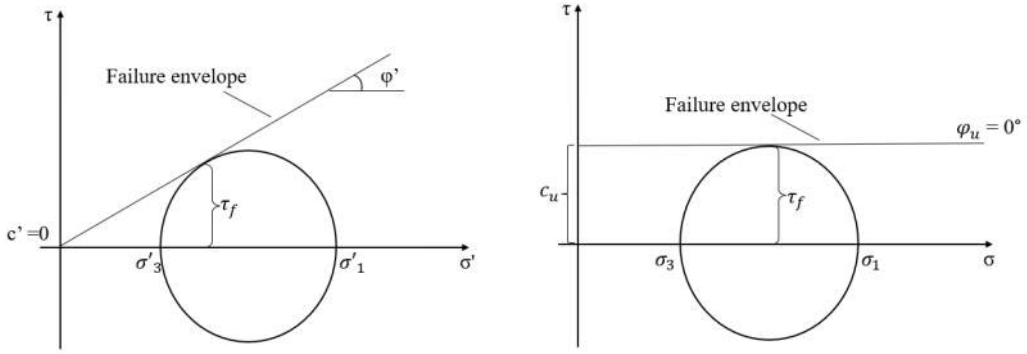

(a) *Drained shear strength* ***(b)*** *Undrained shear strength*

Figure 2.4: *Mohr-Coulomb failure criterion for different drainage conditions. Figure modified from (Knappet & Craig, 1974).*

2.2 Ground investigation

Ground investigations are done to identify and classify soil (Knappet & Craig, 1974). The number of boreholes and its locations should be planned to enable the investigation of the geologic structure for the whole site of interest. Soil samples are obtained to be used in laboratory tests for determination of soil parameters. In-situ

tests can also be performed to assess soil characteristics. The result should provide sufficient information for a suitable design of an engineering project.

Soil samples can be divided in to two categories, disturbed and undisturbed samples (Knappet & Craig, 1974). The soil structure is damaged in a disturbed sample and it is generally used for visual classification as well as for classification and compaction tests. It can be obtained by hand from the auger as the borehole is drilled. An undisturbed sample is obtained with techniques that aims to preserve the soil structure such that shear strength and consolidations tests can be performed. In general soft soil is sensitive to sampling disturbance. Piston sampler is an example of instrument which can conduct undisturbed samples in soft soil. It is pushed down below the bottom of a borehole, such that a tube can be pushed past the piston, bypassing the disturbed soil, and then withdrawn as a locking device holds the piston such that the soil retains in the tube.

2.2.1 In-situ tests

A cone penetration test (CPT) is performed at site to determine the soil stratigraphy and several standard geotechnical parameters (Knappet & Craig, 1974). In fine-grained soils it is usually used to assess the undrained shear strength. A CPT is done by pushing a cone penetrometer vertically into the soil at a constant rate. It measures continuously such that a complete soil profile with its varying soil parameters is achieved. The results from the CPT should be validated against another in-situ test or by laboratory tests.

A field vane test (FVT) is simple test to directly assess the undrained shear strength of especially saturated clays. A rectangular vane, with four plates fixed at 90 degrees angle to each other, is pushed into the soil to a desired depth and then rotated such that the shear strength can be measured.

2.2.2 Laboratory tests

For classification and identification of soil general tests in laboratory are performed (Swedish Standard Insititute, 2007). Bulk density, water content as well as its liquid and plastic limits can be determined. Also the undrained shear strength for a clayey soil can be determined by rapid and simple methods, such as a fall cone test. It has to be considered that the values evaluated represent the state of the soil in the laboratory.

Oedometer test can be performed in laboratory to determine the compressibility and consolidation of soil (Swedish Standard Insititute, 2007). If it is done with continuous loading and constant rate of deformation it is called a CRS. The common values evaluated by the CRS test are the pre-consolidation pressure (σ'_p) and oedometer elasticity modulus (E_{oed}).

To determine effective shear strength of soils direct shear test can be performed in the laboratory (Swedish Standards Institue, 2019). It is done by laterally restrain

a soil specimen and shear it along a mechanically induced horizontal plane while a vertical stress is applied normal to that plane.

2.3 Load from tracked plant

The load (F) caused by a tracked plant, such as a pile rig, imposes a ground bearing pressure from the tracks (Topolnicki et al., 2021). A common problem during design of working platforms is to determine the maximum pressure. The distribution of pressure along the tracks is dependent on the centre of gravity of the rig which is dependent on the orientation of the body of the rig with respect to the orientation of the tracks. Figure 2.5 shows a track system where this angle is presented as θ. The eccentricities (e_x and e_y) are the distances from the geometrical center of the model to the centre of gravity of the rig.

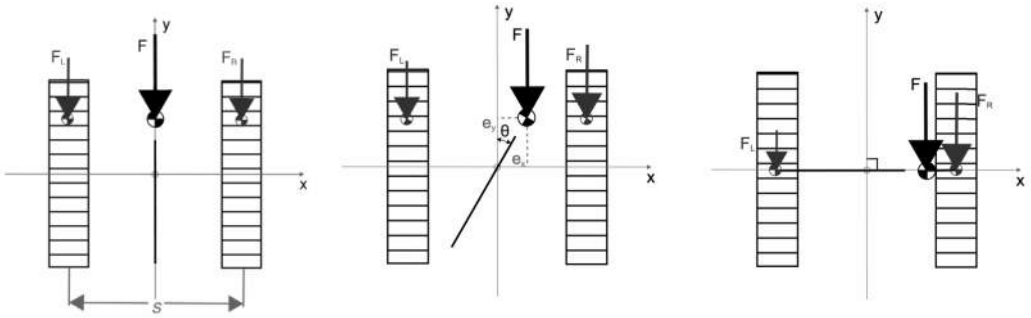

(a) *Rig in orientation of the tracks direction.* ***(b)*** *Rig in θ° rotation from the tracks direction.* ***(c)*** *Rig in 90° rotation from the tracks direction.*

Figure 2.5: *Track system with different orientations of the rig seen from above. Figure made by author.*

F, which includes plant weight and operational loads, are acting in the centre of gravity but distributes it on the left and right track such that the equilibrium Equation 2.6 fulfils (Topolnicki et al., 2021). The Equation is dependent on the eccentricities as well as the track spacing (s). The distribution of the loads F_L and F_R generates either a trapezoidal or triangular distribution over the length of the tracks and are generally simplified to act on the eccentricities.

$$F = F_L + F_R \tag{2.6}$$

where;

$$F_L = F\left(\frac{1}{2} - \frac{e_y}{s}\right) \tag{2.7a}$$

$$F_R = F\left(\frac{1}{2} + \frac{e_y}{s}\right) \tag{2.7b}$$

For example, ground conditions, can cause movements of the resulting vertical load on one track (Topolnicki et al., 2021). This would cause a tilt of the rig. In this case the eccentricities, e_x and e_y, might not be equal to the distance from the geometrical model centre of the track to F_L or F_R. Furthermore, it can cause tracks to lose contact with the ground. Which could cause the distribution to not be equal on both tracks as well as it question how much track area is effective. Several methods have been discussed in the article by Topolnicki et al. (2021) and field studies have been made and discussed to study the distribution of the ground bearing pressure between the tracks of a machine. It have been seen that the simplified method with eccentricities e_x and e_y either can over- or underestimate the ground bearing pressure, depending on the leaders position. On the other hand, for leader position θ=0°, 90° and 270° the results have been more accurate. For the design of a working platform an estimation of the average pressure multiplied with an empirical safety factor have generally been used and have then been calculated as a shallow foundation with the need of bearing capacity of the calculated maximum ground bearing pressure.

2.4 Stress distribution

A method used to estimate the change in vertical stress distribution beneath a shallow foundation is that of Boussinesq (Bergdahl, Ottosson, & Stigson Malmborg, 1993). The method is used to calculate the stress in any point of the soil using superposition. This method however assumes the soil to be an elastic, weightless, homogeneous, isotropic and semi-infinite material. The Boussinesq equation for a strip footing with uniformly applied pressure can be seen in Equation 2.8 and was retrieved from Knappet and Craig (1974).

$$\Delta\sigma_v = \frac{q}{\pi}[\alpha_1 + \sin\alpha_1 \cos(\alpha_1 + 2\alpha_2)] \tag{2.8}$$

where;
q = uniform pressure over the load width (B)
α_1 and α_2 = the angles as presented in Figure 2.6.

Another common method for calculations of the stress distribution is the 2:1 method (Bergdahl et al., 1993). It assumes that the applied load on the surface is spread in the soil with a load spread angle (β) often taken as 2:1 (26.57°) for design purposes and thus distributed over a larger area with increasing depth. This is illustrated in Figure 2.7a and the change in vertical stress assuming the load spread angle of 2:1 can be calculated with Equation 2.9. The drawback of the method is that it assumes a homogeneous and isotropic soil, which is rarely the case in reality. Furthermore, it assumes that the stress is evenly distributed over the area when in reality the stress is larger in the center and smaller at the sides (Temporary Works forum, 2019). This can result in an underestimation of the stress in the center and overestimation of the stress at the sides, this is illustrated in Figure 2.7b.

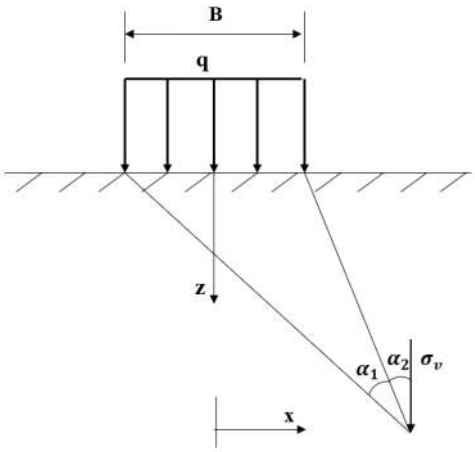

Figure 2.6: *Boussinesq method for strip footings. Figure modified from Knappet and Craig (1974).*

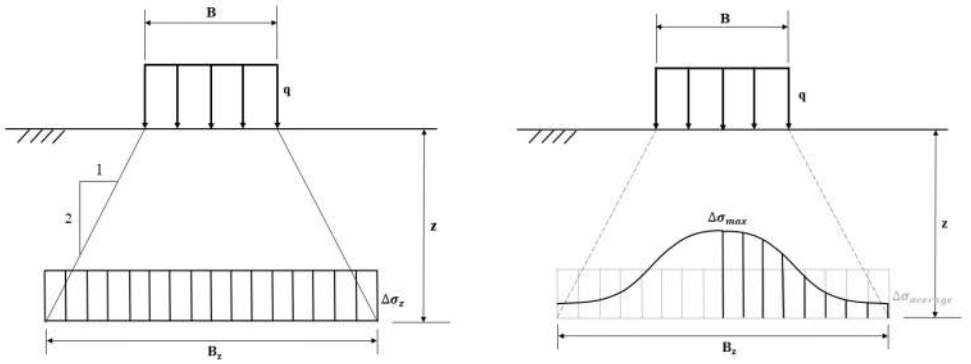

(a) *2:1 load spread method.* ***(b)*** *Actual stress distribution.*

Figure 2.7: *Load spread and stress distribution. Figures modified from Temporary Works forum (2019).*

$$\Delta\sigma_z = \frac{q}{(1+\frac{z}{B})(1+\frac{z}{L})} \tag{2.9}$$

where;
B = with of loaded area
L = length of loaded area.

2.5 Vertical bearing capacity

Several methods have been found by several researchers for calculation of vertical bearing capacity (Bergdahl et al., 1993).

A general bearing capacity equation is used with the assumptions that it is for shallow continuous foundations on a subgrade for cohesive or non-cohesive soils (Bergdahl et al., 1993). It calculates the general shear failure and considers the shear strength of the soil, the surcharge as well as the soil self weight. ϕ of the soil is considered through the bearing capacity factors, with functions based only on ϕ. The bearing capacity equation in its general form is seen in Equation 2.10. Later several researchers have supplemented and suggested correction factors to the general bearing equation to be used when a foundation deviates from the general assumptions. One of those correction factors (s_c^0, s_c, s_q, s_γ) considers the shape of the foundation as a non-continuous foundation.

$$q_u = cN_c\xi_c + \sigma_b' N_q \xi_q + 0.5\gamma' B_{ef} N_\gamma \xi_\gamma \tag{2.10}$$

where;
q_u = ultimate bearing capacity
c = cohesion of underlying soil
σ_b' = effective stress at the bottom of the foundation
γ' = effective unit weight of soil
B_{ef} = effective width of foundation
N_c, N_q, N_γ = bearing capacity factors
ξ_c, ξ_q, ξ_γ = correction factors.

The bearing capacity factors are calculated according to Equation 2.11, 2.12 and 2.13.

$$N_c = \pi + 2, \qquad \text{if } \phi = 0 \tag{2.11a}$$
$$N_c = (N_q - 1)\cot\phi, \qquad \text{if } \phi \neq 0 \tag{2.11b}$$

$$N_q = \frac{1+\sin\phi}{1-\sin\phi} e^{\pi \tan\phi} \tag{2.12}$$

$$N_\gamma = F(\phi)\left[\frac{1+\sin\phi}{1-\sin\phi} e^{\frac{3\pi}{2}\tan\phi}\right] \tag{2.13a}$$

where;

$$F(\phi) = 0.08705 + 0.3231 sin2\phi - 0.04836 sin^2 2\phi \tag{2.13b}$$

If there is a moment or eccentric load acting at the foundation the resulting load will not be at the geometric centre of the foundation (Bergdahl et al., 1993). An effective area (A_{ef}) should in this case be considered as in Equation 2.14. The distance between the geometric centre and the resultant force are represented as e_B for B_{ef} and e_L for the effective length (L_{ef}). Within the A_{ef} the load is assumed evenly distributed.

$$B_{ef} = B - 2e_B \tag{2.14a}$$
$$L_{ef} = L - 2e_L \tag{2.14b}$$
$$A_{ef} = B_{ef} L_{ef} \tag{2.14c}$$

If the foundation has a shape that is not continuous, the bearing capacity factors has to be multiplied by a shape factor according to Equation 2.15 (Bergdahl et al., 1993)

N_c: $$s_c^0 = 1 + 0.2\frac{B_{ef}}{L_{ef}}, \quad \text{if } \phi = 0 \tag{2.15a}$$
$$s_c = 1 + \frac{N_q}{N_C}\frac{B_{ef}}{L_{ef}} \quad \text{if } \phi \neq 0 \tag{2.15b}$$
N_q: $$s_q = 1 + (tan\phi)\frac{B_{ef}}{L_{ef}} \tag{2.15c}$$
N_γ: $$s_\gamma = 1 - 0.4\frac{B_{ef}}{L_{ef}} \tag{2.15d}$$

2.5.1 Non-cohesive soil overlaying clay

According to the guideline provided by SAFE a method that considers the bearing capacity of both the working platform and the subgrade should be used when designing a working platform.

One method is a correction factor to the general bearing capacity equation (Tcheng, 1957). It can be used to calculate the bearing capacity for a non-cohesive soil layer, with a thickness H, overlaying clay according to Equation 2.16 or 2.17.

When $0 < \frac{H}{B_{ef}} < 1.5$:

$$q_b = N_c^* \xi_c c_u \tag{2.16a}$$

where;

$$N_c^* = 4(1 + \frac{H}{1.5B_{ef}}) \tag{2.16b}$$

When $1.5 < \frac{H}{B_{ef}} < 3.5$:

$$q_b = N_c^{**}\xi_c c_u + 0.5\gamma' B_{ef} N_\gamma^* \xi_\gamma \tag{2.17a}$$

where;

$$N_c^{**} = 4.5(3.5 - \frac{H}{B_{ef}}) \tag{2.17b}$$

and

$$N_\gamma^* = 1.38\left[\frac{\sqrt{H}}{B_{ef}} - 1.23\right] N_q \tag{2.17c}$$

and N_q is calculated according to Equation 2.12 for the non-cohesive soil.

For a dense sand layer overlaying a soft clay Meyerhof (1974) suggested that rather than that the platform helped spreading the load it was the development of punching shear resistance in the platform that supported the applied load as shown in Figure 2.8.

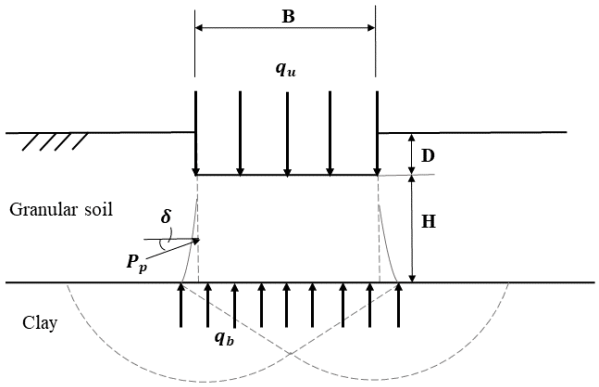

Figure 2.8: *Failure mode of punching shear. Figure modified from Meyerhof (1974).*

The forces acting on the failure surface can be assumed to be equal to a total P_p developed as the material is pushed down inclined with an angle (δ) against the vertical plane. The angle of δ is often taken as $2\phi/3$ as this was found to be the average value of this parameter. The bearing capacity for a platform with B and depth D can therefore be described as in Equation 2.18a

$$q_u = cN_c + 2P_p sin\frac{\delta}{B} + \gamma D \tag{2.18a}$$

where γ is the unit weight of the sand and P_p can be expressed as;

$$P_p = 0.5\gamma H^2(1 + \frac{2D}{H})\frac{K_p}{cos\delta} \tag{2.18b}$$

where K_p is passive earth pressure coefficient and can be assumed to have following relationship with the punching shear resistance coefficient (K_s);

$$K_s tan\phi = K_p tan\delta \tag{2.18c}$$

where;
ϕ = friction angle of sand.

With the above stated relationships in Equations 2.18a, 2.18b and 2.18c q_u can be written as:

$$q_u = cN_c + \frac{\gamma H^2(1 + \frac{2D}{H})K_s tan\phi}{B} + \gamma D \tag{2.19}$$

The relationship in Equation 2.18c has been utilized such that K_s can be retrieved for different friction angles from the diagram in Figure 2.9.

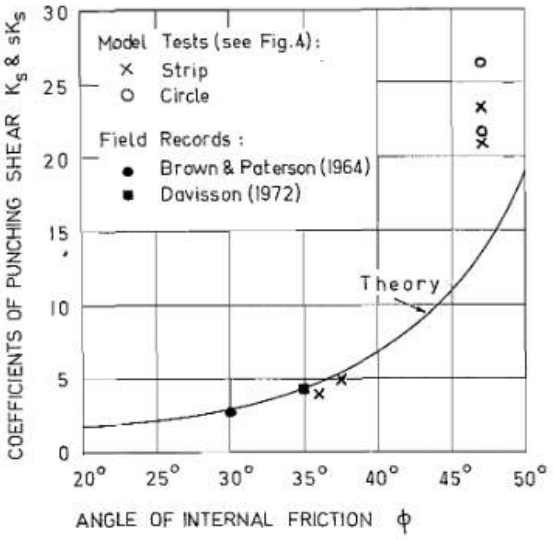

Figure 2.9: *Coefficient of punching shear resistance (Meyerhof, 1974).*

While these equations applies to strip footings, correctional supplementary equations for circular and rectangular footings are provided by Meyerhof (1974). Tests were performed where different kind of footings were loaded until failure on a dense sand overlaying soft clay to validate the theory. The coefficient of K_s was analysed and found to fit well with the proposed theory. Finally the q_u was found to be largely dependent on H, the footing dimensions as well as the ratio between D and B.

The guidlines by SAFE suggest that the theory by Meyerhof and Hanna (1978) can be used to determine the thickness of a working platform with a subgrade of clay. This theory is an extended version of the punch shear resistance theory by Meyerhof (1974) to cover inclined loading conditions. It consider the failure of

a shallow foundation, with an inclined load at an angle α, as an inverted uplift problem as seen in Figure 2.10.

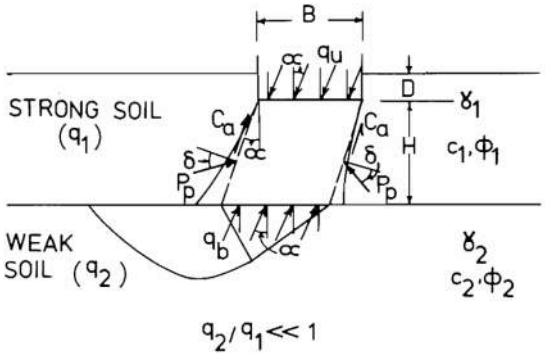

Figure 2.10: *Failure of soil below footing under an inclined load on strong layer overlying a weak deposit (Meyerhof & Hanna, 1978).*

From the applied load a triangular shape of the stronger soil layer is pushed into the weaker soil layer, with an approximate direction of α. As for the case of a vertical load the forces on the actual punching failure surface in the upper layer is assumed to be equivalent to P_p as well as a total adhesion (C_a) with an unit cohesion (c_a). But for the case with an inclined load those are inclined with the angle of δ acting upwards on an assumed plane passing through the foundation edge which is inclined at angle α to the vertical. The vertical component (q_{uv}) of q_u in the direction of the load is then calculated according to Equation 2.20 with C_a and P_p calculated according to Equation 2.21. q_{bv} are the vertical component of the ultimate bearing capacity of the subgrade (q_b) under the inclined load.

$$q_{uv} = q_{bv} + 2(C_a + P_p sin\delta)\frac{cos\alpha}{B} - \gamma_1 H \tag{2.20}$$

$$C_a = \frac{c_a H}{cos\alpha} \tag{2.21a}$$

$$P_p = 0.5\gamma_1 H^2(1 + \frac{2Dcos\alpha}{h})\frac{K_p}{cos\delta} \tag{2.21b}$$

The Building Research Establishment in United Kingdom (BRE) published the handbook *"BR 470 Working Platforms for Tracked Plant"* in 2004. The handbook is a good practice guide that provides support considering design, specification, installation, operation and maintenance of working platforms. BR 470 provides Equation 2.22 where the bearing resistance for the system of the granular layer and clay subgrade can be calculated. This method is also based on the theory of punching shear

resistance by Meyerhof (1974). Dobie, Lees, Buckley, and Bhavsar (2019) discusses the method for design calculation of working platforms provided in BR 470.

$$q_u = q_b + q_p \tag{2.22}$$

The equation considers both q_b and the punching shear resistance component from the platform of granular layer (q_p). q_b and q_p are calculated according to Equation 2.23a and 2.23b respectively.

$$q_b = s_u N_c s_c \tag{2.23a}$$

$$q_p = \frac{\gamma_p K_p H^2 tan\delta s_p}{B} \tag{2.23b}$$

Where;
s_u = undrained shear strength of the subgrade
γ = unit weight of sand
$s_p = 1 + \frac{B}{L}$.

Dobie et al. (2019) discusses the applicability of the method and according to the authors the method is only suited for s_u values between 20 and 80 kPa as well as for small platform depths that satisfies $\frac{H}{B} < 1.5$.

In an article by Burd and Frydman (1997) a parametric study using finite element and finite difference methods is performed to analyse the bearing capacity of plain strain footings on sand overlaying clay. The results from the two independent numerical methods aligns very well with one another which is taken as validation to continue analyse the bearing capacity and load spread angle. The results of the study is compared with established analytical models such as the load spread and punching shear model. The parametric study showed that q_u reached a maximum value (plateu) independent on the shear strength ratio (s_u/γH). This is seen in Figure 2.11. This is contrary to the linear relationship between shear strength and bearing capacity stated in Equation 2.19.

Furthermore, results for β for different shear strength ratios of the clay and ϕ of the sand using Equation 2.24 showed that β was considerably higher for a larger ϕ but also considerably lower for larger shear strength ratios. The load spread method is however very simplified and thought not to be suitable when the failure is confined to the granular layer.

$$tan\beta = \frac{\frac{q_u B}{s_u N_c} - B}{2H} \tag{2.24}$$

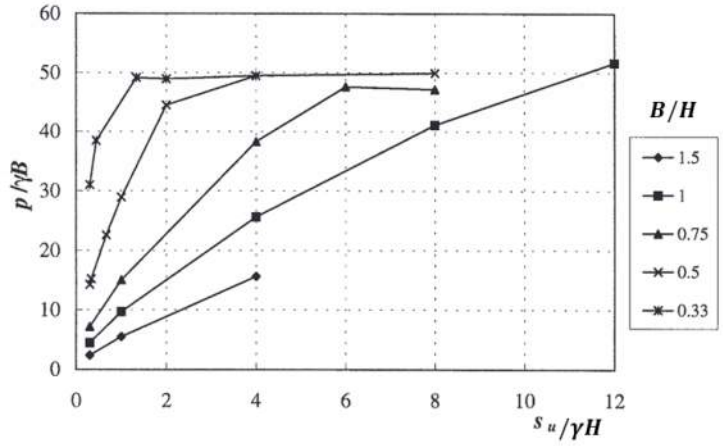

Figure 2.11: *Variation of $p/\gamma H$ and $s_u/\gamma H$ for ϕ=40° (Burd & Frydman, 1997).*

In a technical note for the BR 470 method, Miller (2013) offers correctional factors to the K_p to make the method applicable for s_u beyond the range of 20-80 kPa. This was based on the work by Burd and Frydman (1997) and a finite element analysis. Miller came to a conclusion that the work provided by Burd and Frydman was on the more conservative side concerning the bearing capacity compared to the BR 470 method, even when using large safety factors. This was especially prominent for subgrades with low shear strength. The derived equation for the correctional factor can be seen in Equation 2.25.

$$y = 0.1704ln(x) + 1.2021 \tag{2.25}$$

where;
x = $\frac{c_u N_c \xi_c}{0.5\gamma' b_{ef} N_\gamma \xi_\gamma}$.

2.5.2 Working platform reinforced with log mats

When using log mats as a load-distributing element they can be considered as a shallow foundation (Rankka et al., 2022). For design of working platforms with log mats, both conditions of the soil and the log mats should be considered. When the bearing capacity of the working platform is estimated it is assumed that the log mat has an infinite stiffness and is causing a uniform pressure at the platform. The stiffness of the log mats should however be considered according to its conditions such that an overestimation of its capacity to distribute load is not made.

Methods for stress distribution and bearing capacity in Section 2.4 and 2.5 respectively are all applicable for shallow foundations. Hence they are applicable for working platforms reinforced with log mats and the behaviour of stress distribution

can be estimated as well as bearing capacity can be calculated according to those methods. However, it has not been found that any of those methods have been validated for working platforms with log mats or an shallow foundation which is not infinitely stiff.

2.5.3 Working platform reinforced with geogrids

The article by Dobie, Lees, and Khanardnid (2018) is discussing two case studies with geogrid stabilised working platforms constructed over soft dredged silt. The first case study is a field trial from 1987 in Malaysia. A working platform was built with two layers of geogrids within the platform and it was then loaded with a heavy crane. Several years later the trial was extended and a working platform with two layers of woven geotextiles was built and loaded with a heavily loaded crawler crane. The results from the two trials could then be compared and the performance of the geogrid and geotextile was compared. The trial concluded in a distinction between the functions of geogrids and geotextiles. The geogrid provided mechanical stabilisation where the geotextile acted as reinforcement. Mechanical stabilisation takes place when soil particles interlock with the aperture of a stiff geogrid. This can be considered as a composite if the geogrid interacts effectively.

In a publication by Jewell (1996) guidance on use and design of geosynthetics in working platforms are provided. The method relies on the load spread mechanism and that the geosynthetic supports the outward shear stress and improves the bearing capacity through a reinforcement mechanism. To be able to use the design equations provided for bearing capacity in the guidance the load spread angle of the platform material has to be known.

In an article by Saha Roy and Deb (2017) the bearing capacity of rectangular footings on a geogrid reinforced granular layer overlaying soft soil was studied. A number of laboratory test where performed with different footing dimensions as well as different numbers of geogrid layers to evaluate the effect on bearing capacity, load spread angle and settlements. The results showed that increment in numbers of geogrids reduced settlements and increased bearing capacity as well as the load spread angle. However, it was found that a single geogrid layer had the largest rate of improvement on the bearing capacity while two geogrid layers contributed to the largest rate of reduction in settlements. The effect of the geogrids on both settlements, bearing capacity and load spread angle diminished after the second layer.

In the article by Dobie et al. (2019) the BR 470 method for calculating the bearing capacity of a geogrid reinforced granular working platform over soft soil is discussed. The method is based on adding bearing resistance contributed by the geogrid (q_g) to Equation 2.22. q_g are calculated according to Equation 2.26.

$$q_g = \frac{T_{ult}}{B} \tag{2.26}$$

where;
T_{ult} = geogrid tensile strength.

Dobie et al. (2019) brings up concerns surrounding Equation 2.26 as it either ignores the effect of the footing dimensions (shape factor) or it only considers q_g alongside the punching shear surface. This suggests that considerably large deformations of the platform as high strains of the geogrid are necessary for q_g to contribute to the bearing resistance of the system. However, in 2011 BRE released a supplementary document considering geosynthetic reinforcement where alternative approaches are embraced as long as safety is preserved. It also acknowledge that the contribution of the geogrid is not because of added reinforcement due to its tensile strength but rather the mechanism of mechanical stabilisation.

To investigate the phenomena of surcharge transfer in granular layers stabilised with geogrid a two-dimensional generic finite element analysis was made by Lees (2017) to propose a design method. A geogrid was modeled as a c'-profile which was simulated by a soil structure as the stabilising effect in the granular layer by an addition of apparent cohesion. It was found that the c'-profile acted as interlocking between the geogrid and the granular layer, counteracting particles to rearrange. It showed that stabilisation resist punching shear through the granular layer and allowed more transfer of load across the shear plane. The c'-profile was further studied as a parametric finite element analysis. In the model s_u of the clay varied from 5 to 80 kPa. The additional cohesion in the c'-profile (c'_{max}) was set to 0 kPa when no geogrid was simulated and it was set to 15 kPa when geogrid was simulated. When H was 0.45 m and higher, a second layer of geogrid was placed 0.3 m above the base of the granular layer. As the study was conducted in two-dimensions, the ratio of B/L was set to 0 for a plain strain model and to 1 for axisymmetric cases.

The parametric study resulted in remarkably linear relationships between the ratio of q_u/q_b and H/B. The slope of the linear relationship was called the load transfer efficiency (T). The relationship does also show that the surcharge transfer effect depends primarily on the properties of the granular layer and do not change significant in terms of s_u. But as it effects q_b it affects the ratio of q_u/q_b and therefore becomes higher when the clay subgrade becomes weaker. This is seen in Figure 2.12 as T varies exponentially with s_u.

The relationship developed to a proposed design method, called the T-method, which is relatively simple as the only material parameters needed is the s_u and the T-value. When the relationship is established, with laboratory tests, the needed bearing capacity of the granular layer can be calculated according to Equation 2.27.

$$\frac{q_u}{q_b} = 1 + T\frac{H}{B} \tag{2.27}$$

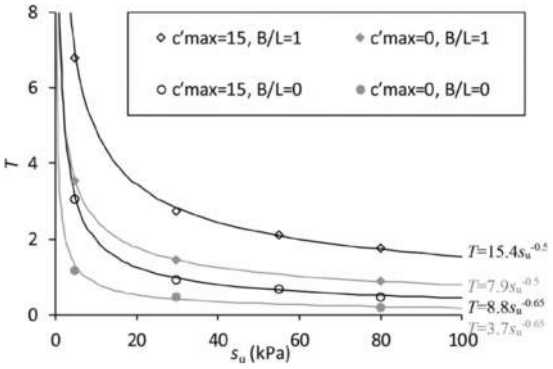

Figure 2.12: *Relationship between load transfer efficiency (T) and undrained shear strength (s_u) from parametric study (Lees, 2017).*

A field trial was performed in Laem Chabang, Thailand (Dobie et al., 2018). A working platform was built with two layers of geogrid and loaded until failure in the stabilised layer was seen. The results was back-calculated according to the T-method. The relationship between T and s_u could be derived and plotted with the parametric study. The result was close to the parametric line for $B/L = 1$, hence it provided good validation for the T-method.

A modification have been made to the T-method by another parametric study with different types of granular fills (Lees & Matthias, 2019). A trend was seen for the different types when s_u was normalised with the effective vertical stress at the base of the granular layer (σ'_0) such that Equation 2.28 can be applied to similar granular materials. Different types of geogrids might still act differently and should still be full scale tested for validation. It was also seen that the T-value increased with ϕ for the granular fill which is consistent with the higher shear strength of the clay. As a low shear strength of the subgrade have larger effects on the bearing capacity, the outputs of T-value becomes sensitive as s_u/σ'_0 are lower and when they fall below 1.25 the corrected T-value (T_{corr}) in Equation 2.29 should be used instead.

$$T = 2.9 \left(\frac{s_u}{\sigma'_0} \right)^{-0.32} - 0.6 \tag{2.28}$$

When $s_u/\sigma'_0 < 1.25$:

$$T_{corr} = \frac{T}{1 + 0.2(1.25 - s_u/\sigma'_0)} \tag{2.29}$$

2.6 Measurement instrumentation

Measurement instrumentation can, in addition to what was stated in Section 2.2.1, be used to monitor performance in the ground, often during a project (Dunnicliff, 1988). Often measurements of total stress and deformations are involved.

2.6.1 Measurement of total stress

An instrument that measure total stress is an earth pressure cell (GEOKON, 2021). The cell will respond not only to soil pressures, but also to the pore water pressure. An earth pressure cell can be installed such that it measures the total stress within a soil mass or at the face of a structural element, but there are several factors that will affect the measurements (Dunnicliff, 1988). Some of the factors that has to be considered are soil/cell stiffness ratio, calibrations as well as field placement effects.

A hydraulic earth pressure cell has two flat plates that are welded at the periphery and separated with a small gap which is filled with a hydraulic fluid (GEOKON, 2021). The earth pressure acts to squeeze those plates together. The gap with hydraulic fluid are connected to a pressure transducer. The transducer converts the hydraulic fluid pressure to an electrical signal. One of the most common transducer are functioning with a vibrating wire principle (Hunt, 2005). It means that it measures wire oscillations within a magnetic field. The change in measured quantity causes the wire in the transducer to change frequency through change in stress. The frequency can then be transmitted to a receiving instrument where it can be read as a value.

It is important that the pressure is uniform over the plate and that the cell is as stiff as the soil (GEOKON, 2021). In practice this is difficult to achieve and for example if the cell is stiffer than the soil, it will over register soil pressure. The cell will then attract soil pressure as the soil immediately around the cell is sheltered by the cell and does not experience the full pressure. This results in a slightly higher stress concentration at the rigid rim which would not be obtained if the cell was not present and the measured total stress is higher than the mean soil stress.

All instruments must be calibrated to make sure that its readings becomes useful (Dunnicliff, 1988). Calibration consist of applying known pressures on the cell and measuring its response. Before shipment from the factory calibrations are done. Then it is wisely to do preliminary test on the earth pressure cells when they are received at site and before they are installed in soil (GEOKON, 2021). This can be done by just pressing the cell and a change in readout digits should be seen. One of the most used calibration methods are dead weight calibration (DWC) (Hunt, 2005) as it is a easy to perform and requires little time. A known weight are placed on the cell and the readings are checked.

All measurement instrumentation have uncertainties (Dunnicliff, 1988). The hysteresis effect is one uncertainty that can be measured during calibration. A cyclic load test can be performed and measures are taken during loading and unloading in several steps. If the measured values are plotted against the actual value and the loading and unloading curves does not correspond well the separation between the curves are a measure of hysteresis. The effect is commonly caused by friction and backlash and if a large hysteresis effect is seen the measurements are not suitable for rapidly changing parameters.

Experience have shown that measuring earth pressures within a fill often meets with failure (GEOKON, 2021). This is due to problems of stress distribution within the fill and how the installed cell influences the actual stress distribution. But there are recommendations for installation of earth pressure cells within a fill. A recommendation is that each cell should be individually installed in small pockets (Dunnicliff, 1988). Each pocket should be twice the size of the cell and the pockets should be separated by at least 1 m. The pockets should carefully be hand dug and the cell should be placed and checked for correct functioning, alignment and level. The pocket can then be back filled with stone-free soils, but similar to the surrounding soil. A 10-20 cm thick layer of embankment material, with rocks larger than the size of the cell removed, can then be filled and compacted by hand-operated equipment before completing the fill.

2.6.2 Measurement of deformation

There are several methods and instruments to measure deformation depending on the application (Dunnicliff, 1988). Deformation can be monitored as the changing distance between two points on surface or on a structure, or between one point on the surface and one point on a structure.

A dial indicator is an inexpensive instrument to use for measurements of deformation (Dunnicliff, 1988). It can be attached to a bracket on one side which works as machined reference surface and it measures deformations as it bears against a surface on the other side where deformations are expected.

Another instrument for measurement of deformation are crackmeters. A vibrating wire crackmeter is designed with a spring that is connected to the wire at one end and to a connecting rod at the other (GEOKON, 2020). When the connected rod is pulled out from the gauge body the spring elongates causing increase in tension which is sensed in the vibrating wire. A transducer with the function of vibrating wire principle, as described in Section 2.6.1, converts the signals, which is proportional to the extension of the crackmeter and can be read in a receiving instrument.

For installation of crackmeters there are different types of anchors (GEOKON, 2020). Groutable anchors can be used to install it in concrete or rock. Depending on the crackmeter model and anticipated direction of movement they should be installed with appropriate spacing distances according to the supplier. The crackmeter should be extended till the desired reading is obtained, its position should be measured and then it can be anchored in those points. As for the earth pressure cells, the crackmeters are calibrated in the factory before shipment, and as they are installed readings should be made and checked with calibration sheets.

3 Planning and Execution of Field Trial

When a field trial is to be carried out with geotechnical instrumentation a systematic approach for planning should be used (Dunnicliff, 1988). It is significant that site conditions is known, as for example the project type, subsurface stratigraphy and engineering properties of subsurface.

When this is known predictions of what controls the behavior in the ground can be made and should be stated as questions that can be answered by the measurements that will be conducted. Based on this, the purpose of the instrumentation can be defined and the parameters that should be monitored must be selected. It is important to not only measure the primary parameter of interest, both causes and effects must be considered to be able to develop a relationship between those parameters. A prediction of the magnitudes of the parameters has to be made to be able to choose required instrumentation considering ranges, accuracy and sensitivities. When this have been considered the instrumentation and its location can be selected.

A list of each instrumentation, its location and its purpose can be made and a plan for the installation process should be made. In the plan it is important that calibration of the instrument is considered. While measuring during the field trial, it is finally important to record factors that may influence the measured data and procedures for ensuring reading correctness.

This chapter will describe the methods used and choices made during the planning and execution phase of the field trial.

3.1 Site conditions

The first step of planning the field trial was to find a suitable site where the clay was undisturbed. A construction site in Erikssund, where a new bridge was about to be built, was found to meet these requirements. The construction site is located outside Stockholm and an area on the site could be spared for the field trial to be performed. The site and its location is seen in Figure 3.1.

When the site was set for the field trial a ground investigation could be done. Two boreholes were drilled, one in the center of each platform that was planned to be build. A disturbed sample was taken from an auger in one of the boreholes and a visual classification of the soil was made. A piston sampler was used to get undisturbed samples, at 1.5 m, 2.5 m and 3.5 m depth, from the other borehole and in the same borehole a FVT was conducted. In each borehole a CPT was conducted to a depth of 15 m.

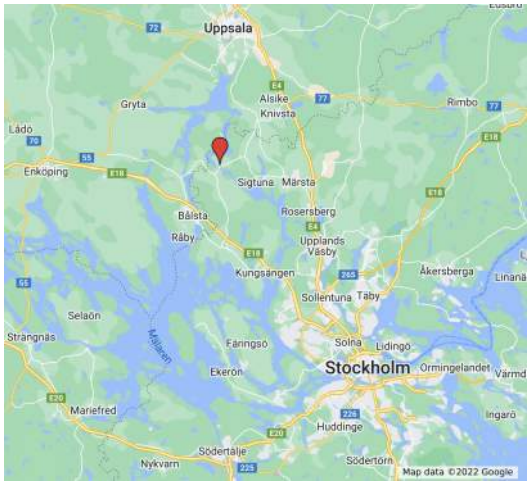

(a) Map of where the site is located (Google Maps, 2022).

(b) Drone image of the site when the two platforms have been built.

Figure 3.1: *Site in Erikssund.*

The samples was sent to the laboratory. General tests as well as a CRS test was made on the samples conducted from the piston sampler. The sampling were considered to be successful and the samples could be considered as undisturbed. Therefore, also a direct shear test could be performed on those samples.

The results from the ground investigation was analysed and parameters for the clay was evaluated and could further be used in the project. The unit weight (γ) was set to 16 kN/m^3, the undrained shear strength (s_u) to 10 kPa and compressibility modul (M_0) to 1 MPa. All results from the ground investigation can be seen in appendices A.1 to A.6.

3.2 Applied load

The applied load for the field trial was supposed to simulate the weight of a tracked pile rig. For simplification, it was decided to use concrete weights to simulate one track of the pile rig as well as the pressure imposed by that track.

Dimensions used for the track was 4.2 m x 0.9 m, s as shown i Figure 2.5, was set to 3.8 m and the weight of the pile rig (F) was set to about 700 kN according to the example given in the guidelines by Swedish Association for Foundation Engineering (2020). For simplification of the field trial a uniform ground bearing pressure was wanted along the track, hence F_R was calculated to 617 kN according to Equation 2.7 for the rig in 90° rotation from the tracks direction. This load would correspond to a ground bearing pressure of 163 kPa. Seven concrete weights of 67.5 kN was decided to be used for the field trial and was to be stacked on each other on an fixed area of 4.2 m x 0.9 m such that it would correspond to a ground bearing pressure of 125 kPa. For further design of the working platform this maximum ground bearing pressure was used.

During the field trial nine concrete weights of 54 kN with the dimension of 4.5 m x 1 m was used instead. Those were stacked directly on the working platform such that the area of one weight simulated one track of a pile rig. This corresponded to an applied pressure of 108 kPa.

3.3 Design of working platforms

The field trial was to be performed with three different working platforms, one working platform without reinforcement, one reinforced with log mats and one reinforced with geogrid. On each platform a test was to be executed. The tests are further called test F, L and G respectively.

Two platforms were built as test F and L could be performed on the same platform. The platforms were named A and B. The platforms had to be as identical as possible regarding dimensions and execution. The theoretical difference was that platform A was built without reinforcement and platform B was reinforced with a geogrid. Both platforms were built such that one log mat with length of 5.5 m could fit on the width of the platform with 0.5 m to spare on the sides from the slope. Lengthwise six log mats besides each other, each one 0.9 m wide, needed to fit such that a pile rig would fit on the log mats. Additional length space was added such that three dimensional effects could be discarded and plain strain conditions would apply. The slope was inclined with and angle of 1:1. An overview of the platforms A and B is seen in Figure 3.2 with one weight applied as the simulated track.

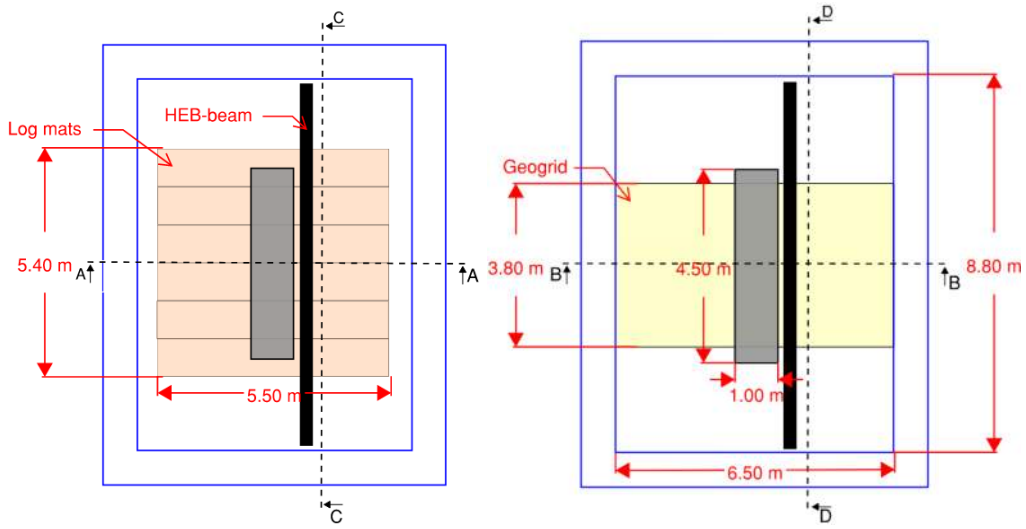

(a) Platform A reinforced with log mats. *(b) Platform B reinforced the geogrid within the platform.*

Figure 3.2: *An overview of the platforms with one weight applied as the simulated track.*

Platform A is in Figure 3.2b seen reinforced with log mats, however the platforms were designed considering the unreinforced platform as it is assumed to be the

platform with the lowest bearing capacity. It was desired not to reach failure during the trial considering the safety on site. For the design of the working platform the ultimate bearing capacity of the clay was calculated with the general bearing capacity equation, Equation 2.10. The load was calculated as a centric load hence B_{ef} was set to 0.9 m and L_{ef} was set to 4.2 m. $q_{u,clay}$ was calculated to 54 kPa. The calculation can be seen in Appendix B.

To decide the thickness of the platforms several calculations were performed. The 2:1 method was used to estimate the distribution of stress due to the applied load, q=125 kPa. To not reach failure in the clay, in accordance with $q_{u,clay}$=54 kPa, the thickness of the platform had to be higher than 0.8 m. The correction factor method by Tcheng (1957) was used to calculate the thickness of the platform. As this was done, the boundary conditions of Equation 2.16 and 2.17 was not full-filled and the method was considered not to be accurate for calculations of the platform thickness. As no inclined loads was to be induced for the trial, the method by Meyerhof and Hanna (1978) and Equation 2.20 was not considered suitable. Instead, the punching shear resistance method by Meyerhof (1974) and Equation 2.19 was used. Parameters for the fill was set according to Trafikverket (2014), with γ_{fill}=18 kN/m^3 and $\phi_{fill} = 45°$. q_u was set to 125 kPa. H was calculated to 0.6 m. Equation 2.22 from BR 470 with and without the correction factor by Miller (2013) (Equation 2.25) was also used to calculate the thickness of the platform. q_u was set to 125 kPa, B to 0.9 m, K_p was set according to Swedish Standards Institute (2005) and H could be calculated to 0.6 m without the correction factor by Miller (2013) and 0.7 m with the correction factor. During the design process, the general bearing capacity equation combined with the 2:1 method was, due to lack of time, mostly considered and therefore the thickness of the platform was set to 0.8 m. This can be seen in Figure 3.3 which is sections as viewed in Figure 3.2 of each platform with the final design of the platforms for load step 6.

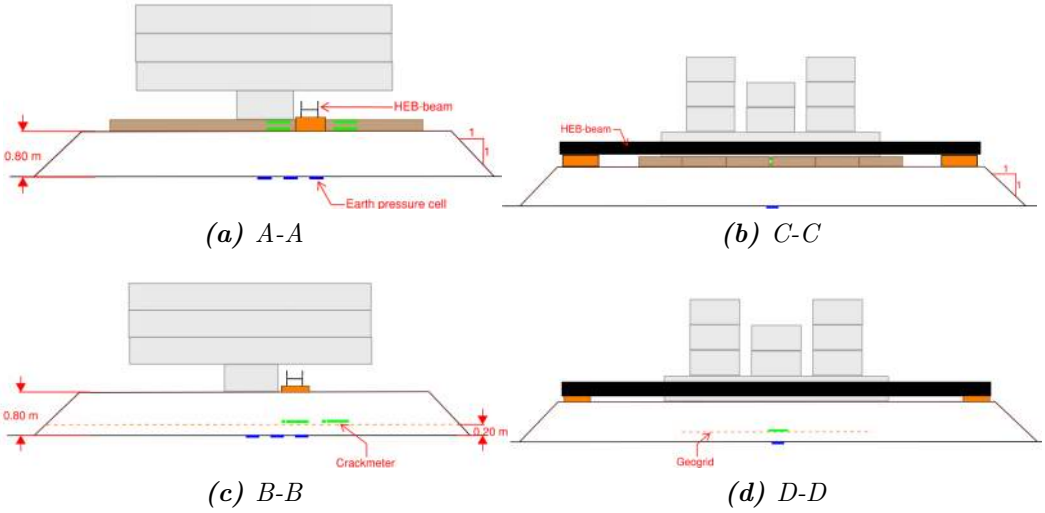

(a) A-A *(b) C-C*

(c) B-B *(d) D-D*

Figure 3.3: *Sections from figure 3.2. Final design and installation of measurements of the two platforms.*

When the thickness of the working platform was set and when it later was known that other weights was to be used during the field trial recalculation of the ultimate bearing capacity of the clay was made. It was still about 54 kPa with the general bearing capacity equation. With the 2:1 method it was also seen that the clay would be close to failure for this thickness during the case with the working platform of only fill. All calculations made for the design of the working platform are seen in Appendix B.

For platform B a geogrid was installed within the granular fill. Geogrids are installed within or beneath the granular platform and acts in tension such that when the platform is loaded, it restrains in an outward movement of the fill (Temporary Works forum, 2019). In order to mobilise its tensile strength it has to strain. For a correct installation of the geogrid, the particle size of the fill has to be related to the mesh size of the grid such that the effects of interlocking is achieved. The load spread angle of a geogrid reinforced granular platform are often taken as 1:1 for design purposes.

The geogrid used in the field trial was a triaxial geogrid with a width of 3.8 m. It was placed centered under the simulated track as seen in Figure 3.2b, 3.3c and 3.3d. The geogrid used is seen in Figure 3.4 and a specification of it is seen in Appendix C. The article by (Saha Roy & Deb, 2017) concludes that one layer of geogrid had the highest rate of improvement of bearing capacity and that after two layers the effects diminishes. The T-method was based on numerical studies where a second layer of geogrid was added when the thickness of the platform was 0.45 m and higher. Considering those aspects of layers of geogrid, it was decided to install one layer of geogrid 20 cm above the clay to simplify the analyses.

Figure 3.4: *Geogrid used in field trial.*

3.4 Measurement instrumentation

To measure the performance of the three types of platforms it was decided to measure total stress, the deformation in the log mat and geogrid as well as the settlement under the simulated track.

To measure total stress three earth pressure cells was installed in each platform. The earth pressure cells used was a hydraulic type with circular stainless steel plates and a vibrating wire transducer. The cell had a pressure range up to 2 MPa. A full specification of the model used can be found in Appendix D.

The earth pressure cells were decided to be installed at the same locations for both working platforms. Cell 1 was placed under the centre of the simulated track and Cell 2 directly under the edge of the simulated track, which resulted in a center to center distance of 0.45 m as the concrete weight used for design was 0.9 m wide. Cell 3 was placed with the same centre to centre distance from Cell 2, and was therefore placed 0.9 m from Cell 1. The positions for each cell is seen from above in Figure 3.5a with the earth pressure cells marked with blue circles. To be sure that all cells would give readings a load spread angle of 2:1 was assumed which resulted in a stress distribution that would reach 0.85 m from the center of the platform and hence it was decided to be okay with positioning the third cell 0.9 m from centre. The recommendation of at least 1 m between each cell was neglected as it was considered more important that a change in total stress would be measured, which was not certain according to the calculation performed if the center to center distance was further apart. For test L a larger distance between each cell could have been considered. However, as test F and test L was to be executed at the same platform this was not possible.

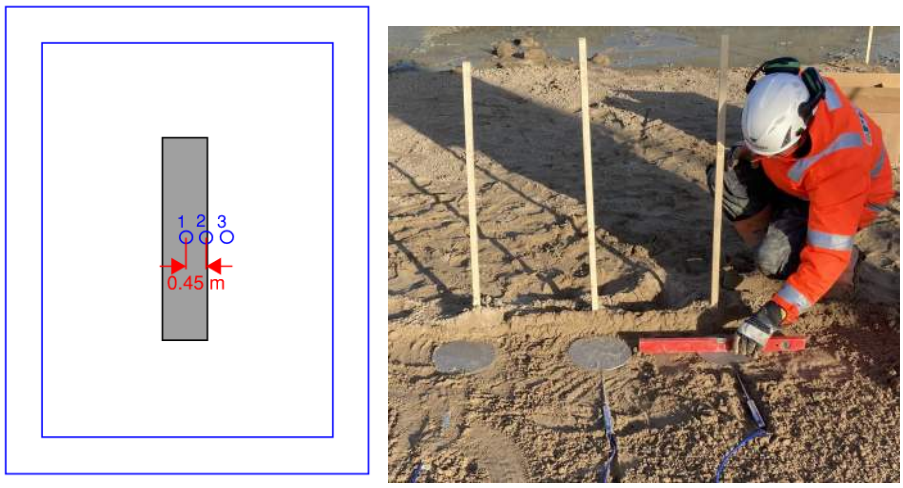

(a) *Position of earth pressure cells (blue circles) in both platforms.*

(b) *Earth pressure cells during installation for the field trial.*

Figure 3.5: *Earth pressure cells used in field trial.*

The earth pressure cells were to be installed between the platform and the clay. This is seen in the sections in Figure 3.3. It was decided to add a 0.1 m thick layer of sand above the clay and over the whole working platform area. Due to the shorter center to center distance, in the sand layer, a larger pocket, instead of separated pockets, was hand dug with care such that all three earth pressure cells was installed horizontally. This was also done to protect the cells and such that no large fractions from the granular soil were pressing against the cells and resulting in

an nonuniform pressure. Figure 3.5b shows the earth pressure cells used and how they were positioned before they were covered with sand within the sand layer.

For test L on platform A, four crackmeters called L1, L2, L3 and L4, were installed on a log mat. The specification on the crackmeters used can be seen in Appendix D. They were installed according to the drawing in Figure 3.6 were the crackmeters are marked in green. Two crackmeters were installed at the upper part of the log mat and those were expected to measure compression. Two crackmeters were installed in the lower part of the log mat and those were expected to measure extension. L1 and L2 were positioned from the center of the platform and L3 and L4 were positioned with a distance of 1.2 m from L1 and L2 such that a behaviour of the deformation along the log mat could be measured. The installed crackmeters on the log mat can be seen in Figure 3.7a.

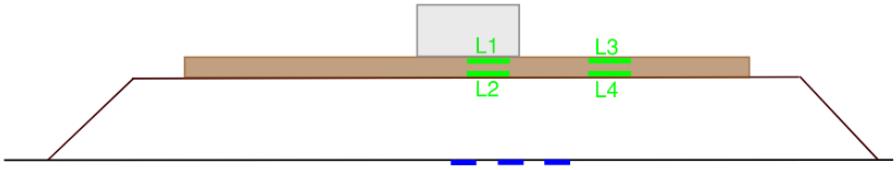

Figure 3.6: *Section A-A as seen in figure 3.2a. Position of crackmeters, seen in green, in platform A for test L. Earth presseure cells are seen in blue.*

(a) *Crackmeters installed on a log mat.*

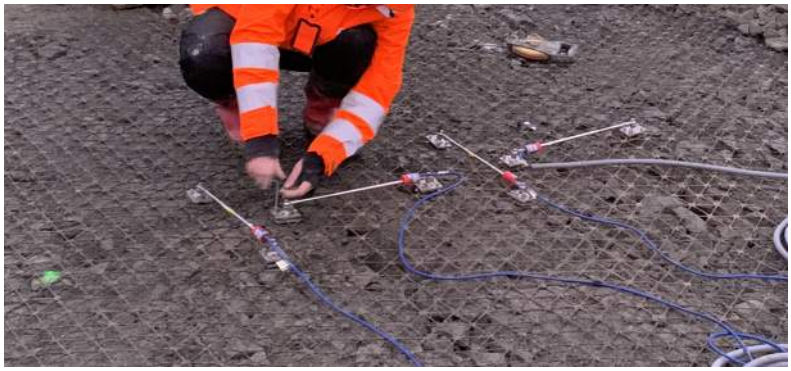

(b) *Crackmeters installed on the geogrid.*

Figure 3.7: *Crackmeters installed for the reinforced working platforms.*

For platform B four crackmeters were installed using clamps on the geogrid according to the drawing in Figure 3.8. Their positions were decided to be in the same cross section as the earth pressure cells and in two directions to be able to measure the deformation of the geogrid in two directions. Two cells were positioned under the edge of the simulated track and two cells were positioned about 1.5 m from the center of the platform to measure if the geogrid would deform differently in relation to where the load was applied. The crackmeters installed in the geogrid in the field are seen in Figure 3.7b. When the crackmeters were installed in the geogrid a zero reading would have been desired to see how much the geogrid would strain as the rest of the working platform was built. As there was no time, a zero reading was not retrieved and instead the values measured when the platform was built had to be compared to zero readings from before the crackmeters were installed and an estimation of the strain in the geogrid could be done. It was seen that the geogrid did not strain significantly during construction and compaction of the working platform.

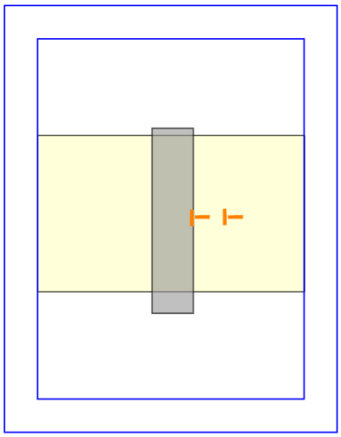

Figure 3.8: *Overview of platform B with the positions of crackmeters, marked in orange, for test G. Simulated track is marked in gray.*

During the field trials the earth pressure cells and crackmeters were read with a logger. During test L and G the cells and crackmeters measurements were logged once every minute. For test F, as only the cells were to be measured, they could be logged every 15th second.

The settlement under the simulated track was measured with dial indicators. This was done by placing a HEB-beam with the ends resting on a build-up at the edges of the platform such that it did not rest on the area that was about to be loaded. This can be seen in Figure 3.2 and 3.3. The dial indicator was fastened with a magnet on the HEB-beam and was measuring against the first weight. As it was measuring against the first weight, the zero reading was taken after the settlement of the first load step. For further load steps the dial indicator could be read for each load step. For test L one dial indicator was placed in the middle along one side of the weight. For test F and G two dial indicators was placed at the ends and on the same side of the weight, such that the deformation in the middle along the weight could be calculated. The installation of the dial indicators in the field trial can be seen for each test in Figure 3.9.

(a) Test L *(b) Test G* *(c) Test F*

Figure 3.9: *Dial indicator installation for the field trial.*

3.4.1 Preliminary test and load tests

Before the earth pressure cells was installed in the granular fill preliminary tests was performed. The DWC method was used by standing on each cell and checking the readings with a portable readout device, model GK-404 VW, which is seen in Figure 3.10. According to the supplier, the readings during the preliminary test should be compared to readings from the provided calibration sheet (GEOKON, 2021). This was done and all cells was tested successfully.

Figure 3.10: *Portable readout device, model GK-404 VW, used the preliminary tests and load tests.*

When the earth pressure cells were installed and the working platforms were built a loading test was performed to make sure that the cells worked properly and that they gave reasonable readings. The platform was loaded and unloaded in three steps of 54 kN. This was done to validate that the earth pressure cells gave the same readings for the same load and to find out if there was a hysteresis effect. The concrete weights were placed according to the drawing in Figure 3.11 such that the three cells theoretically would give same readings.

Each load step of the load test had a duration of about 10 *min* for platform A and 5 *min* for platform B. Readings were taken with a portable readout hand device and the measure was firstly read for cell 1, then 2 and lastly cell 3.

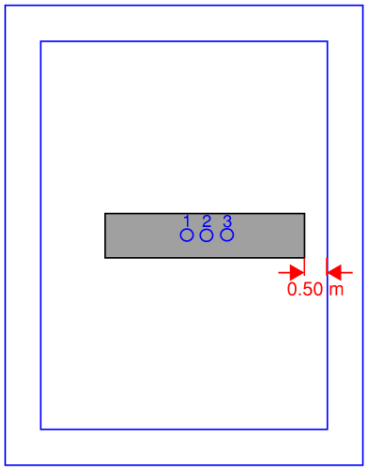

Figure 3.11: *Overview of load test with weight centered over the earth pressure cells (blue circles).*

After the load test was performed it was noticed that the design of the weights were not laying flat against the ground. This is seen in the drawing of the weight in Figure 3.12a and also Figure 3.12b which is a photograph taken during the load test of platform B.

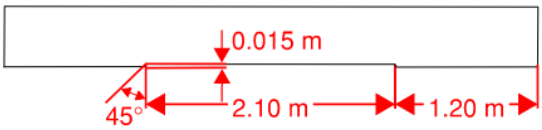

(a) *Drawing of concrete weight.*

(b) *Photograph from load test of working platform B.*

Figure 3.12: *Drawing of concrete weight and photograph of the weight during the load test.*

3.5 Field trial

When the site was excavated to build the working platform directly on the undisturbed clay, it was found that the dry crust was thicker than what was predicted. The excavation had to be deeper which took more time than planned, and the building of the platforms as well as the installation of the measurement instrumentation got postponed. The deeper excavation also led to a problem with the ground water. In the excavation, where the platform was to be built, was about 10 cm of water. Both during the building of the platform as well as during the field trials this water had to be pumped out as it was not desired to affect the field trials. When the water was pumped the working platforms could start to be built.

When the earth pressure cells was installed in the sand layer granular fill could be added. For platform A it was built with a 0.7 m layer of 0-90 granular fill. This was built in layers and compacted as it would have been done in a construction project. For platform B a 0.1 m layer of the granular fill was added above the sand layer. Then the geogrid was rolled out above. Crackmeters were installed on the geogrid and then the rest of the platform could be built. 0.6 m of the granular fill was added in layers and compacted as it would have been done in a construction project. When the working platforms were built and all measurements instrumentation were installed the field trials could begin.

There are some guidelines concerning the load steps for when a field trial is to be performed on plates (Bergdahl et al., 1993). It is recommended that each step should be about 10 % of the calculated failure load and all steps should have equal weight. The duration of each step depends of the aim of the study, but in cohesive soils the duration is often about 8 minutes. Maintained loading is a test method that is usually used to determine the failure load of piles in a field trial (Olsson & Holm, 1993). The loading is also done stepwise and each step has equal duration at about 15 minutes. For each load step the load increment should be about 5 % of the calculated failure load. For a field trial of piles with a static compression method the first loading step should be a maximum of 5 % of the final total load in order to check the measurement equipment (Swedish Standard Institute, 2018). Then each loading should increase with even steps and the total load should be reached in minimum 8 steps. When approaching the final load the loading increment may decrease. It is recommended that the minimum duration for a step is 60 minutes but can be extended if creep rate or displacement rate is studied and have not stabilised.

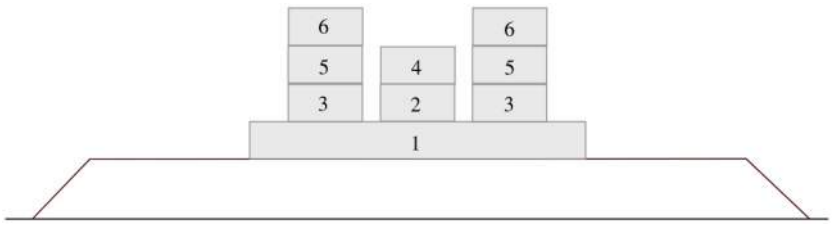

Figure 3.13: *Section A-A and B-B in figure 3.2. Load steps as it was executed in the field trial.*

Considering those guidelines, but also that pile rigs are a temporary load the duration for each loading step was decided to be at least 15 minutes. Furthermore, it was hard to find weights suitable for the field trial, therefore the weights had to be placed as shown in Figure 3.13. This resulted in a choice between uneven load steps or unevenly distributed loads. Since it was thought that the data would be easier to analyse if the load was evenly distributed, the loading was done with uneven load and it resulted in total of 6 steps. In Figure 3.13 it is seen which weights corresponded to which load step and Table 3.1 shows the applied load and pressure for each step.

Table 3.1: *Applied pressure for each load step as it was executed in the field trial.*

Load step	**Applied load** (kN)	**Applied pressure** (kPa)
1	54	12
2	108	24
3	216	48
4	270	60
5	378	84
6	486	108

The field trial with log mats were the first to be performed. The log mats were placed on platform A. Test L was deliberately performed before test F as test L was not expected to lead to failure or large settlements. Test F could therefore be performed on platform A afterwards as well. Before the loading could begin the problem concerning the contact surface of the simulated track against the platform had to be solved. The entire area of the simulated track had to be in contact with the log mat to ensure an uniform pressure such that an applied load could be assumed when analysing the results. This was done, as seen in Figure 3.14a, by using two layers of 2 cm thick plywood boards to fill the cavity between the simulated track and the log mat.

The first weight corresponding to load step 1 could then be placed on the platform. The dial indicator was installed and the loading could further proceed according to plan. Photographs of test L is seen in Figure 3.15 as it is fully loaded.

Next field trial was performed on platform B with the geogrid. For this field trial only one layer of plywood boards was used to get the simulated track in contact with the working platform. This is seen in Figure 3.14b. A photograph of test G is seen in Figure 3.16 as it is fully loaded.

Test F was performed lastly on working platform A with only the granular fill. As seen in Figure 3.14c, for this test two layers of plywood boards had to be used to ensure contact with the platform. A photograph of test F is seen in Figure 3.17 as it is about to be loaded with the first weight of load step 6.

(a) Log mat *(b) Geogrid* *(c) Only fill*

Figure 3.14: *Solution with plywood boards to ensure contact of the simulated track with working platform.*

(a) *(b)*

Figure 3.15: *Photographs of test L as it is fully loaded.*

Figure 3.16: *Photograph of test G as it is fully loaded.*

Figure 3.17: *Photograph of test F as it is about to be loaded with the first weight of step 6.*

4 Finite Element Method

This chapter will present information on numerical models and the methodology of the numerical analysis made to enable comparison with the field trial results.

Plaxis is a finite element program, developed to analyse deformation, stability and groundwater flow in geotechnical engineering by finite element method (Bentley, 2021a). Plaxis 2D is the software package that analyses geotechnical engineering problems in two dimensions. As many geotechnical problems include issues with modeling of structures and the interaction between structures and soils Plaxis are equipped with features to deal with the complex problems.

4.1 Model of field trial in Plaxis

The field trial with the working platform without reinforcement was firstly modeled in Plaxis 2D as a two-dimensional plane strain Finite Element Analysis with 4th order 15-node triangular elements. This was done to enable comparisons and validation of the results from the field trial as well as with results from analytical methods.

The boundaries of the model was set from 0 to 40 on the x-axis and from 0 to -12 on the y-axis. It was set such that the boundaries was sufficiently distant from the working platform. The clay was modelled as a 12 m thick soil layer and the working platform was modeled as a structure with material properties of granular fill. The model was built with the same dimensions as for the field trial as seen in Figure 3.2 and 3.3a but without the log mats. Ground water was not considered in the model, hence the ground water table was set on level -12. The mesh was modeled as a "very fine" mesh which resulted in 3202 elements. The mesh in the platform, as well as for the area in the clay below the working platform, was designed with a refined mesh such that it was concentrated in the highly stressed zone. The Plaxis model with mesh is seen in Figure 4.1.

The Mohr-Coulomb material model with "undrained B" behaviour was used for the clay layer where stiffness is defined using effective input parameters and strength is defined as undrained shear strength. The properties of unit weight (γ) and undrained shear strength (s_u) were set as evaluated from the field measurements. The E'-modulus was set to $3M_0$. All parameters used in the clay layer are seen in Table 4.1. The Mohr-Coulomb model uses a linear elastic perfectly plastic model to approximate soil behaviour. The linear elastic and perfectly plastic part of the model are based on Hooke's law and the Mohr-Coulumb failure criterion respectively (Bentley, 2021b). This model, however, is a simplification of real soil behavior which is neither linear or isotropic.

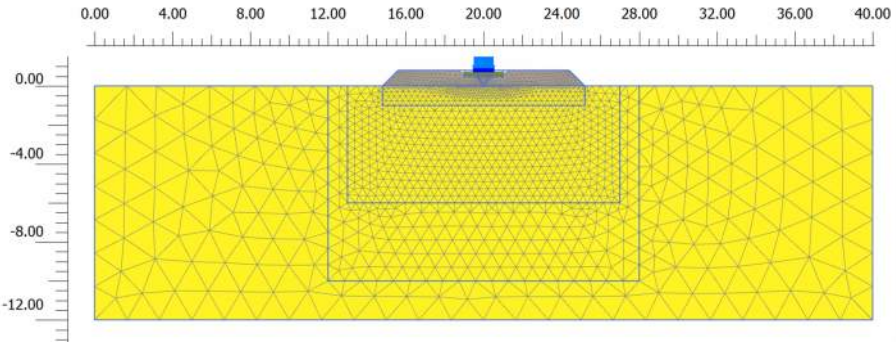

Figure 4.1: *Field trial model created in Plaxis.*

Table 4.1: *Parameters for the clay layer.*

	γ (kN/m^3)	E' (MPa)	v' (-)	$s_{u,ref}$ (kPa)	$s_{u,inc}$ (kPa/m)	K_0 (-)
Clay	16	3	0.3	10	0.5	1

The sand layer in the working platform was neglected in the Plaxis model and the whole platform was simulated as granular fill. The Mohr-Coulomb material model with drained behaviour as effective parameters were used to simulate the soil behaviour of the platform. The unit weight was set in accordance with Trafikverket (2014). The friction angle was originally set in accordance with Trafikverket (2014) but was further varied to better fit the field trial results. All parameters used for the granular fill are seen in Table 4.2.

Table 4.2: *Parameters for the granular fill layer.*

	$\gamma_{unsat}/\gamma_{sat}$ (kPa)	E' (MPa)	v' (-)	c'_{ref} (kPa)	ϕ' (°)	Ψ (°)	k_x=k_y (m/day)	K_0 (-)
Granular fill	18/21	40	0.3	10	40, 45, 50	15	10	0.234

A plate was simulated with stiff material properties to model the concrete weights that was used in the field trial as the simulated track. The material properties used in Plaxis are seen in Table 4.3. An interface was used in-between the plate and fill and was set to 0.67. The load was simulated as a line load on the plate. The load was increased in several construction stages in steps of 12 $kN/m/m$ until the total load of 108 $kN/m/m$ was reached in accordance with the field trial.

Table 4.3: *Parameters for the concrete plate.*

EA_1 (kN/m)	EI $(kN\ m^2/m)$
$7.875{\cdot}10^7$	$1.64{\cdot}10^6$

Numerical models for the reinforced working platforms were created as well. For the working platform reinforced with log mats one plate was modeled with stiffness parameters according to Table 4.4 to simulate the log mats. The plate was modeled with the width of 5.5 m corresponding to the width of the log mats during test L.

Table 4.4: *Parameters for log mat plate.*

EA_1 (kN/m)	EI $(kN\ m^2/m)$
$3.22{\cdot}10^6$	$1.073{\cdot}10^4$

The working platform reinforced with geogrids was not modeled with the geogrid tool that is integrated in Plaxis. Instead the geogrid was modeled with a structure with a material that was created trying to resemble the mechanical stabilisation of the geogrid. This was done by raising the cohesion with 15 kPa in the granular material consequent with the findings in the article by Lees and Matthias (2019). It was further suggested by Lees and Matthias (2019) that the geogrid has an influence area of about 0.15 m above and below where the geogrid is installed. Therefore a layer in the platform of 0.1 m below and 0.15 m above where the geogrid was placed in the field trial was assigned this new material as can bee seen in Figure 4.2.

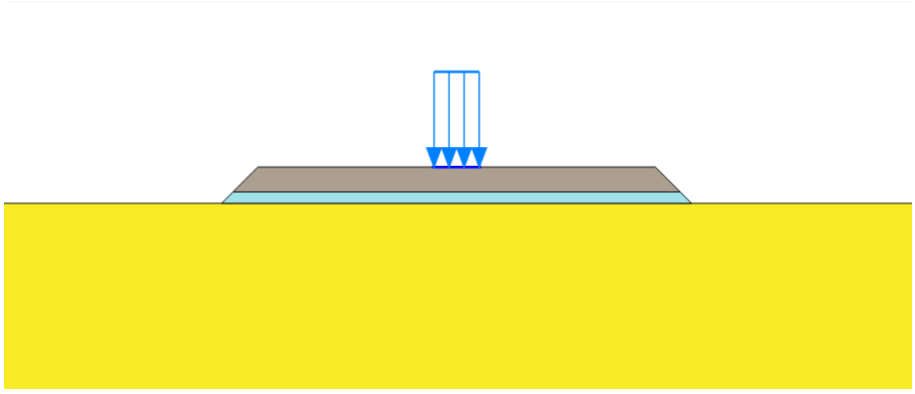

Figure 4.2: *Model of the working platform reinforced with a geogrid.*

5 Results and Discussion

This chapter will present the results retrieved from the load test, field trial and numerical analysis as well as analytical calculations on bearing capacity and load spread angles. A discussion of the results will be provided based on the findings in Chapters 2, 3 and 4.

5.1 Load test

The results from the load test described in Section 3.4.1 is seen in Figure 5.1 for the earth pressure cells in each platforms respectively. What is seen is that the measured total stresses are generally higher in platform A compared to platform B. Furthermore, cell 1 measures highest total stresses and cell 3 measures the lowest total stresses in both working platforms. A small hysteresis effect was noted for all cells as the measured stress was not exactly the same during the unloading as for the the first loading step. During reloading, all cells measured higher stresses compared to the first loading. Finally, it is seen that the behaviour for each cell is very similar in each platform. Cell 1 measures largest differences during loading, unloading and reloading, while cell 3 measures most similar measures when loading, unloading and reloading for both platforms.

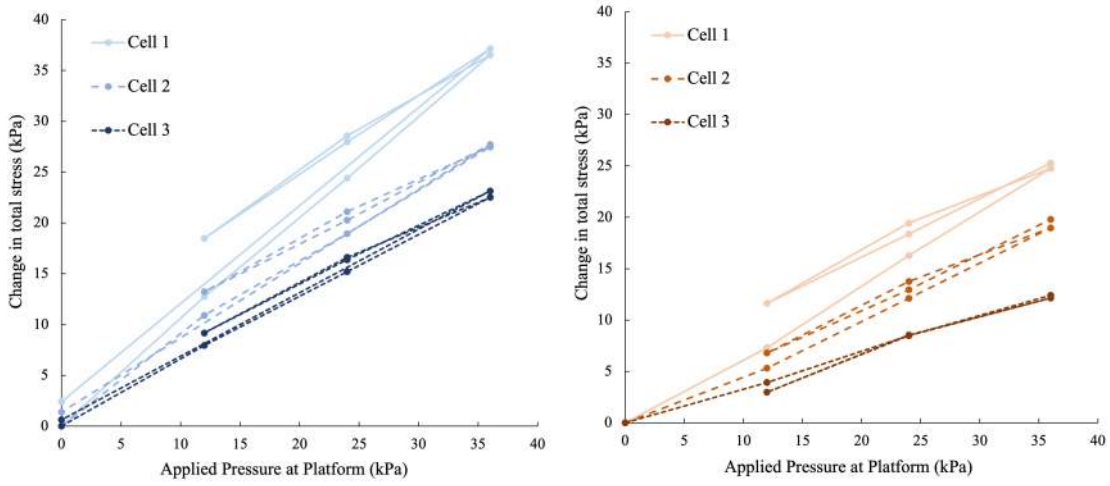

(a) Cells in platform A. *(b) Cells in platform B.*

Figure 5.1: *Results from the load test.*

The test was performed such that equal stresses was expected from all cells in both platforms. According to theory of the Bousinessq method and actual stress distribution, cell 2 was expected to measure a slightly higher stress and cell 1 and 3 was expected to measure the same stress. There are many possible explanation as to why this was not the result. Why the cells in platform B generally measured lower stresses than in platform A can be explained as the result of mechanical stabilisation due to the geogrid as discussed in Section 2.5.3. This would suggest that mechanical stabilisation has occurred and consequently improved the load spread efficiency. Another explanation is that it could also be dependent on the accuracy of the earth pressure cells as it according to the specification is $\pm$5-10 kPa. Finally it could be due to effects from the construction of the two platforms, such as compaction of the granular fill.

The two later explanations, however, do not correlate with the very similar behaviours of the corresponding cells in each platform. Explanations as to why the individual cells in each platform measures different stresses but with similar behaviour in both platforms can be that the weight was centered over cell 2 which made the simulated track closer to the slope (0.5 m) compared to the other side where the distance to the slope was 1.5 m. It is uncertain if and how this could influence the stress distribution under the weight.

After the load test was performed it was found that the simulated track surface was not laying flat against the working platform. This lead to a higher pressure at the ends of the weights as the surface of the weight was not in contact with the platform at the center. This, however, would expect to give results of similar higher stresses in cells 1 and 3 and slightly lower stresses in cell 2. As the results measured do not align with this theory the uncertainties concerning the contact surface of the simulated track do not give an complete explanation of the behaviour seen in Figure 5.1. Hence more uncertainties has to influence the results from the load test.

As the total stresses was taken by a hand device, measures for each cell could not be taken at the same time. Looking at the time readings from the field trial in Appendix E it is seen that for most load steps the first readings are higher, especially for cell 1, and after a few minutes it stabilises and shows lower stresses. The higher stresses recorded in cell 1 could therefore be explained by that the stresses had not yet stabilised by the time of the measurement while the measures for cell 2 and 3 are taken as the stress state have stabilised and are therefore lower. On the other hand, again looking at the time readings for the field trial, this effect is mostly seen in the later load steps. During the load test those loads were not reached and the effect might not have been present and would therefore not be an explanation to the results retrieved from the load test.

Considering the hysteresis effect and the unexpected stresses measured there are too many uncertainties concerning the load test. The results from the load test can therefore not be used to calibrate the earth pressure cells or to normalise the field trial results. However, many uncertainties were found during the load test that may not have been found if the field trial was performed directly. Therefore these results

will still be considered and compared with the field trial results. Finally, the load test gave results that suggested that the earth pressure cells were working and show a behaviour where it increases and decreases linearly to the loading, unloading and reloading.

5.2 Field trial

Results from the field trial are presented in Figure 5.2 where the measured change in total stress against applied pressure at platform for all field trial tests can be seen for each cell. It can clearly be seen that the rate of measured change in total stress decreases for each load step. For cell 1 and 2 stresses as high or even higher than the applied pressure are registered for the first load steps. For all cells, test F has registered the highest stresses and for test G it shows the lowest stresses at cell 1 and 3 but reaches stresses almost as high as for test F at cell 2. Furthermore, the stresses measured in cell 2 surpasses the stresses measured in cell 1 for test G after the third load step. Another effect that can be seen is that the stress paths for test F and L are roughly the same at all cells for the two first load steps but then parts as the rate of stress decreases faster for test L. The original data from the field trial where the measured change in total stress against time is presented in Appendix E.

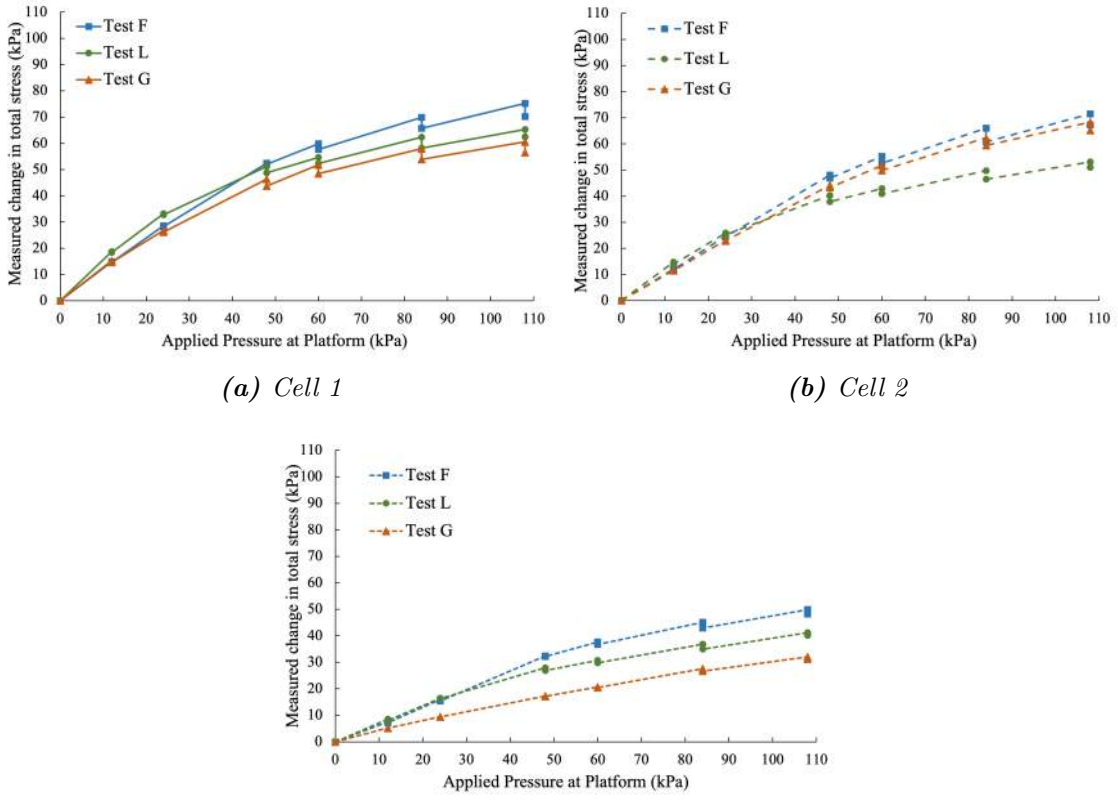

(a) Cell 1

(b) Cell 2

(c) Cell 3

Figure 5.2: *Measured change in total stress from each cell.*

The results show higher change in total stress than the pressure thought to be applied at the platform. This is unexpected. A likely explanation of this is that the earth pressure cells are to stiff and the effect described in Section 2.6.1, where the cell over register the stress has occurred. The same effect could be due to the hysteresis effect shown during the load test. If this is the case, the real change in total stress will most likely be lower than what has been measured by all the cells. Although, the effect of the load spread can still be analysed through these result if not considering the exact value of the stresses.

Another explanation is that the earth pressure cells measured the stress correctly but the applied pressure is much larger than what is thought since it is uncertain if the entire surface of the simulated track were in contact with the platform. This can also be an explanation to why the graph shows that the rate of stress decreases for larger load steps as more of the simulated track comes in contact with the platform for each load step and the pressure does not increase as much for each load step. Therefore, the reliance on the results are higher for the later rather than the earlier load steps.

Test F shows the largest measured change in stress as no reinforcement have helped to distribute the load. As for test L the stresses measured for the lower loading steps are the same as for without reinforcement. This indicates that the log mats did not effectively spread the load for these steps. This aligns with circumstances of the field trial as it was seen that the entire surface of the log mats were not in contact with the platform for these early load steps. The larger the load, the more of the log mat surface was in contact with the platform and could therefore spread the load more efficiently.

The result from test G shows unexpected results. The measured stresses at cell 2 where not expected to surpass those measured by cell 1 according to either the Boussinesq theory or the load spread theory. This can be due to different causes. One cause can be that cell 2 is over-registering due to a larger fraction in contact with the earth pressure cell creating a large point load or that the concrete weight was tilting towards cell 2. Another explanation could be that the earth pressure cell was not laying horizontally for the time of the field trial due to the compaction of the platform during construction. It could also be due to the placement of cell 2 as it lays directly beneath the edge of the simulated track, if punching shear has occurred, as described by Meyerhof (1974), large stresses would have been distributed vertically downward to the cell. Because of the many different explanations it is difficult to say anything about the load spread efficiency of the geogrid.

5.2.1 Strain

The results from the deformation measurement by the crackmeters on test L and G can be seen in Figure 5.3 as strain in the log mat and the geogrid respectively. The strains measured in both cases are very small and shows unexpected behaviour. Especially crackmeters L3 and G4 shows deviating results compared to the others. However, it can be seen that for most crackmeters there is a reaction during loading.

For test L the results are irregular. It can, however, be seen that L2 and L4 is elongated while L1 and L3 is in compression for most of the larger loading steps. This aligns with the placement of the meters on the log mat and the bending moment that would occur in the log mats when loaded in this way. However, the strains are very small and consequently the deformations of the log mats are very small.

For test G all crackmeters show elongation except G4 which is displaying compression. While G1 is showing good alignment with the loading steps the others are showing more discrete results of strain during loading. As G1 is placed closest to the loaded area this could be an explanation to this behaviour.

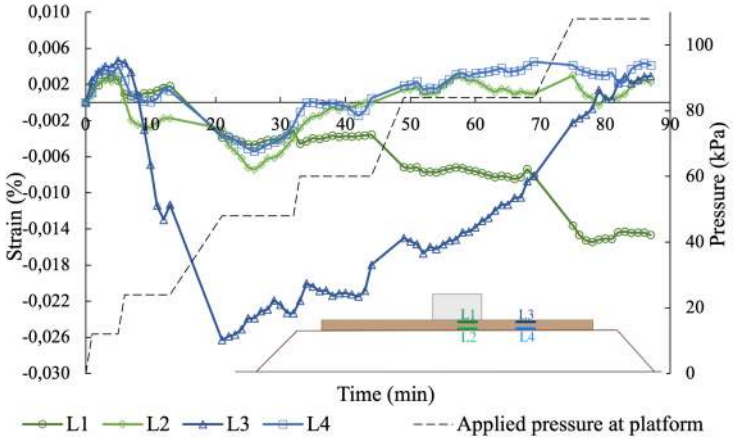

(a) *Crackmeters from the log mat.*

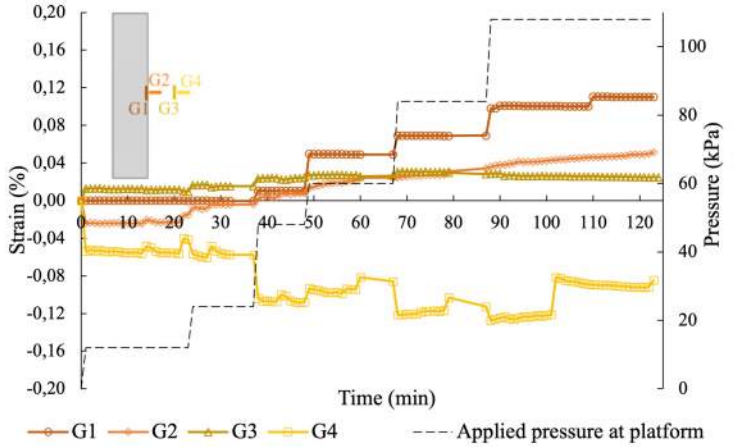

(b) *Crackmeters from the geogrid.*

Figure 5.3: *Results from crackmeters.*

Platform A was not executed such that the log mats entire area could be in contact with the platform. This resulted in the log mats tipping back and forth, which could explain the unexpected results from the early load steps in test L.

For test G it can be seen that the geogrid is strained close to the loaded area. The strains are very small which could suggest that the geogrid is not efficiently

used. However, when comparing the stresses from test F and G in Figure 5.2 it is clear that the geogrid is contributing to lower stresses. This might suggest that the interlocking mechanism of mechanical stabilisation has occurred despite the small strain. Another explanation can be that the crackmeters were interlocked in the fill and thus counteracting strain in the geogrid at the placement of the crackmeters.

As the results, for both the log mat and the geogrid, show lower strains than what could be expected as well as irregular behaviour it is difficult to conclude anything from these results. The uncertainties surrounding the results are too large and too many to be reliable.

5.2.2 Settlements

The results read from the dial indicator on deformation of the platform beneath the load can be seen in Figure 5.4. The result from test F is seen to be very linear while test L show a decreasing rate of settlement after the second load step. This is contrary to test G where the rate of settlement increases after the second load step. In accordance with the results from the earth pressure cells (Figure 5.2), it is seen that test F displays the largest settlements. However, the platform reinforced with geogrid shows the smallest settlements until the last load step where the settlements are smallest for the platform with log mats.

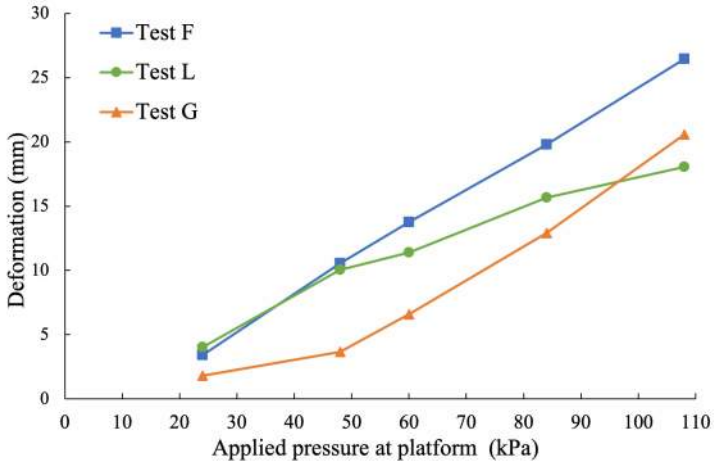

Figure 5.4: *Measured settlement of concrete weight in field trial*

If the settlements would have shown an increasing rate a failure could have been expected. For all test the settlements increased linear with the applied pressure. This is an indication that the platforms are still stable and not approaching failure.

The result of settlement suggests that the log mat spreads the load more efficiently than the geogrid for larger loads. In that case it is complicated to evaluate the most effective solution for a working platform where different conditions apply. Since these results imply that the effective area of the log mats vary during loading it can be hard to estimate the effective area during design of working platforms with log mats.

The settlement results of test G are unexpected as the rate of settlements increases after the second load step. The results in Figure 5.3 shows larger strains after the second load step which could explain the larger rate in settlement. If the mechanism of reinforcement is considered for the geogrid this would suggest that the geogrid is only beginning to activate. Furthermore, the results in Figure 5.1 and 5.2 shows that the geogrid already has an effect on the stress before this load step.

There are some uncertainties concerning the measurement of the settlements. The measurement was taken in the middle along one side of the weight, the settlements on the other side is unknown as the weight might have been tilted one way or the other. A better point to measure the settlements would have been in the middle of the weight directly beneath it. As the concrete weights might have been tilting different ways during the different tests there are large uncertainties concerning these results.

5.2.3 Stress distribution

The results of stress distribution for all field trial tests can be seen in Figure 5.5. The graph shows the horizontal distance from the centre of the platform at a depth of 0.8 m against the change in total stress for the final load step of an applied pressure of 108 kPa. Only the final load step is analysed in this way as it is believed to show the most reliable results, as explained before. It is plotted with the measured change in total stress against the horizontal distance from the centre of the platform, which is the location of cell 1. In the same figure, the stress distribution according to Equation 2.8, the Boussinesq theory, with a strip footing with B=1 m is seen. This is corresponding to the conditions during test F. It is seen that all tests show different stress distributions.

The result of stress distribution from test F shows highest stresses compared to the two other tests. Similar stresses are seen straight under the simulated track and then a decrease of stress from the edge of the simulated track. When comparing the result with the stress distribution with the Boussinesq theory similar behavior is seen as well as a similar inclination of the load spread from the edge of the simulated track. The stress distribution from test L shows a linear decrease of stress distribution from the centre of the platform. The result of stress distribution from test G shows highest stresses in cell 2, which is placed directly below the edge of the simulated track. For cell 1 and 3 it shows the lowest total stress.

Looking at the results of stress distribution from the field trial and comparing them to the Boussineq theory it is seen that significantly higher stresses are measured in the field trial. As this is the the final load step it can be assumed, as discussed, that most of the simulated track surface is in contact with the working platform, and the uncertainties of the actual applied load can be discarded. The Boussinesq theory is based on several assumptions about the soil and does not account for any type of soil parameters. However, it can still be considered as an indication that in the field trial, the earth pressure cells have been to stiff compared to the surrounding soil, and have attracted soil pressure and over-registered stress.

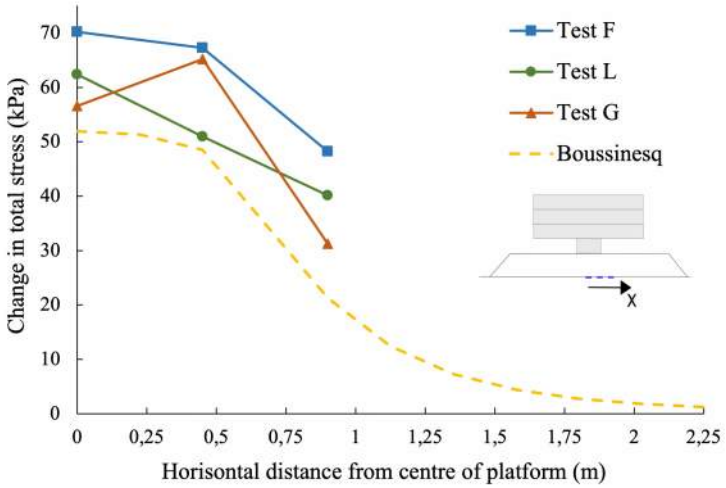

Figure 5.5: *Measured total stress for 108 kPa applied pressure at platform and calculated total stress with Boussinesq.*

As discussed, it is uncertain for test L how much of the surface of the log mat was in contact with the granular platform. Furthermore, it is also unknown how much of the weight surface was in contact with the log mat. This can further give uncertainties about where the load is distributed in relation to the cells. As the granular platform was very uneven the load might not have been distributed evenly. If this is the case it is more difficult to analyse the result and compare it with the other tests as well as with theory. To be able to analyse the behaviour this uncertainty has to be neglected, and so it can be interpreted to spread the load more evenly than the other tests.

The result from test G, as discussed, are the most unexpected received. As very little theories have been found of the stress distribution in a platform with geogrids there are uncertainties in how reliable the measured behavior is. Most theories found about the contribution of geogrid is that of mechanical stabilisation. If it is assumed that this is what have occurred in the field trial it can be considered as a part of the working platform has become stiffer. If it is assumed that cell 2 have over-registered the total stress as discussed, the behaviour of the stress distribution curve can be considered as similar to the Boussinesq theory. Then, comparing test G and F it is seen that lower change in total stress is measured for test G. Hence, with those assumptions it can be concluded that the geogrid has the effect of mechanical stabilisation in the field trial. On the other hand, because of all uncertainties concerning the measurement and as there are little to compare the behaviour of a geogrid with, it could just as likely be that the measured behaviour actually is the stress distribution when influenced by a geogrid.

When the field trial was planned the three earth pressure cells was positioned in the center, by the edge of the simulated track and the third cell with the same center to center distance. It was also assured that a change in stress was to be seen in all three cells according to the 2:1 method for test F. Looking at the result and comparing it

to the Boussinesq theory it can be read that a change in total stress also would have been measured at a horizontal distance further away from the centre of the platform. If assuming that the result from the field trial would continue follow the behaviour of Boussinesq it could be interpolated that test L would distribute a higher stress on a further distance while test G would distribute a lower stress on a shorter distance. However, lower stresses indicate that the platform is further away from soil failure. For further studies, it would be interesting to study the behaviour further from the center of the platform to confirm the stress distribution behavior compared to the Boussinesq theory.

From the result of stress distribution in the field trial it would have been desired to conclude what type of reinforcement is the better in terms of load spread efficiency. Test G converges well with the Bousinessq theory and shows lower stresses in two out of three cells compared to test F and L. But the result for test L shows that the log mats have more equal stress distribution. Hence, it is not possible to say what is the better option.

5.3 Finite element results

The first result from the finite element model in Plaxis is seen in Figure 5.6. It is compared with the field trial result for test F as the platform was fully loaded. The result from Plaxis is with a line load of 108 kPa. A sensitivity analysis was performed to see the influence of the granular fill friction angle. Therefore a case with three different friction angles, 40°, 45° and 50° was simulated. This was done to try and fit the Plaxis results with the field trial results. Since the parameters of the clay where obtained from the ground investigation, only the granular fill parameters were modified, as there were large uncertainties considering the granular fill parameters. Furthermore, the Boussinesq curve with conditions corresponding to test F is plotted for reference. The results from Plaxis shows smaller stresses than what was measured during the field trial. The results from the model aligns very well with the Boussinesq curve.

There are not large differences in stress distribution for the different friction angles. However, from the results of the sensitivity analysis it can be seen that a friction angle off 40° shows best agreement with the behaviour in the field. Therefore in further numerical models this friction angle was used for the granular fill.

The results from the numerical analysis shows good agreement with the behaviour of the field trial result, but it shows magnitude of stress more like that of the Boussinesq theory. Even though the simplifications are many for the Boussinesq theory it aligns very well with the results from the numerical analysis and this could further strengthen the theory that the earth pressure cells have attracted soil pressure. However, because the field trial results fits well with the behaviour modeled in Plaxis and calculated using Boussinesq this can be taken as validation that the field trial result show accurate stress distribution behaviour.

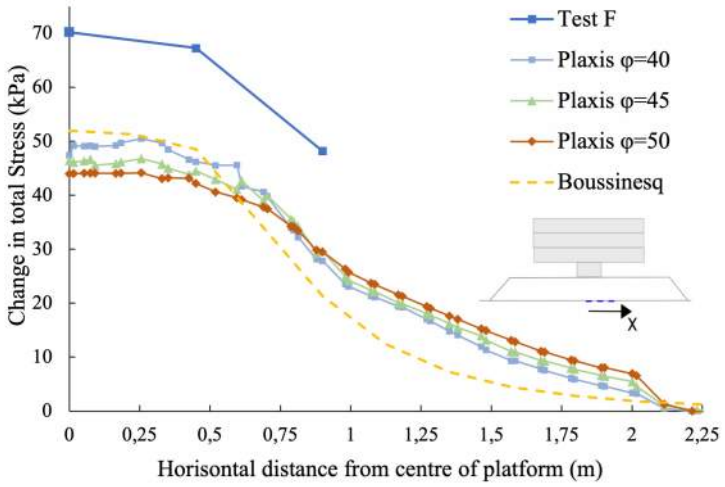

Figure 5.6: *Field trial result for fully loaded working platform compared with results from Plaxis with three different friction angels in the granular fill.*

5.3.1 Numerical model with log mats

The results of the numerical model and field trial results for test L can be seen in Figure 5.7. The stress distribution for the Plaxis model without reinforcements has also been plotted for reference as well as the Boussinesq curve for a plate with a width of 5.5 m. Similar to previous results in Figure 5.5 and 5.6 the measured stress is higher than the numerical analysis or Boussinesq results. However, contrary to the results for the case of only fill the Plaxis result for the platform with log mat does not align as well with the Boussinesq result and shows stresses up to 15 kPa larger.

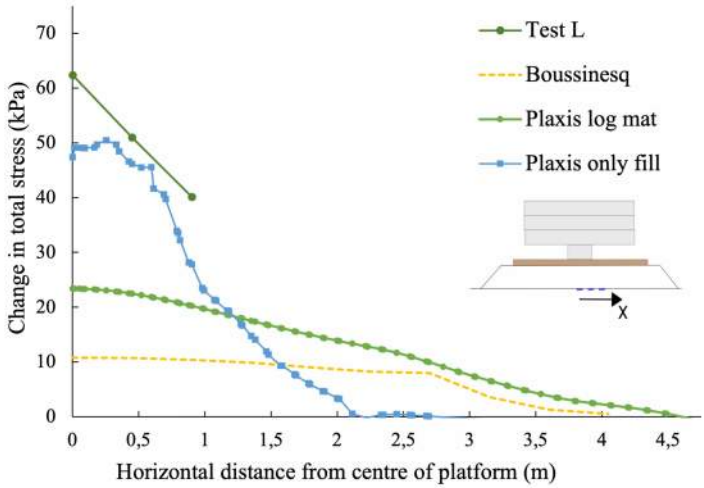

Figure 5.7: *Field trial result for a fully loaded working platform with log mats compared with results from Plaxis with a friction angle of 40°.*

The results from the numerical model differs more for this case than for the model without reinforcements. This can be due to the way the log mat is modeled. In the numerical model, it assumes that the entire area of the log mat is in contact with the granular platform. As discussed, there are uncertainties concerning this and therefore also how much of the log mat that could efficiently spread the load. These results strengthens the suspicion that the effective area of the log mat was a lot smaller than 100 %. As the field trial results from test L show more similar results to the numerical model without reinforcements it suggests that the effective area of the log mat was not much larger that that of the simulated track on the log mat. However, as suggested considering the results in Figure 5.2 the log mat distributes the load more efficiently for higher load steps. Although, if large loads, settlements and deformations are needed for the log mat to efficiently spread the load there might be risks concerning that the load is large enough to cause soil failure before the log mat has been activated. This would be important to keep in mind when designing working platforms with log mats. The effective area of the log mat should be carefully considered and it is of importance that the construction of the granular platform is carefully executed such that the tolerance of irregularities of the surface are achieved to improve the conditions for the log mat to spread the load efficiently over a larger area.

5.3.2 Numerical model with geogrid

The results from the numerical model with geogrid are in Figure 5.8 plotted with the result from the model without reinforcement. The results show a very similar behaviour with the results from the model without reinforcements and does not align as well with the results from the field trial test G.

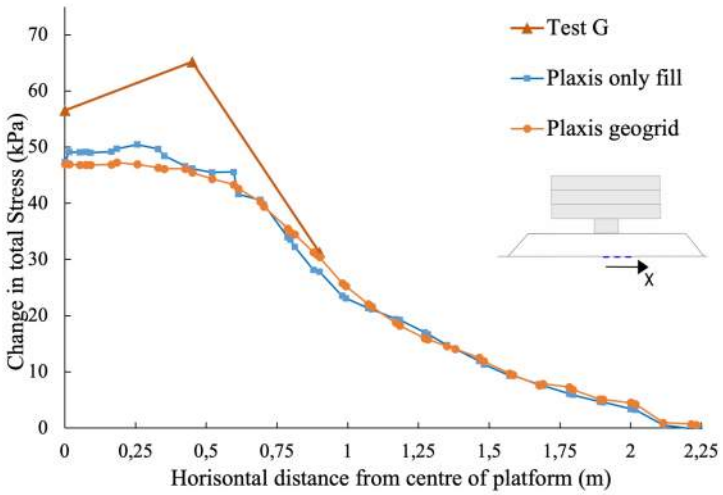

Figure 5.8: *Field trial result for a fully loaded working platform reinforced with geogrid compared with results from Plaxis with a friction angle of 40°.*

The result of the numerical analyse of the working platform with geogrid show very similar results to that of the numerical analyse of the model without reinforcements.

This is probably due to the model as the material parameters are the same as for only fill except for the cohesion. This result would suggest that the geogrid has no influence on the stress distribution, which contradicts the field trial results where test G displays lower stresses than for test F. An explanation to this is that the numerical model needs to be corrected to display lower stresses compared to the case of only fill in accordance with Figure 5.5. It is however, hard to fit the geogrid numerical model to the field trial results as cell 2 is showing unexpected and most likely unreliable results.

5.4 Vertical bearing capacity and load spread angle

As a friction angle of 40° for the fill was found to be the best fit from the Plaxis analysis the vertical bearing capacity for the system of the 0.8 m high working platform of granular fill overlaying the subgrade of clay could be recalculated. It was calculated with the same methods and equations as for the design of the platform, as well as using the graph by Burd and Frydman (1997) in Figure 2.11. With the calculated ultimate bearing capacities for the system the load spread angle could be calculated with Equation 2.24 for each method used. The results for a working platform without reinforcements are presented in Table 5.1. It is seen that the bearing capacity varies between 64 and 163 kPa and that the load spread angle varies between 9 and 54°. However, note that some of the methods for example Meyerhof (1974) and BR470 are not suitable for clay with shear strength lower than 20 kPa and as the clay on the Erikssund site had a shear strength of around 10 kPa this should be kept in mind.

Table 5.1: *Calculated vertical bearing capacity and load spread angle for the unreinforced working platform.*

Method	**Bearing capacity** (kPa)	**Load spread angle** (°)
Tcheng (1957)	63.96	8.67
Meyerhof (1974)	162.58	53.50
BR470	131.40	44.20
BR470+Miller (2013)	113.04	36.83
Burd and Frydman (1997)	90.00	25.13
Plaxis	112.46	36.58

Calculations were also made for the bearing capacity of the working platform with log mats. This was done using the same methods as for only fill, but instead using the dimensions of the log mats. It could be assumed that because of the large stiffness of the log mats, they would evenly distribute the load from the weights over the entire log mat area. Thus resulting in a lower pressure on the granular platform. The ultimate pressure of the weights on the log mats could then be calculated. Further, was the load spread angle calculated with Equation 2.24 with p as the calculated vertical bearing capacity. The results for the case of the working platform with log

mats are presented in Table 5.2. It is seen that the ultimate applied pressure is varying between 276 and 508 kPa and that the load spread angle varies between -20° and 60°.

Table 5.2: *Calculated vertical bearing capacity and load spread angle for the working platform with log mats.*

Method	**Bearing capacity** (kPa)	**Ultimate applied pressure** (kPa)	**Load spread angle** (°)
Tcheng (1957)	45.76	302.01	-20.72
Meyerhof (1974)	59.32	391.54	27.87
BR470	76.98	508.04	59.66
BR470 + Miller (2013)	66.39	438.16	45.03
Plaxis	-	276.13	-

To estimate the bearing capacity of the working platform reinforced with geogrid calculations were performed as well. As the load spread angle was not known for the granular fill the guidance provided by Jewell (1996) could not be used. Instead the method from BR470 with an addition of bearing resistance by the added geogrid was used. The T-method was also used to calculate the bearing capacity. Equation 2.9 was used with the corrected T-value according to Equation 2.28 and 2.29. Further, the load spread angle was calculated with Equation 2.24. The results for the case of the working platform with geogrid are presented in Table 5.3. The bearing capacity is varying between 109 and 481 kPa and the load spread angle is varying between 35° and 79°.

Table 5.3: *Vertical bearing capacity and load spread angle of the working platform reinforced with a geogrid.*

Method	**Bearing capacity** (kPa)	**Load spread angle** (°)
BR470	481.40	79.17
T-method	180.37	57.46
Plaxis	109.18	35.08

All analytical calculations made for the ultimate bearing capacities and load spread angle are seen in Appendix F.

All methods were found to differ a lot in bearing capacity for each working platform. The field trial was not taken to failure hence it can not be used as a validation of the methods.

For the bearing capacity the results for a working platform reinforced with log mats result in the highest possible applied pressure. However, these results are calculated using the assumption that the entire surface of the log mat is in contact with the granular fill as the log mats are considered as a shallow foundation for these calculations. When estimating the effective area of a shallow foundation,

in Equation 2.14, the only considered aspect is where the resulting load is acting. Further, the contact area of the shallow foundation with the platform is not consider when estimating the effective area. As the results from the field trial compared with the numerical results and Boussinesq suggests this is affecting the effective area significantly and therefore the bearing capacity may be overestimated.

As the results vary considerably for the respective situations there are large uncertainties considering the bearing capacity of a working platform. As the field trial is loaded with a pressure of 108 kPa and failure was not reached for any case all methods suggesting an ultimate bearing pressure smaller that that can be discarded. Some methods gives results of bearing capacities close to 108 kPa, these are also unlikely to be true as the results of settlement in Figure 5.4 show no signs of increment in rate.

Plaxis results show larger bearing capacity for a platform without geogrid than with. This is very unlikely to be the case and is most likely due to numerical errors in the program. Even if the geogrid had no effect on the working platform it should not be decreasing the bearing capacity. Furthermore, as seen in the field trial results the geogrid does contribute to a more efficient load spread which would indicate that the bearing capacity would be higher.

The results in Table 5.2 and 5.3 show mostly larger bearing capacities for a working platform reinforced with a log mat compared to a geogrid. However, as the calculations assume a 100 % effective area of the log mats this result can be misleading. Therefore, it cannot be drawn any conclusions which reinforcement contributed to a larger bearing capacity.

The load spread angle in a working platform is widely discussed in found research. Commonly, in purpose of design, the load spread angle it set to 2:1 for the working platforms and for working platforms with geogrid is said to be set to 1:1. With the Equation from Burd and Frydman (1997) it was possible to calculate the load spread angle with bearing capacities calculated by different methods and it is noted that the load spread angle is varying a lot for all three cases of working platforms. As can be seen in the tables the load spread angle is larger than 2:1 for most methods. This means that if the 2:1 method is used for design of a platform, it might lead to an underestimation of the load spread.

6 Conclusion

This study set out to analyze the efficiency of load spread in working platforms reinforced with log mats and with geogrid.

From results of a field test, numerical analyses as well as analytical calculations, the main findings about load spread in a reinforced working platform are that they show lower stresses compared to an unreinforced working platform. However, the results do not show unambiguously which type of reinforcement that spreads the load more efficiently. While the field trial results show that the log mat spread the load more evenly and resulted in lower settlements for the final load step the geogrid show results of lower stresses for 2 out of 3 earth pressure cells compared to the log mat.

The results from analysing a working platform reinforced with log mats further showed that the efficiency of the log mat is connected to the surface in contact with the granular platform. Hence, when designing a working platform with log mats the assumption on the effective area of the log mat is of great importance.

From the results on the geogrid reinforced working platform it could be seen that the behaviour was similar to that of the unreinforced platform. It showed, however, smaller stresses and resulted in smaller settlements. Therefore it could be suggested that the mechanism of mechanical stabilisation has occurred even though no large strains were measured.

Worth noting is that the behaviour for these different working platforms when approaching failure is unknown. The results suggest that the log mat would activate more at larger loads and settlements and as only small strains on the geogrid was measured it might not have been fully activated. Therefore, it is hard to connect the results of stress distributions to the vertical bearing capacity of each platform.

The lack of time and knowledge led to many uncertainties concerning the field trial results. Therefore, a final conclusion that can be drawn from this master's thesis is that detailed planning as well as execution of a field trial greatly affects the quality of the results.

6.1 Further studies

To further learn about the behaviour in working platforms the ultimate vertical bearing capacity should be studied. Research and theories concerning working platforms and shallow foundations usually studies the ultimate bearing capacity as opposed to the load spread efficiency. To enable comparison between results from the field

trial, analytical calculations and numerical models it would be of interest to perform a full scale load test on the working platforms where failure is reached.

The vertical bearing capacity should further be investigated as the behaviour of the geogrid concerning the different mechanisms are not fully investigated. This should be done to study if the load spread efficiency is in direct relation with the bearing capacity.

Finally, as this thesis do not include studies of slope stability for working platforms with different reinforcements this could be further studied to give another dimension to the issue concerning safety of working platforms for tracked plant.

Bibliography

Bentley. (2021a). *PLAXIS General Information Manual* (V22.00 ed.). Plaxis bv, Bentley Systems, Incorporated.

Bentley. (2021b). *PLAXIS Material Models Manual*. Plaxis bv, Bentley Systems, Incorporated.

Bergdahl, U., Ottosson, E., & Stigson Malmborg, B. (1993). *Plattgrundläggning*. Stockholm: AB Svensk Byggtjänst.

Burd, H. J., & Frydman, S. (1997). Bearing capacity of plane-strain footings on layered soils. *Canadian Geotechnical Journal*, *34*, 241–253.

Dobie, M., Lees, A., Buckley, J., & Bhavsar, R. (2019). Working platforms for tracked plant - BR 470 guideline and a revised approach to stabilisation design with multiaxial hexagonal geogrids..

Dobie, M., Lees, A., & Khanardnid, J. (2018). Case study: performance of a geogrid stabilised working platform constructed over extremely soft dredged silt. Seoul, Korea: International Conference on Geosynthetics. Retrieved from `https://www.researchgate.net/publication/327881174`

Dunnicliff, J. (1988). *Geotechnical Instrumentation for Monitoring Field Performance*. Wiley.

GEOKON. (2020). *Model 4420 Series Vibrating Wire Crackmeter.*

GEOKON. (2021). *Model 4800 Series VW Earth Pressure Cells Instruction Manual.* Retrieved from `https://www.geokon.com/content/manuals/4800_Earth_Pressure_Cells.pdf`

Google Maps. (2022). *Site in Erikssund.* Retrieved from `https://www.google.se/maps/@59.6450069,17.6112101,17z/data=!3m1!4b1!4m2!6m1!1s1bw27vahbapH_KgKGrRntB9NpiONz8RUN?hl=en`

Hunt, R. E. (2005). *Geotechnical engineering investigation handbook* (2nd ed.). CRC Press.

Jewell, R. A. (1996). *Soil reinforcement with geotextiles*. London: Construction Industry Research and Information Association.

Knappet, J. A., & Craig, R. F. (1974). *Craig's soil mechanics* (8th ed.). Abingdon: Spon Press.

Lees, A. (2017). Bearing capacity of a stabilised granular layer on clay subgrade. *Bearing Capacity of Roads, Railways and Airfields*, 1135–1142.

Lees, A., & Matthias, P. (2019). Bearing capacity of a geogrid-stabilised granular layer on clay. *Ground engineering*, 28–33.

Markskydd. (n.d.). *Stockmatta trä.* Retrieved from `https://www.markskydd.se/product/timber-bogmats/`

Meyerhof, G. G. (1974). Ultimate Bearing Capacity of Footings on Sand Layer Overlying Clay. *Canadian Geotechnical Journal*, *11*(2), 223–229.

Meyerhof, G. G., & Hanna, A. M. (1978). Ultimate bearing capacity of foundations on layered soils under inclined load. *Canada Geotechnical Journal*, *15*(4),

565–572. Retrieved from https://cdnsciencepub.com/doi/abs/10.1139/t78-060

Miller, K. S. (2013). *Technical Note on Use of BR470 in Soft Clay.* Federation of Piling Specialists. Retrieved from https://www.fps.org.uk/content/uploads/2017/05/Technical_Note_on_Use_of_BR470_in_Soft_Clay.pdf,

Olsson, C., & Holm, G. (1993). *Pålgrundläggning.* Stockholm: AB Svensk Byggtjänst, Statens geotekniska institut.

Rankka, W., Liedberg, S., Rudebeck, D., & Dehlbom, B. (2022). *Säker uppställning av tunga anläggningsmaskiner.* AB Svensk Byggtjänst.

Saha Roy, S., & Deb, K. (2017). Bearing Capacity of Rectangular Footings on Multilayer Geosynthetic-Reinforced Granular Fill over Soft Soil. *International Journal of Geomechanics*, *17*(9).

Sällfors, G. (2013). *Geoteknik* (5th ed.). Göteborg: Cremona.

Swedish Association for Foundation Engineering. (2020). *Säker arbetsplatform - Riktlinjer.* Stockholm. Retrieved from https://www.svenskgrundlaggning.se/wp-content/uploads/2020/09/sg-arbetsplattform-v1-0_200616.pdf

Swedish Standard Insititute. (2007). *Eurocode 7: Geotechnical design Part 2: Ground investigation and testing.* Stockholm.

Swedish Standard Institute. (2018). *Geotechnical investigation and testing – Testing of geotechnical structures –Part 1: Testing of piles: static compression load testing.* Stockholm.

Swedish Standards Institue. (2019). *Geotechnical investigation and testing Laboratory testing of soil Part 10: Direct shear tests.*

Swedish Standards Institute. (2005). *Eurocode 7: Geotechnical design –Part 1: General rules.* Stockholm.

Tcheng, Y. (1957). Fondations superficielles en Milieu Stratifié Proc. *Fourth International Conference Soil mechanics Fondation Engineering*, *1*, 449–452.

Temporary Works forum. (2019). *Working Platforms - Design of granular working platforms for construction plant - A guide to good practice.* London.

Topolnicki, M., Wäger, J., Schweizer, S., Koller, A., Brzozowski, T., & Sołtys, G. (2021). Field test verfification of ground bearing pressure under rig tracks and implications for working platform design. *Ground Engineering*, 26–38. Retrieved from https://www.researchgate.net/publication/350836532

Trafikverket. (2014). *Trafikverkets tekniska krav för geokonstruktioner TK Geo 13.*

A Ground Investigation

A.1 Visual classification from disturbed sample

ELU

FÖRSÖKSRAPPORT FÄLT/ GEOTEKNIK

Sida 2

Uppdragsnamn: **Erikssund**

Uppdragsnummer: 40394

Upprättat av: Christian Ramel

Ort, datum: Stockholm, 2022-02-23

Dokumentnummer:

Provtagningsprotokoll — Störd provtagning

Provtagning utförd enligt SS-EN 1997-2 samt SS-EN 22475-1 /Ver. SGF 2014:1

Uppdragsnummer HJ	Uppdrag KP		Undersökningspunkt HK
40394	Edriksberg		22E101
Positionering/inmätning	❑Mäts i annan ordning ❑Se separat plan ❑Se skiss		Datum KD
Sekt: HH	Sida: HV/HL	Z: HZ	20220216
Borrigg T	Utrustning	Utförande på vatten	Utförd av HQ
505 FM		❑Ja, se separat prot.	BoÅb
Foderrör (m)	Foderrör (ϕ)	Återfyllning (mtrl)	Typ av provtagare
			❑Skr ❑Sp ❑Ps ❑K ❑
Provtagningskategori Ny	Provlängd (m)	Provdiameter (ϕ)	Djup vattenyta i borrhål HG
❑A ❑B ❑C			XXX
Förborrning (m) HO	Neddrivning		Stoppkod
	❑Statisk ❑Dynamisk ❑Rotation ❑		

Protokoll			
Djup, m.u.my D	Fältklassificering av jordart		
start - slut	enligt SS-EN ISO 14688-1	Prov nr	Anmärkning
0 - 0,3	Hu	Ej	
0,3 - 0,9	Cldc sa	1	
0,9 - 1.5	gyCl si_	2	
1.5 - 5	Cl	3	
5 -	Avslut på 5m		
-			
-			
-			
-			
-			
-			
-			
-			
-			
-			
-			
-			
-			
	*Fältklassificering av jordart enligt SS-EN ISO 14688-1		

Avbrott under arbetet, avvikelse från standard, kommentarer, markskada m m K

Filnamn - digitalt provtagningsresultat	GW-rör eller Pp installerat	Se baksida ❑
	❑Se separat protokoll	Blad _ (__)

####

A.2 Field vane test

ELU

FÖRSÖKSRAPPORT FÄLT/ GEOTEKNIK

Sida 4

Uppdragsnamn
Erikssund

Uppdragsnummer
40394

Upprättat av
Christian Ramel

Ort, datum
Stockholm, 2022-02-23

Dokumentnummer

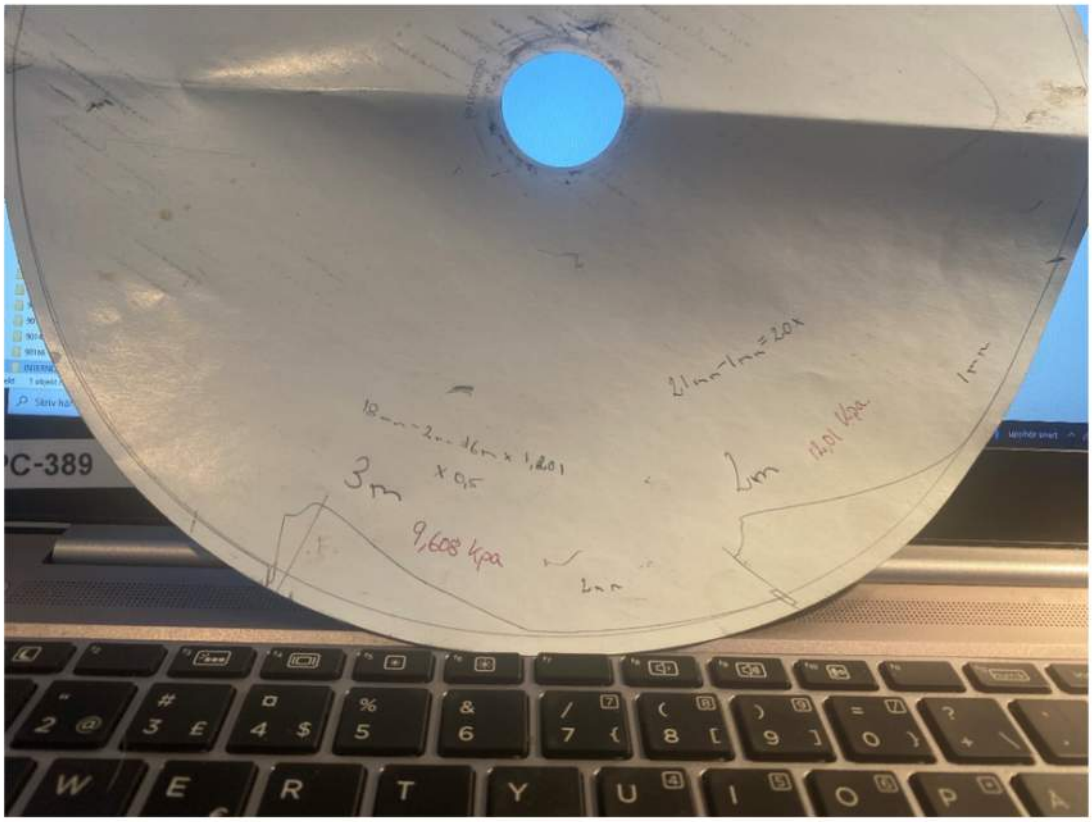

A.3 Cone penetration test

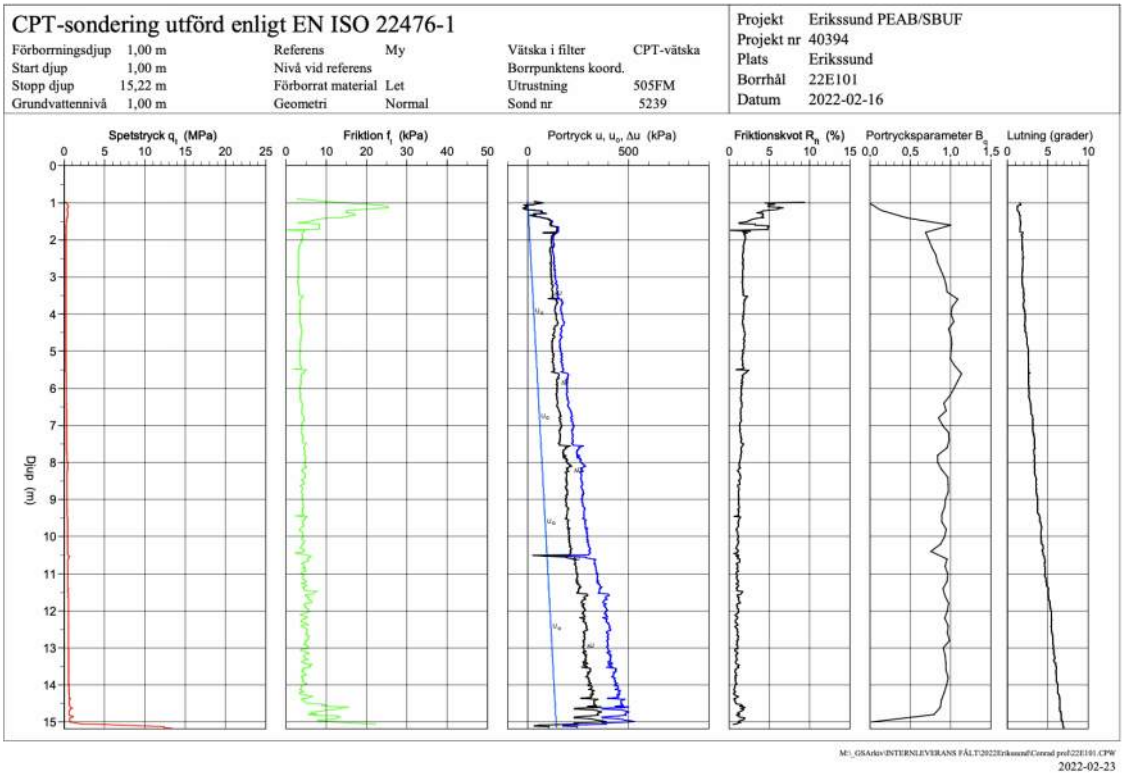

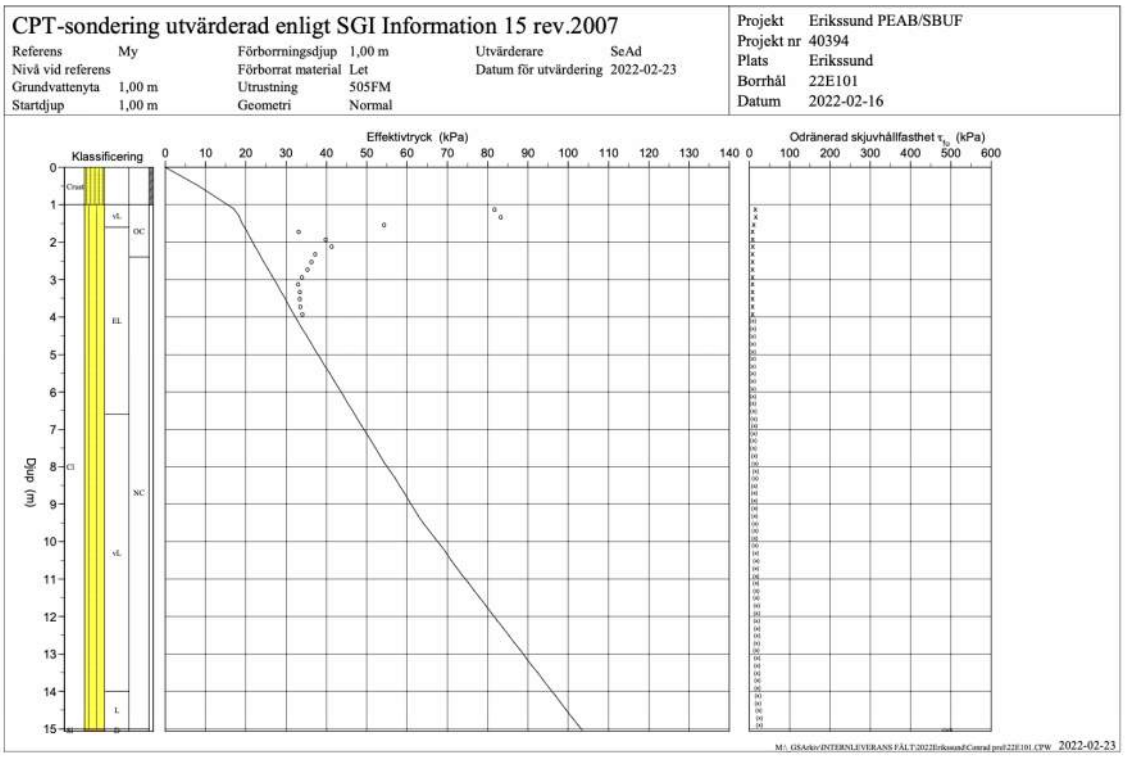

C P T - sondering

Projekt
Erikssund PEAB/SBUF 40394

Plats Erikssund
Borrhål 22E101
Datum 2022-02-16

Förborrningsdjup	1,00 m	Förborrat material	Let
Startdjup	1,00 m	Geometri	Normal
Stoppdjup	15,22 m	Vätska i filter	CPT-vätska
Grundvattenyta	1,00 m	Operatör	Bo Åberg
Referens	My	Utrustning	505FM
Nivå vid referens		[x] Portryck registrerat vid sondering	

Kalibreringsdata

Spets	5239	Inre friktion O_c	0,0 kPa
Datum		Inre friktion O_f	0,0 kPa
Areafaktor a	0,825	Cross talk c_1	0,000
Areafaktor b	0,000	Cross talk c_2	0,000

Nollvärden, kPa

	Portryck	Friktion	Spetstryck
Före	253,30	123,80	2,89
Efter	267,80	123,00	2,90
Diff	14,50	-0,80	0,01

Skalfaktorer

Portryck Område	Faktor	Friktion Område	Faktor	Spetstryck Område	Faktor

[ ] Använd skalfaktorer vid beräkning

Korrigering

Portryck	(ingen)
Friktion	(ingen)
Spetstryck	(ingen)

Bedömd sonderingsklass 2

Portrycksobservationer

Djup (m)	Portryck (kPa)
1,00	0,00

Skiktgränser

Djup (m)

Klassificering

Djup (m) Från	Till	Densitet (ton/m³)	Flytgräns	Jordart
0,00	1,00	1,70		Crust
1,00	2,00	1,52	0,72	
2,00	3,00	1,57	0,61	
3,00	4,00	1,55	0,61	

Anmärkning

M:_GSArkiv\INTERNLEVERANS FÄLT\2022Erikssund\Conrad prel\22E101.CPW

C P T - sondering

Projekt
Erikssund PEAB/SBUF
40394

Plats Erikssund
Borrhål 22E101
Datum 2022-02-16

Djup (m) Från	Till	Klassificering		ρ t/m³	w_L	τ_{fu} kPa	ϕ °	σ_{vo} kPa	σ'_{vo} kPa	σ'_c kPa	OCR	I_D %	E MPa	M_{OC} MPa	M_{NC} MPa
0,00	1,00	Crust		1,70				8,3	8,3						
1,00	1,20	Cl vL	OC	1,52	0,72	15,1		18,0	17,0	81,7	4,82				
1,20	1,40	Cl vL	OC	1,52	0,72	15,6		21,2	18,2	83,3	4,57				
1,40	1,60	Cl vL	OC	1,52	0,72	11,2		24,1	19,1	54,3	2,85				
1,60	1,80	Cl EL	OC	1,52	0,72	7,6		27,2	20,2	33,1	1,64				
1,80	2,00	Cl EL	OC	1,52	0,72	8,9		30,2	21,2	39,7	1,88				
2,00	2,20	Cl EL	OC	1,57	0,61	8,6		33,2	22,2	41,3	1,86				
2,20	2,40	Cl EL	OC	1,57	0,61	7,9		36,2	23,2	37,1	1,60				
2,40	2,60	Cl EL	NC	1,57	0,61	7,9		39,3	24,3	36,3	1,49				
2,60	2,80	Cl EL	NC	1,57	0,61	7,8		42,4	25,4	35,2	1,39				
2,80	3,00	Cl EL	NC	1,57	0,61	7,6		45,5	26,5	33,9	1,28				
3,00	3,20	Cl EL	NC	1,55	0,61	7,5		48,6	27,6	33,0	1,20				
3,20	3,40	Cl EL	NC	1,55	0,61	7,6		51,6	28,6	33,3	1,17				
3,40	3,60	Cl EL	NC	1,55	0,61	7,7		54,6	29,6	33,4	1,13				
3,60	3,80	Cl EL	NC	1,55	0,61	7,7		57,7	30,7	33,5	1,09				
3,80	4,00	Cl EL	NC	1,55	0,61	7,9		60,7	31,7	34,0	1,07				
4,00	4,20	Cl EL	NC	1,60		(8,6)		63,8	32,8		1,00				
4,20	4,40	Cl EL	NC	1,60		(8,6)		66,9	33,9		1,00				
4,40	4,60	Cl EL	NC	1,60		(8,1)		70,0	35,0		1,00				
4,60	4,80	Cl EL	NC	1,60		(7,5)		73,2	36,2		1,00				
4,80	5,00	Cl EL	NC	1,60		(7,3)		76,3	37,3		1,00				
5,00	5,20	Cl EL	NC	1,60		(7,8)		79,5	38,5		1,00				
5,20	5,40	Cl EL	NC	1,60		(7,8)		82,6	39,6		1,00				
5,40	5,60	Cl EL	NC	1,60		(7,6)		85,7	40,7		1,00				
5,60	5,80	Cl EL	NC	1,60		(8,2)		88,9	41,9		1,00				
5,80	6,00	Cl EL	NC	1,60		(8,2)		92,0	43,0		1,00				
6,00	6,20	Cl EL	NC	1,60		(8,4)		95,2	44,2		1,00				
6,20	6,40	Cl EL	NC	1,60		(9,0)		98,3	45,3		1,00				
6,40	6,60	Cl EL	NC	1,60		(9,9)		101,4	46,4		1,00				
6,60	6,80	Cl vL	NC	1,60		(10,4)		104,6	47,6		1,00				
6,80	7,00	Cl vL	NC	1,60		(11,7)		107,7	48,7		1,00				
7,00	7,20	Cl vL	NC	1,60		(10,9)		110,9	49,9		1,00				
7,20	7,40	Cl vL	NC	1,60		(10,1)		114,0	51,0		1,00				
7,40	7,60	Cl vL	NC	1,60		(10,1)		117,1	52,1		1,00				
7,60	7,80	Cl vL	NC	1,60		(11,4)		120,3	53,3		1,00				
7,80	8,00	Cl vL	NC	1,60		(13,8)		123,4	54,4		1,00				
8,00	8,20	Cl vL	NC	1,75		(14,8)		126,7	55,7		1,00				
8,20	8,40	Cl vL	NC	1,60		(13,3)		130,0	57,0		1,00				
8,40	8,60	Cl vL	NC	1,60		(12,1)		133,1	58,1		1,00				
8,60	8,80	Cl vL	NC	1,60		(12,1)		136,3	59,3		1,00				
8,80	9,00	Cl vL	NC	1,60		(12,2)		139,4	60,4		1,00				
9,00	9,20	Cl vL	NC	1,60		(12,5)		142,5	61,5		1,00				
9,20	9,40	Cl vL	NC	1,60		(13,0)		145,7	62,7		1,00				
9,40	9,60	Cl vL	NC	1,75		(13,4)		149,0	64,0		1,00				
9,60	9,80	Cl vL	NC	1,75		(13,6)		152,4	65,4		1,00				
9,80	10,00	Cl vL	NC	1,75		(13,2)		155,8	66,8		1,00				
10,00	10,20	Cl vL	NC	1,75		(13,7)		159,3	68,3		1,00				
10,20	10,40	Cl vL	NC	1,75		(14,9)		162,7	69,7		1,00				
10,40	10,60	Cl vL	NC	1,60		(16,8)		166,0	71,0		1,00				
10,60	10,80	Cl vL	NC	1,75		(15,2)		169,3	72,3		1,00				
10,80	11,00	Cl vL	NC	1,75		(15,8)		172,7	73,7		1,00				
11,00	11,20	Cl vL	NC	1,75		(15,5)		176,1	75,1		1,00				
11,20	11,40	Cl vL	NC	1,75		(16,3)		179,6	76,6		1,00				
11,40	11,60	Cl vL	NC	1,75		(16,9)		183,0	78,0		1,00				
11,60	11,80	Cl vL	NC	1,75		(18,1)		186,4	79,4		1,00				
11,80	12,00	Cl vL	NC	1,75		(17,5)		189,9	80,9		1,00				
12,00	12,20	Cl vL	NC	1,75		(17,7)		193,3	82,3		1,00				
12,20	12,40	Cl vL	NC	1,75		(18,6)		196,7	83,7		1,00				
12,40	12,60	Cl vL	NC	1,75		(18,4)		200,2	85,2		1,00				
12,60	12,80	Cl vL	NC	1,75		(18,0)		203,6	86,6		1,00				
12,80	13,00	Cl vL	NC	1,75		(17,2)		207,0	88,0		1,00				
13,00	13,20	Cl vL	NC	1,75		(18,9)		210,5	89,5		1,00				
13,20	13,40	Cl vL	NC	1,75		(19,0)		213,9	90,9		1,00				
13,40	13,60	Cl vL	NC	1,75		(19,2)		217,3	92,3		1,00				
13,60	13,80	Cl vL	NC	1,75		(19,5)		220,8	93,8		1,00				
13,80	14,00	Cl vL	NC	1,75		(19,3)		224,2	95,2		1,00				
14,00	14,20	Cl L	NC	1,75		(20,5)		227,6	96,6		1,00				
14,20	14,40	Cl L	NC	1,75		(21,2)		231,1	98,1		1,00				
14,40	14,60	Cl L	NC	1,75		(22,9)		234,5	99,5		1,00				
14,60	14,80	Cl L	NC	1,75		(24,6)		237,9	100,9		1,00				
14,80	15,00	Cl L	NC	1,75		(24,9)		241,4	102,4		1,00				
15,00	15,07	Si D		1,95		((490,7))	(36,0)	243,8	103,4				27,5	36,8	29,4

M:_GSArkiv\INTERNLEVERANS FÄLT\2022Erikssund\Conrad prel\22E101.CPW

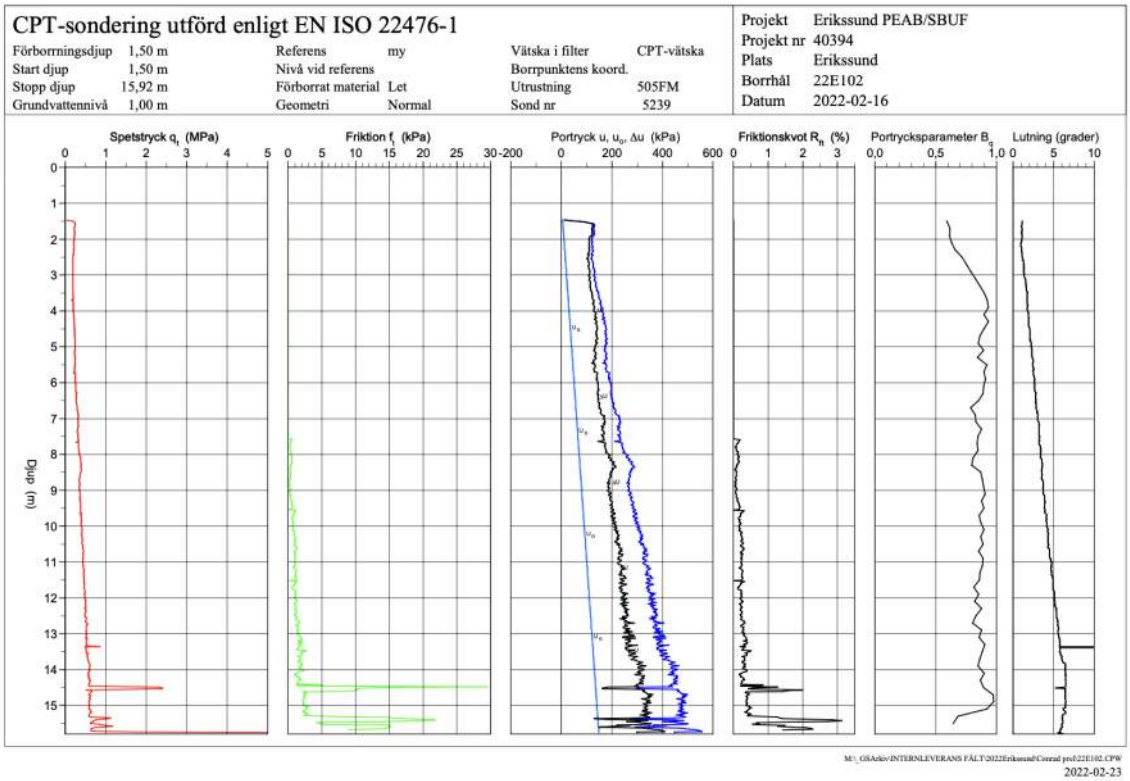
CPT-sondering utförd enligt EN ISO 22476-1
Förborrningsdjup 1,50 m
Start djup 1,50 m
Stopp djup 15,92 m
Grundvattennivå 1,00 m
Referens my
Nivå vid referens
Förborrat material Let
Geometri Normal
Vätska i filter CPT-vätska
Borrpunktens koord.
Utrustning 505FM
Sond nr 5239
Projekt Erikssund PEAB/SBUF
Projekt nr 40394
Plats Erikssund
Borrhål 22E102
Datum 2022-02-16
Spetstryck q_t (MPa)
Friktion f_t (kPa)
Portryck u, u_0, Δu (kPa)
Friktionskvot R_f (%)
Portryckparameter B_q
Lutning (grader)
Djup (m)
2022-02-23

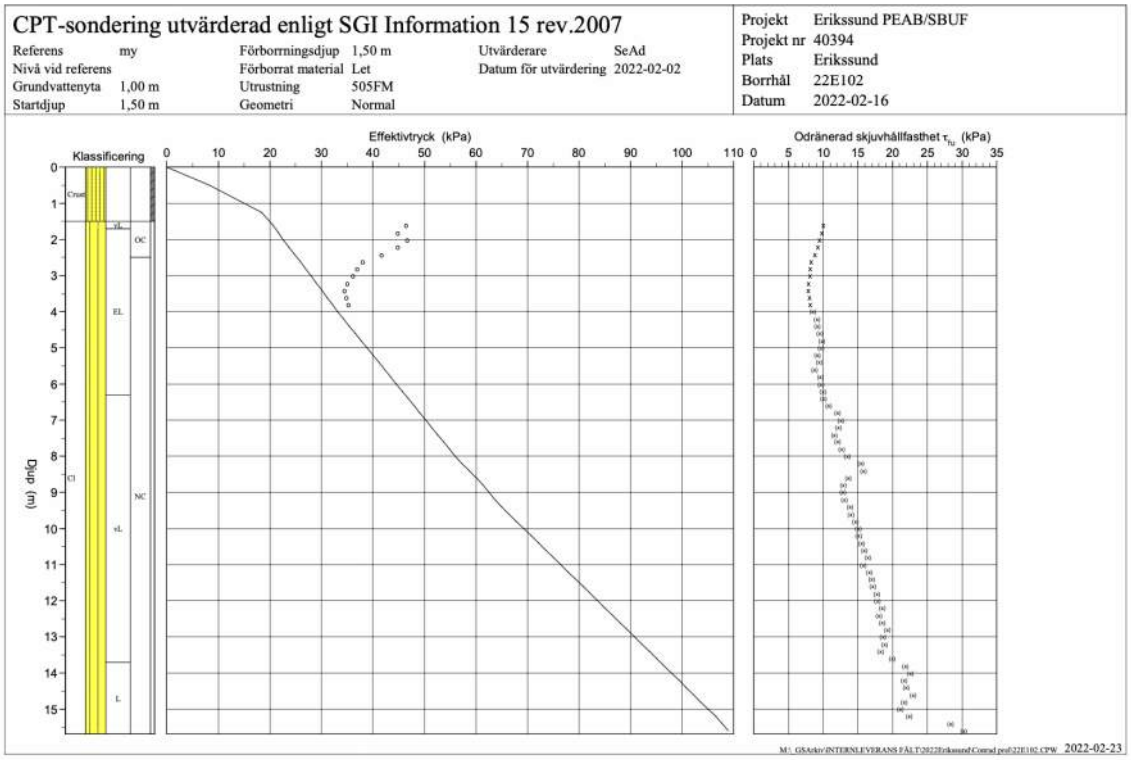
CPT-sondering utvärderad enligt SGI Information 15 rev.2007
Referens my
Nivå vid referens
Grundvattenyta 1,00 m
Startdjup 1,50 m
Förborrningsdjup 1,50 m
Förborrat material Let
Utrustning 505FM
Geometri Normal
Utvärderare SeAd
Datum för utvärdering 2022-02-02
Projekt Erikssund PEAB/SBUF
Projekt nr 40394
Plats Erikssund
Borrhål 22E102
Datum 2022-02-16
Klassificering
Effektivtryck (kPa)
Odränerad skjuvhållfasthet τ_fu (kPa)
Djup (m)
2022-02-23

C P T - sondering

Projekt
Erikssund PEAB/SBUF 40394

Plats Erikssund
Borrhål 22E102
Datum 2022-02-16

Förborrningsdjup	1,50 m	Förborrat material	Let
Startdjup	1,50 m	Geometri	Normal
Stoppdjup	15,92 m	Vätska i filter	CPT-vätska
Grundvattenyta	1,00 m	Operatör	Bo Åberg
Referens	my	Utrustning	505FM
Nivå vid referens		[x] Portryck registrerat vid sondering	

Kalibreringsdata

Spets	5239	Inre friktion O_c	0,0 kPa
Datum		Inre friktion O_f	0,0 kPa
Areafaktor a	0,825	Cross talk c_1	0,000
Areafaktor b	0,000	Cross talk c_2	0,000

Nollvärden, kPa

	Portryck	Friktion	Spetstryck
Före	253,20	123,10	2,90
Efter	252,70	123,10	2,91
Diff	-0,50	0,00	0,01

Skalfaktorer

Portryck Område	Faktor	Friktion Område	Faktor	Spetstryck Område	Faktor

[ ] Använd skalfaktorer vid beräkning

Korrigering

Portryck	(ingen)
Friktion	(ingen)
Spetstryck	(ingen)

Bedömd sonderingsklass 1

Portrycksobservationer

Djup (m)	Portryck (kPa)
1,00	0,00

Skiktgränser

Djup (m)

Klassificering

Djup (m) Från	Till	Densitet (ton/m^3)	Flytgräns	Jordart
0,00	1,50	1,70		Crust
1,50	2,00	1,52	0,72	
2,00	3,00	1,57	0,61	
3,00	4,00	1,55	0,61	

Anmärkning

M:_GSArkiv\INTERNLEVERANS FÄLT\2022Erikssund\Conrad prel\22E102.CPW

C P T - sondering

Projekt
Erikssund PEAB/SBUF
40394

Plats **Erikssund**
Borrhål **22E102**
Datum **2022-02-16**

Djup (m) Från	Till	Klassificering		ρ t/m³	w_L	τ_{fu} kPa	ϕ °	σ_{vo} kPa	σ'_{vo} kPa	σ'_c kPa	OCR	I_D %	E MPa	M_{OC} MPa	M_{NC} MPa
0,00	1,00	Crust		1,70				8,3	8,3						
1,00	1,50	Crust		1,70				20,8	18,3						
1,50	1,70	Cl vL	OC	1,52	0,72	10,0		26,6	20,6	46,4	2,26				
1,70	1,90	Cl EL	OC	1,52	0,72	9,8		29,6	21,6	44,9	2,08				
1,90	2,10	Cl EL	OC	1,57	0,61	9,5		32,5	22,5	46,7	2,07				
2,10	2,30	Cl EL	OC	1,57	0,61	9,3		35,6	23,6	44,9	1,90				
2,30	2,50	Cl EL	OC	1,57	0,61	8,8		38,7	24,7	41,6	1,68				
2,50	2,70	Cl EL	NC	1,57	0,61	8,3		41,8	25,8	38,0	1,47				
2,70	2,90	Cl EL	NC	1,57	0,61	8,1		44,9	26,9	36,9	1,37				
2,90	3,10	Cl EL	NC	1,55	0,61	8,1		48,0	28,0	36,1	1,29				
3,10	3,30	Cl EL	NC	1,55	0,61	7,9		51,0	29,0	35,0	1,21				
3,30	3,50	Cl EL	NC	1,55	0,61	7,9		54,0	30,0	34,5	1,15				
3,50	3,70	Cl EL	NC	1,55	0,61	8,0		57,1	31,1	34,8	1,12				
3,70	3,90	Cl EL	NC	1,55	0,61	8,1		60,1	32,1	35,3	1,10				
3,90	4,10	Cl EL	NC	1,60		(8,5)		63,2	33,2		1,00				
4,10	4,30	Cl EL	NC	1,60		(9,1)		66,3	34,3		1,00				
4,30	4,50	Cl EL	NC	1,60		(9,2)		69,4	35,4		1,00				
4,50	4,70	Cl EL	NC	1,60		(9,5)		72,6	36,6		1,00				
4,70	4,90	Cl EL	NC	1,60		(9,8)		75,7	37,7		1,00				
4,90	5,10	Cl EL	NC	1,60		(9,7)		78,9	38,9		1,00				
5,10	5,30	Cl EL	NC	1,60		(9,2)		82,0	40,0		1,00				
5,30	5,50	Cl EL	NC	1,60		(9,4)		85,1	41,1		1,00				
5,50	5,70	Cl EL	NC	1,60		(8,7)		88,3	42,3		1,00				
5,70	5,90	Cl EL	NC	1,60		(9,6)		91,4	43,4		1,00				
5,90	6,10	Cl EL	NC	1,60		(9,7)		94,5	44,5		1,00				
6,10	6,30	Cl EL	NC	1,60		(9,9)		97,7	45,7		1,00				
6,30	6,50	Cl vL	NC	1,60		(10,0)		100,8	46,8		1,00				
6,50	6,70	Cl vL	NC	1,60		(10,8)		104,0	48,0		1,00				
6,70	6,90	Cl vL	NC	1,60		(12,1)		107,1	49,1		1,00				
6,90	7,10	Cl vL	NC	1,60		(12,5)		110,2	50,2		1,00				
7,10	7,30	Cl vL	NC	1,60		(12,2)		113,4	51,4		1,00				
7,30	7,50	Cl vL	NC	1,60		(11,6)		116,5	52,5		1,00				
7,50	7,70	Cl vL	NC	1,60		(12,1)		119,7	53,7		1,00				
7,70	7,90	Cl vL	NC	1,60		(12,6)		122,8	54,8		1,00				
7,90	8,10	Cl vL	NC	1,60		(13,5)		125,9	55,9		1,00				
8,10	8,30	Cl vL	NC	1,75		(15,4)		129,2	57,2		1,00				
8,30	8,50	Cl vL	NC	1,75		(15,8)		132,7	58,7		1,00				
8,50	8,70	Cl vL	NC	1,75		(13,6)		136,1	60,1		1,00				
8,70	8,90	Cl vL	NC	1,60		(12,9)		139,4	61,4		1,00				
8,90	9,10	Cl vL	NC	1,60		(12,8)		142,5	62,5		1,00				
9,10	9,30	Cl vL	NC	1,60		(13,1)		145,7	63,7		1,00				
9,30	9,50	Cl vL	NC	1,75		(13,8)		148,9	64,9		1,00				
9,50	9,70	Cl vL	NC	1,75		(14,0)		152,4	66,4		1,00				
9,70	9,90	Cl vL	NC	1,75		(14,6)		155,8	67,8		1,00				
9,90	10,10	Cl vL	NC	1,75		(15,0)		159,2	69,2		1,00				
10,10	10,30	Cl vL	NC	1,75		(15,1)		162,7	70,7		1,00				
10,30	10,50	Cl vL	NC	1,75		(15,5)		166,1	72,1		1,00				
10,50	10,70	Cl vL	NC	1,75		(15,9)		169,5	73,5		1,00				
10,70	10,90	Cl vL	NC	1,75		(16,4)		173,0	75,0		1,00				
10,90	11,10	Cl vL	NC	1,75		(15,7)		176,4	76,4		1,00				
11,10	11,30	Cl vL	NC	1,75		(16,6)		179,8	77,8		1,00				
11,30	11,50	Cl vL	NC	1,75		(16,9)		183,3	79,3		1,00				
11,50	11,70	Cl vL	NC	1,75		(17,1)		186,7	80,7		1,00				
11,70	11,90	Cl vL	NC	1,75		(17,7)		190,1	82,1		1,00				
11,90	12,10	Cl vL	NC	1,75		(17,8)		193,6	83,6		1,00				
12,10	12,30	Cl vL	NC	1,75		(18,5)		197,0	85,0		1,00				
12,30	12,50	Cl vL	NC	1,75		(18,0)		200,4	86,4		1,00				
12,50	12,70	Cl vL	NC	1,75		(18,5)		203,9	87,9		1,00				
12,70	12,90	Cl vL	NC	1,75		(19,2)		207,3	89,3		1,00				
12,90	13,10	Cl vL	NC	1,75		(18,6)		210,7	90,7		1,00				
13,10	13,30	Cl vL	NC	1,75		(18,8)		214,2	92,2		1,00				
13,30	13,50	Cl vL	NC	1,75		(18,3)		217,6	93,6		1,00				
13,50	13,70	Cl vL	NC	1,75		(19,9)		221,0	95,0		1,00				
13,70	13,90	Cl L	NC	1,75		(21,8)		224,5	96,5		1,00				
13,90	14,10	Cl L	NC	1,75		(22,6)		227,9	97,9		1,00				
14,10	14,30	Cl L	NC	1,75		(21,6)		231,3	99,3		1,00				
14,30	14,50	Cl L	NC	1,75		(21,9)		234,8	100,8		1,00				
14,50	14,70	Cl L	NC	1,75		(22,9)		238,2	102,2		1,00				
14,70	14,90	Cl L	NC	1,75		(21,6)		241,6	103,6		1,00				
14,90	15,10	Cl L	NC	1,75		(21,1)		245,1	105,1		1,00				
15,10	15,30	Cl L	NC	1,75		(22,4)		248,5	106,5		1,00				
15,30	15,50	Cl L	NC	1,60		(28,3)		251,8	107,8		1,00				
15,50	15,69	Cl L	NC	1,60		(30,3)		254,9	108,9		1,00				

M:_GSArkiv\INTERNLEVERANS FÄLT\2022Erikssund\Conrad prel\22E102.CPW

A.4 General tests

SAMMANSTÄLLNING AV

GEOTEKNISKA LABORATORIEUNDERSÖKNINGAR

Uppdrag	Erikssund
Kund	PEAB Anläggning AB

PROVTAGNING

Utrustning	Kv StII Ø 50 mm
Provtagning	2022-02-16
Prover inkom	2022-02-17
Anmärkning	-

PROVNING

Utförd	2022-02-18 / AS
Granskad	2022-02-21 / PY
Provt. till provn.	2 dygn
Provförvaring	Klimatrum ca 7°C (3 månader)

PROVRESULTAT

Punkt	Djup	Jordartsbenämning	ρ t/m³	w_N %	w_L %	$c_{u,okorr}$ okorr. kPa	c_u korr. kPa	c_{ur} omr. kPa	S_t -	Anm.
22E102	1,5	Grå sulfidfläckig LERA med delar av gyttja. Cl (gy) (su).	(1,54) 1,51 1,52	88 90 91	72	15	12	0,65	23	1)
	2,5	Grå sulfidfläckig LERA. Cl (su).	(1,58) 1,57 1,58	76 72 78	61	11	9,3	0,57	19	2)
	3,5	Grå sulfidfläckig varvig LERA. vCl (su).	1,58 1,57 1,54	78 75 75	61	12	9,9	0,62	19	

För teckenförklaring, information om standarder, utvärdering av skjuvhållfasthet m m, se www.labmind.se/metoder.

ANMÄRKNINGAR

Rutinanalys utförd på övertub, enligt överenskommelse med kund.
1) Tomrum, ca 25 mm, i övertub.
2) Tomrum, ca 10 mm, samt prov insjunket från kanterna ca från ca 10 till ca 25 mm i övertub.

FOTOREDOVISNING

Scanna eller klicka på QR-koden:

A.5 Oedometer CRS

SAMMANSTÄLLNING AV

ÖDOMETERFÖRSÖK, TYP CRS

LAB MIND

Uppdrag	Erikssund
Kund	PEAB Anläggning AB

ALLM.

Utrustning	Kv Stll, Ø 50 mm
Provt. till provn.	7 dygn

PROVRESULTAT

Punkt	Djup	ρ	w_N	Jordart	σ_c'	M_L	σ_L'	M'	k_i	β_k	c_u / σ_c'	$\varepsilon_{0,85\sigma c'}$	Anm.
		t/m³	%		kPa	kPa	kPa	-	m/s	-	-	%	
22E102	1,5	1,49	91	Cl (gy) (su)	28	295	54	11,0	8,1E-10	3,5	0,43	3,0	1)
	2,5	1,58	78	Cl (su)	21	260	40	13,5	1,3E-09	3,9	0,44	1,7	1)
	3,5	1,52	83	vCl (su)	34	270	53	12,0	1,8E-09	4,4	0,29	3,1	1)

För teckenförklaring, information om standarder, utvärdering m m, se www.labmind.se/metoder.

ANMÄRKNINGAR

1) Avvikande empirisk korrelation.

EMPIRI OCH PROVKVALITET

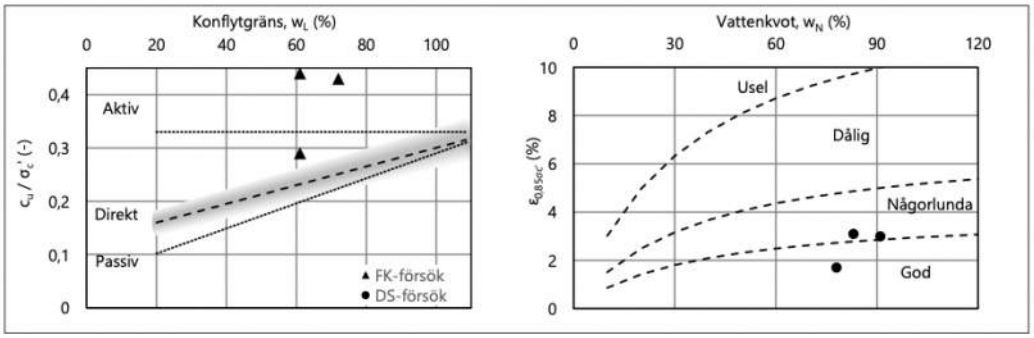

REDOVISNING AV

ÖDOMETERFÖRSÖK, TYP CRS

Uppdrag	Erikssund	**Punkt**	22E102
Kund	PEAB Anläggning AB	**Djup**	1,5 m

ALLMÄNT

CRS-försök			Från rutinanalys		
Jordart	Cl (gy) (su)		**Jordart**	Cl (gy) (su)	
w_N	91	%	w_N	89	%
ρ	1,49	t/m^3	ρ	1,52	t/m^3

PROVNING

Utfört	2022-02-23 / AS
Granskat	2022-02-25 / DG
Provt. till försök	7 dygn
Prov	Kv Stll Ø50 mm

UTVÄRDERING

σ_c'	M_L	σ_L'	M'	k_i	β_k	$k_{ini\ (0,85\sigma c')}$	$\varepsilon_{0,85\sigma c'}$	c_u / σ_c'	M_i/M_L
28	295	54	11,0	8,1E-10	3,5	0,020	3,0	0,43	2,7
kPa	kPa	kPa	-	m/s	-	m/år	%	-	-

Avvikande empirisk korrelation.

REDOVISNING AV FÖRSÖK

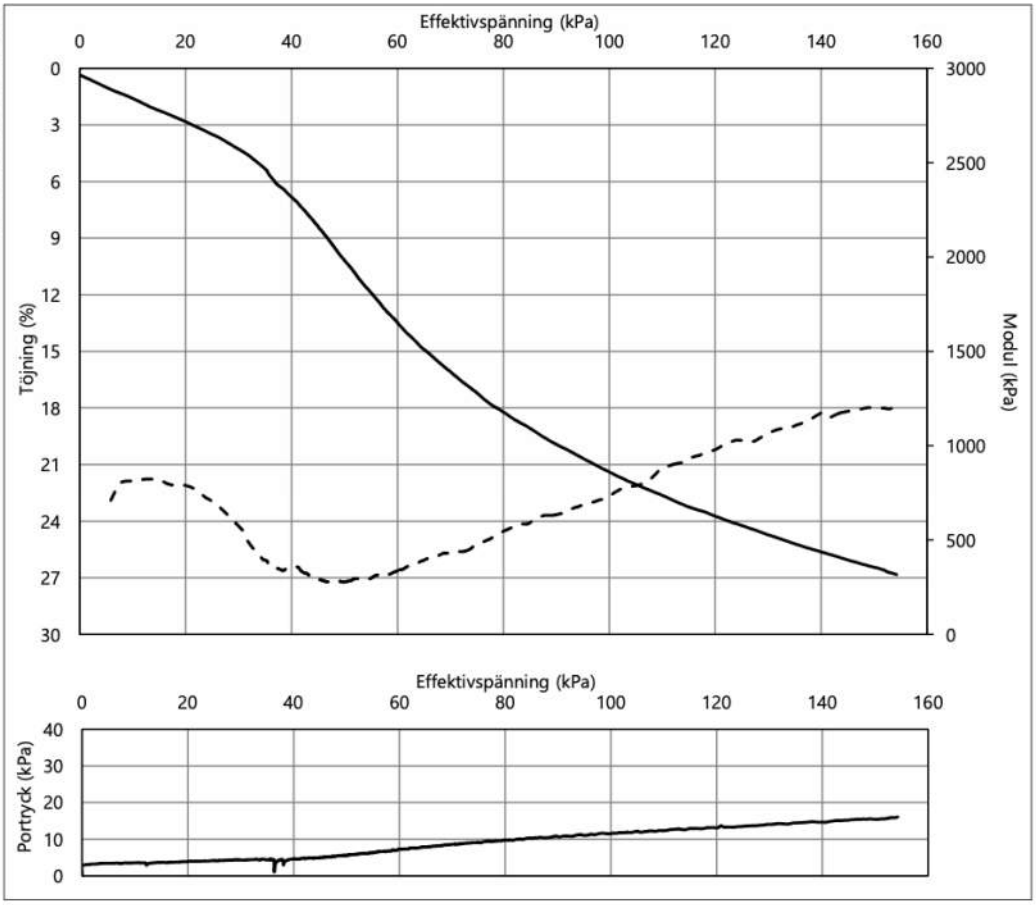

För teckenförklaring, information om standarder, utvärdering m m, se www.labmind.se/metoder.

Provningstemperatur ca 7° (klimatrum). Provdimensioner ca 20x50 mm. Deformationshastighet ca 0,0025 mm/min.

REDOVISNING AV

ÖDOMETERFÖRSÖK, TYP CRS

Uppdrag	Erikssund	**Punkt**	22E102
Kund	PEAB Anläggning AB	**Djup**	1,5 m

REDOVISNING AV FÖRSÖK

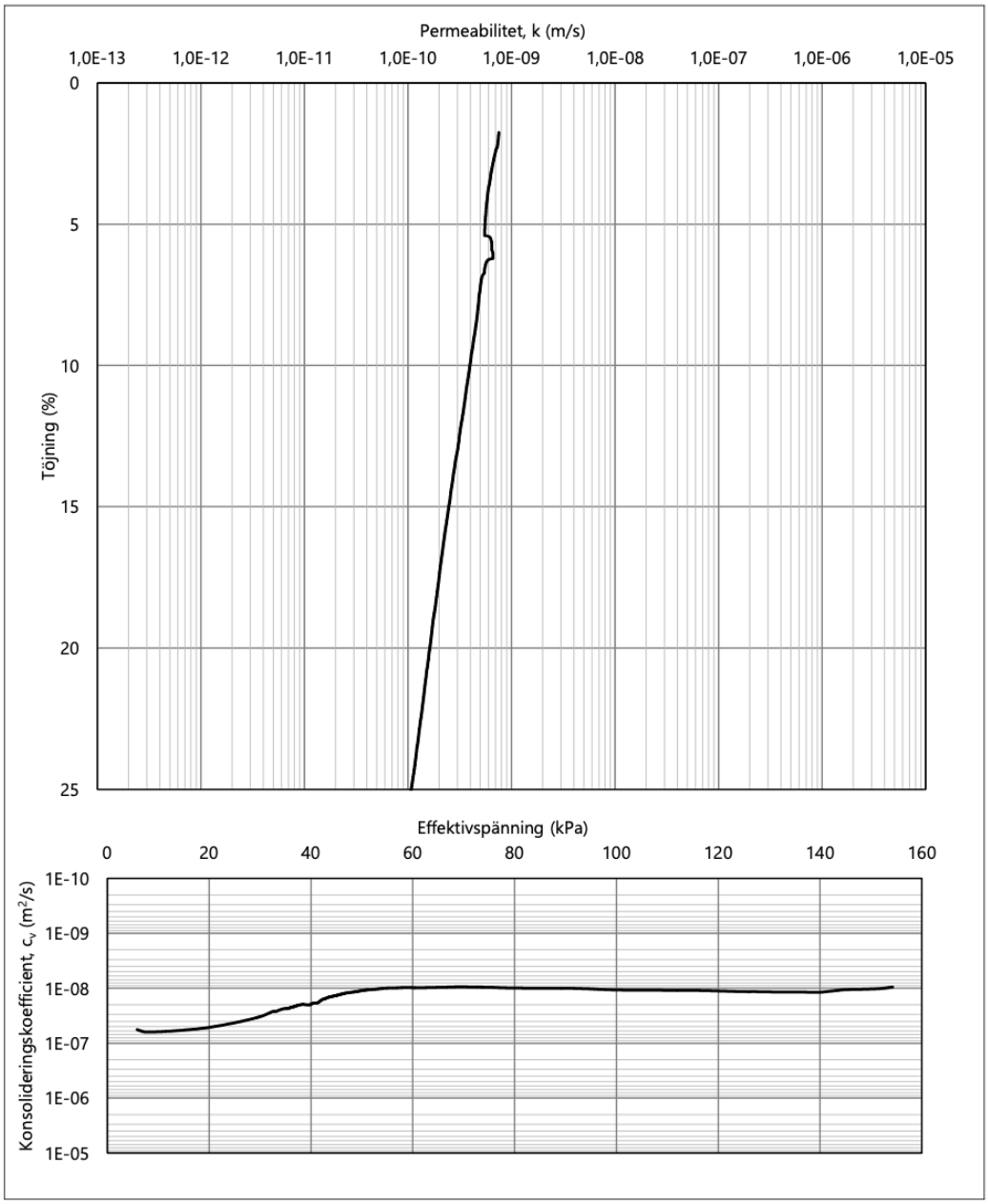

REDOVISNING AV

ÖDOMETERFÖRSÖK, TYP CRS

Uppdrag	Erikssund	**Punkt**	22E102
Kund	PEAB Anläggning AB	**Djup**	2,5 m

ALLMÄNT

CRS-försök			Från rutinanalys		
Jordart	Cl (su)		**Jordart**	Cl (su)	
w_N	78	%	w_N	75	%
ρ	1,58	t/m³	ρ	1,58	t/m³

PROVNING

Utfört	2022-02-23 / AS
Granskat	2022-02-25 / DG
Provt. till försök	7 dygn
Prov	Kv Stll Ø50 mm

UTVÄRDERING

σ_c'	M_L	σ_L'	M'	k_i	β_k	$k_{ini\ (0,85\sigma c')}$	$\varepsilon_{0,85\sigma c'}$	c_u / σ_c'	M_i/M_L
21	260	40	13,5	1,3E-09	3,9	0,035	1,7	0,44	4,2
kPa	kPa	kPa	-	m/s	-	m/år	%	-	-

Avvikande empirisk korrelation.

REDOVISNING AV FÖRSÖK

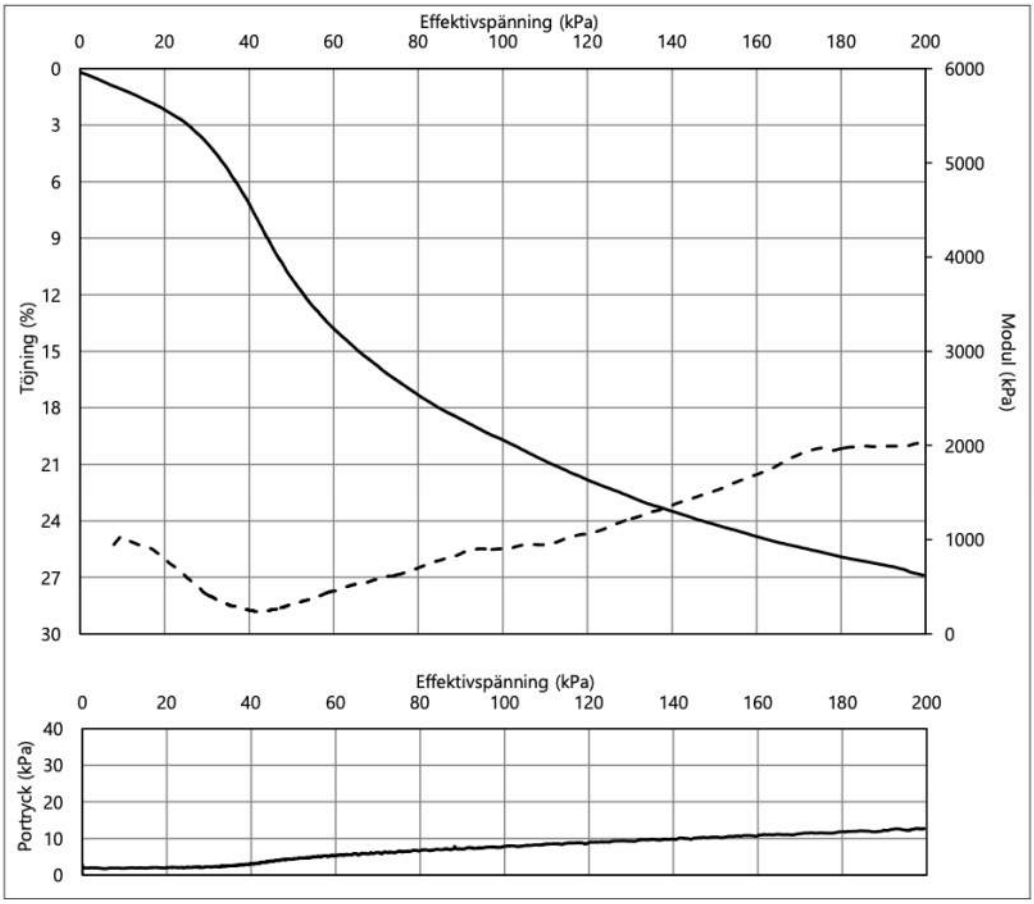

För teckenförklaring, information om standarder, utvärdering m m, se www.labmind.se/metoder.

Provningstemperatur ca 7° (klimatrum). Provdimensioner ca 20x50 mm. Deformationshastighet ca 0,0025 mm/min.

REDOVISNING AV

ÖDOMETERFÖRSÖK, TYP CRS

Uppdrag	Erikssund	**Punkt**	22E102
Kund	PEAB Anläggning AB	**Djup**	2,5 m

REDOVISNING AV FÖRSÖK

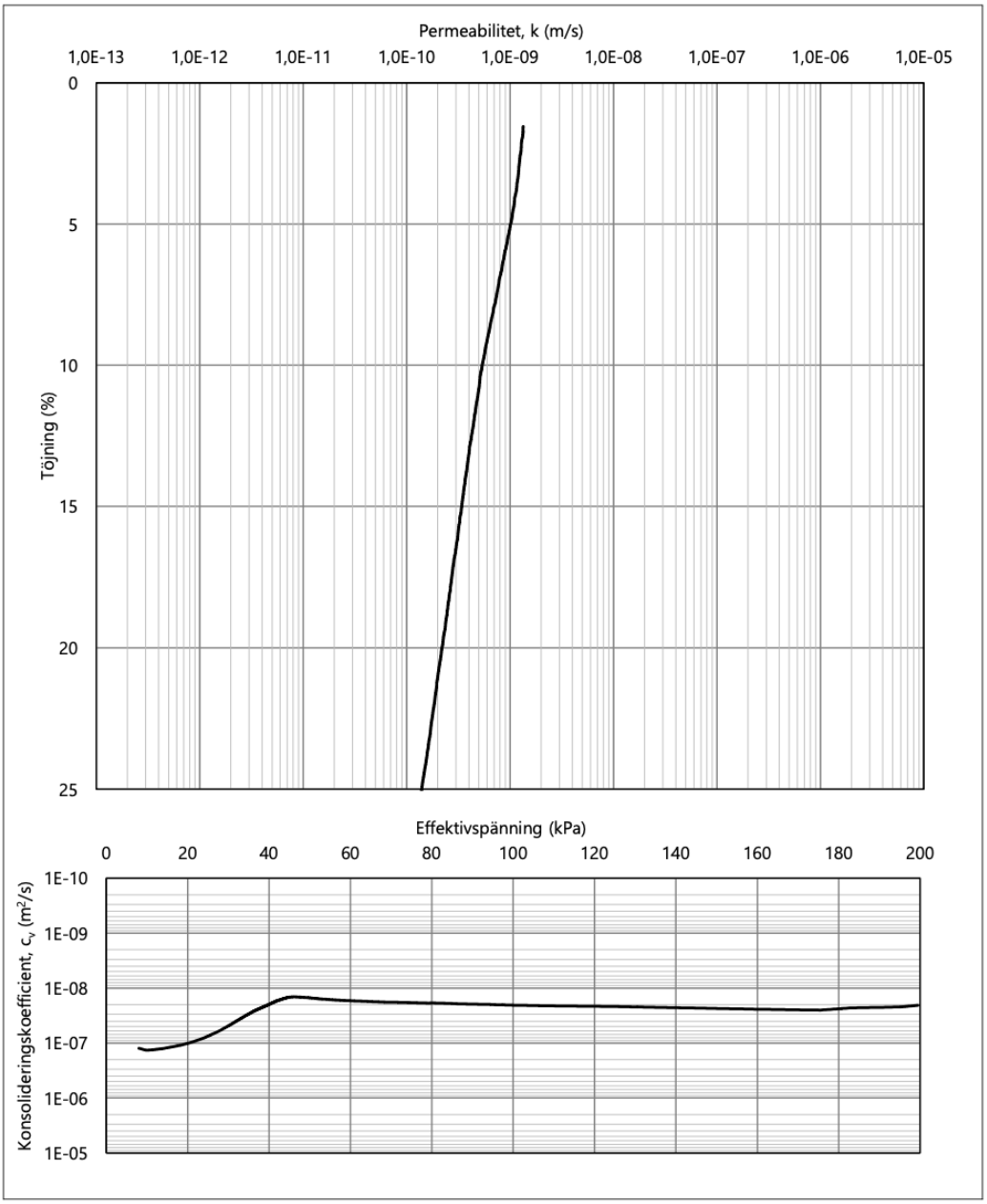

REDOVISNING AV

ÖDOMETERFÖRSÖK, TYP CRS

Uppdrag	Erikssund	**Punkt**	22E102
Kund	PEAB Anläggning AB	**Djup**	3,5 m

ALLMÄNT

CRS-försök			Från rutinanalys		
Jordart	vCl (su)		**Jordart**	vCl (su)	
w_N	83	%	w_N	76	%
ρ	1,52	t/m³	ρ	1,54	t/m³

PROVNING

Utfört	2022-02-23 / AS
Granskat	2022-02-25 / DG
Provt. till försök	7 dygn
Prov	Kv Stll Ø50 mm

UTVÄRDERING

σ_c'	M_L	σ_L'	M'	k_i	β_k	$k_{ini\ (0,85\sigma c')}$	$\varepsilon_{0,85\sigma c'}$	c_u / σ_c'	M_i/M_L
34	270	53	12,0	1,8E-09	4,4	0,041	3,1	0,29	3,5
kPa	kPa	kPa	-	m/s	-	m/år	%	-	-

Avvikande empirisk korrelation.

REDOVISNING AV FÖRSÖK

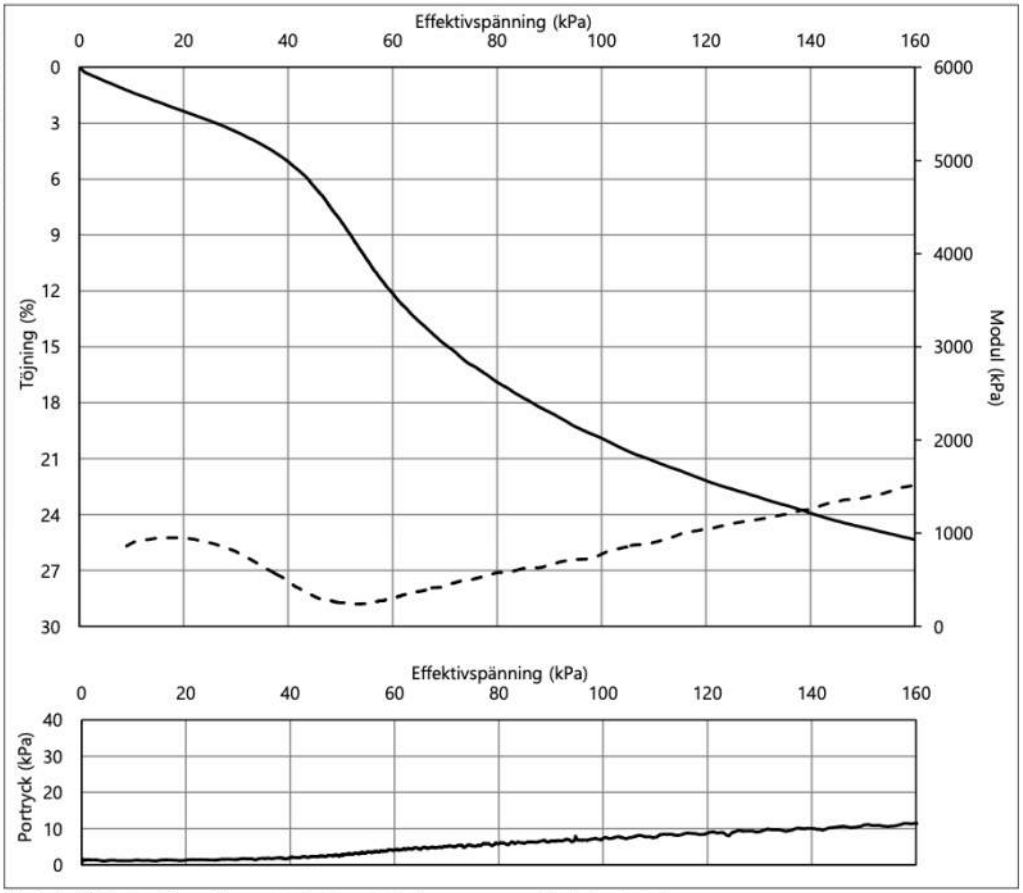

För teckenförklaring, information om standarder, utvärdering m m, se www.labmind.se/metoder.

Provningstemperatur ca 7° (klimatrum). Provdimensioner ca 20x50 mm. Deformationshastighet ca 0,0025 mm/min.

REDOVISNING AV

ÖDOMETERFÖRSÖK, TYP CRS

Uppdrag	Erikssund	**Punkt**	22E102
Kund	PEAB Anläggning AB	**Djup**	3,5 m

REDOVISNING AV FÖRSÖK

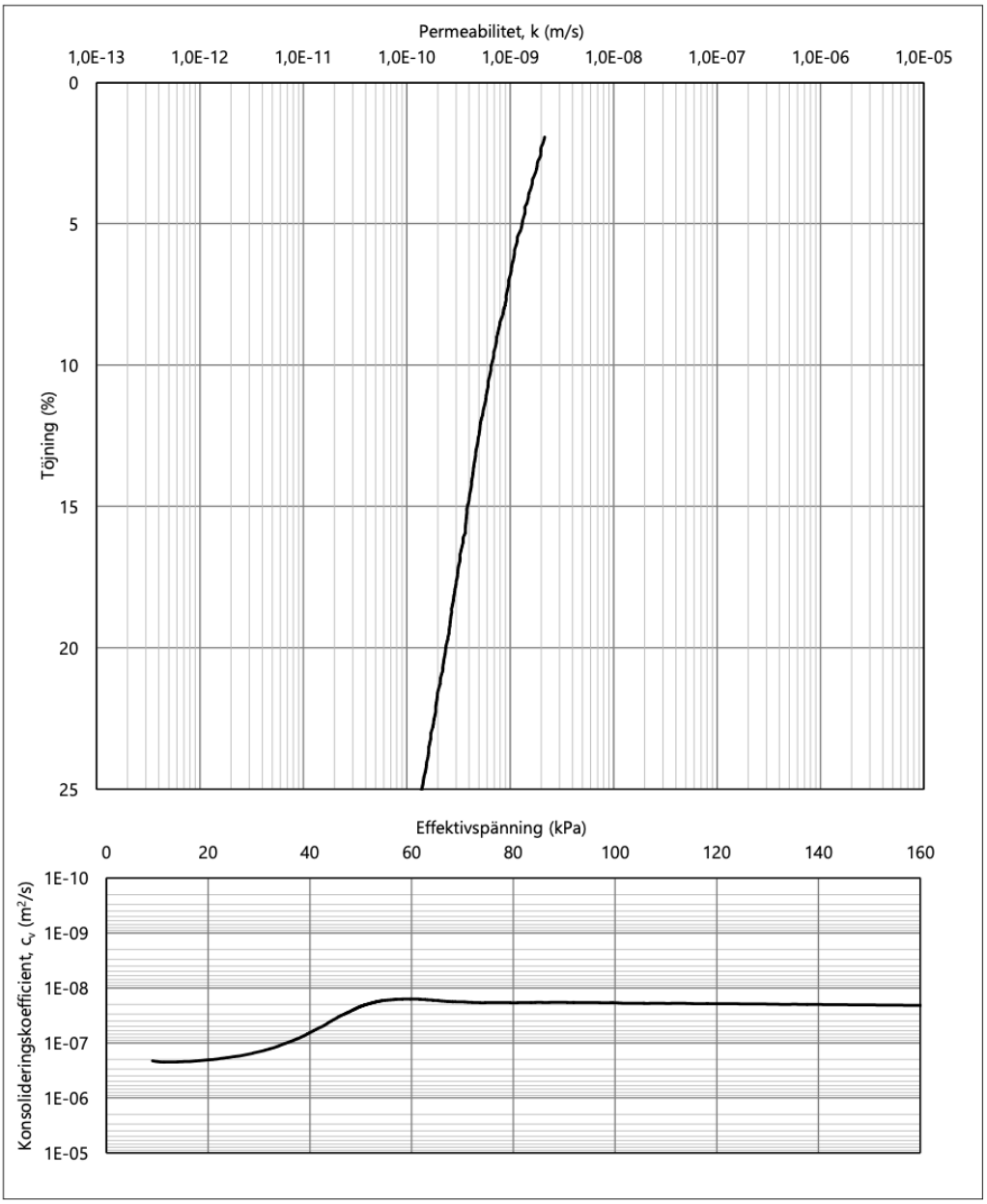

Unr 2203 **LabMind AB** | Värmdövägen 84, 131 54 Nacka | www.labmind.se Sid 2(2)

A.6 Direct shear tests

REDOVISNING AV

DIREKT SKJUVFÖRSÖK

Uppdrag	Erikssund	**Punkt**	22E102
Kund	PEAB Anläggning AB	**Djup**	2,5 m

ALLMÄNT

Jordart	Cl (su)	
w_N	75	%
w_L	61	%
Provt.	Kv Stll Ø 50 mm	

PROVNING

Utfört	2022-03-02 / AS
Granskat	2022-03-04 / DG
Provt. till försök	14 dygn
Typ av försök	Konsoliderat, odränerad skjuvning

RESULTAT

Konsolidering			**Skjuvning**			**Empiri / provkvalitet**		
Kons.spänn.	23,5	kPa	c_u	10,5	kPa	$\varepsilon_{kons.sp.}$	3,7	%
Start skjuvning	23,5	kPa	γ_{brott}	0,06	rad	c_u / σ_c'	0,50	-

Avvikande empirisk korrelation. Något stor töjning under konsolidering.

REDOVISNING AV FÖRSÖK

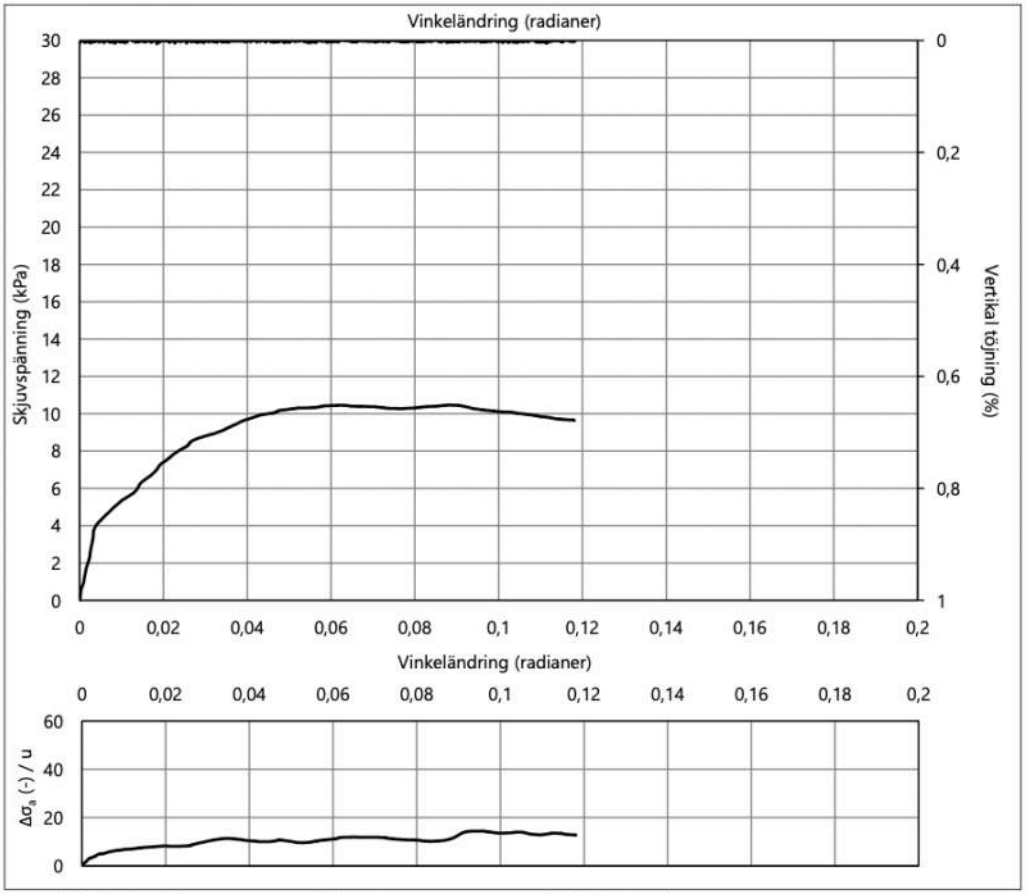

För teckenförklaring, information om standarder, utvärdering m m, se www.labmind.se/metoder.

Provningstemperatur ca 7° (klimatrum). Deformationshastighet vid skjuvning 0,15 rad/dygn.

REDOVISNING AV

DIREKT SKJUVFÖRSÖK

Uppdrag	Erikssund	**Punkt**	22E102
Kund	PEAB Anläggning AB	**Djup**	3,5 m

ALLMÄNT

Jordart	vCl (su)	
w_N	76	%
w_L	61	%
Provt.	Kv StII Ø 50 mm	

PROVNING

Utfört	2022-03-03 / AS
Granskat	2022-03-04 / DG
Provt. till försök	15 dygn
Typ av försök	Konsoliderat, odränerad skjuvning

RESULTAT

Konsolidering			**Skjuvning**			**Empiri / provkvalitet**		
Kons.spänn.	28,5	kPa	c_u	12,0	kPa	$\varepsilon_{kons.sp.}$	3,9	%
Start skjuvning	28,5	kPa	γ_{brott}	0,07	rad	c_u / σ_c'	0,35	-

Avvikande empirisk korrelation. Något stor töjning under konsolidering.

REDOVISNING AV FÖRSÖK

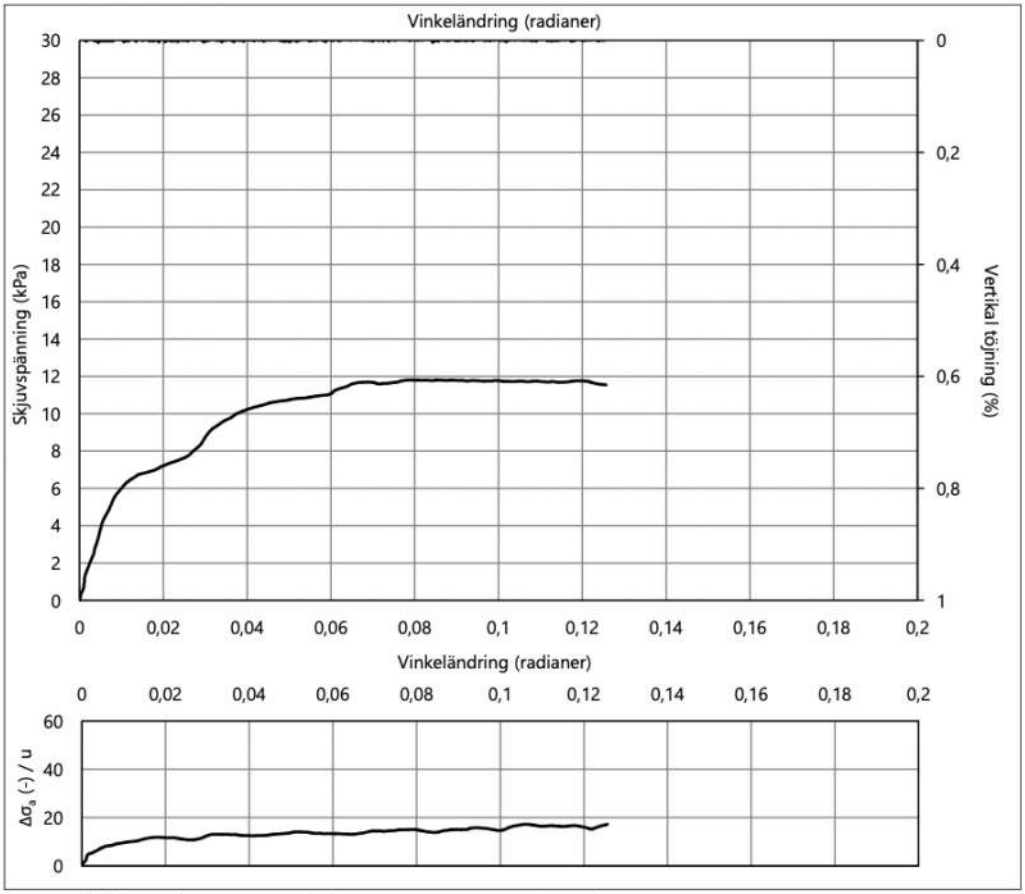

För teckenförklaring, information om standarder, utvärdering m m, se www.labmind.se/metoder.

Provningstemperatur ca 7° (klimatrum). Deformationshastighet vid skjuvning 0,15 rad/dygn.

REDOVISNING AV

DIREKT SKJUVFÖRSÖK

Uppdrag	Erikssund	**Punkt**	22E102
Kund	PEAB Anläggning AB	**Djup**	1,5 m

ALLMÄNT

Jordart	Cl (gy) (su)	
w_N	90	%
w_L	72	%
Provt.	Kv StII Ø 50 mm	

PROVNING

Utfört	2022-03-01 / AS
Granskat	2022-03-04 / DG
Provt. till försök	13 dygn
Typ av försök	Konsoliderat, odränerad skjuvning

RESULTAT

Konsolidering			**Skjuvning**			**Empiri / provkvalitet**		
Kons.spänn.	18,5	kPa	c_u	13,0	kPa	$\varepsilon_{kons.sp.}$	3,8	%
Start skjuvning	18,5	kPa	γ_{brott}	0,11	rad	c_u / σ_c'	0,46	-

Avvikande empirisk korrelation. Något stor töjning under konsolidering.

REDOVISNING AV FÖRSÖK

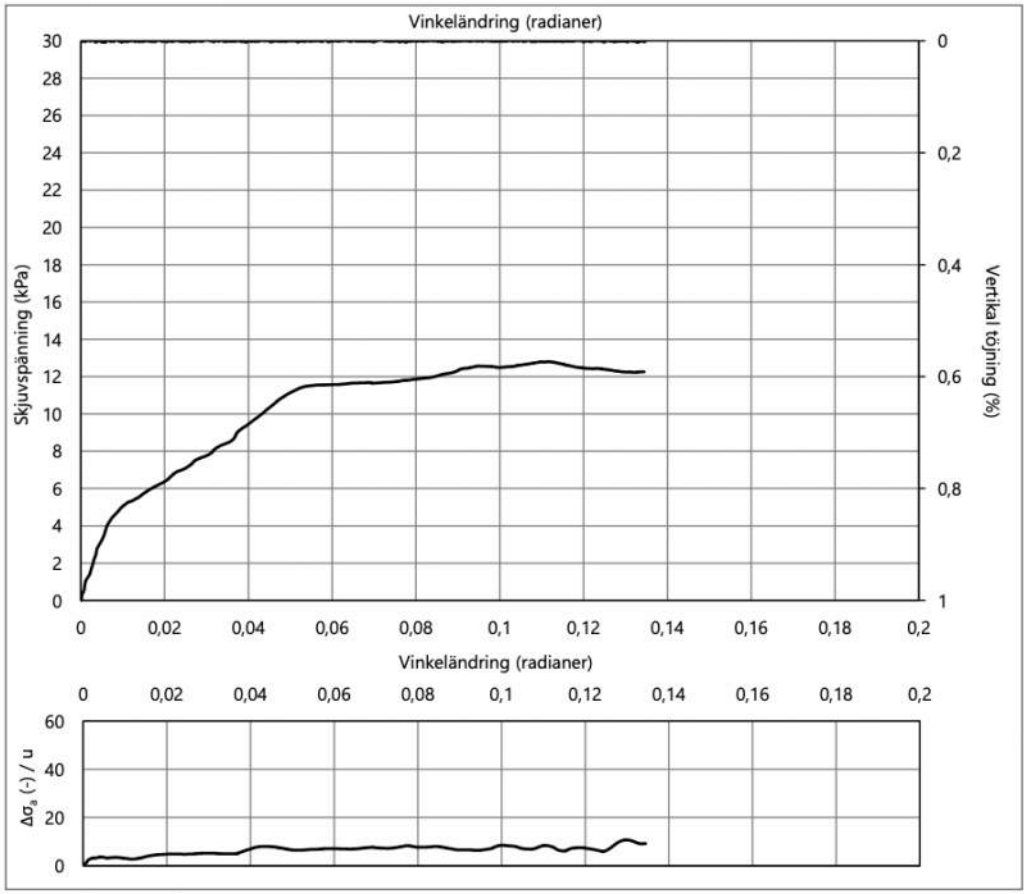

För teckenförklaring, information om standarder, utvärdering m m, se www.labmind.se/metoder.

Provningstemperatur ca 7° (klimatrum). Deformationshastighet vid skjuvning 0,15 rad/dygn.

B Calculations for Design

General bearing capacity equation

Ultimate bearing capacity of clay

		Unit	*Comment*
c	10	kPa	Evaluated from ground investigation
σ'_b	0	kPa	
γ'	16	kN/m3	Evaluated from CPT and general test
ϕ	0		
B_ef	0,9	m	
L_ef	4,2	m	
N_c	5,14		
N_q	0		
F(ϕ)	0,09		
N_γ	0		
s_c^0	1,04		
sq	1		
s_γ	0,91		
ξ_c	1,04		
ξ_q	1		
ξ_γ	0,91		
q_u,clay	53,62	kPa	

2:1 method - design

(Bergdahl et al., 1993)

		Unit
B	0,9	m
L	4,2	m
q	125	kN/m2

z	Δσz (kPa)
0	125,00
0,2	97,62
0,4	79,01
0,6	65,63
0,8	55,59
1	47,82
1,2	41,67
1,4	36,68
1,6	32,59
1,8	29,17
2	26,28

Punching Shear Resistance
(Meyerhof, 1974)
Thickness of platform

		Unit	*Comment*
q_u	125	kPa	
c_clay	10	kPa	Evaluated from ground investigation
γ_fill	18	kN/m3	*(Trafikverket, 2014)*
ϕ_fill	45	°	*(Trafikverket, 2014)*
B	0,9	m	
D	0	m	
N_c	5,14		
K_s	11,5		*(Meyerhof, 1974)*
H	0,57	m	

Punching Shear Resistance - BR 470

(Dobie et al. 2019)

Ultimate bearing capacity of system

		Unit	*Comment*
q_u	125	kPa	
B	0,9	m	
L	4,2	m	
s_u	10	kPa	Evaluated from ground investigation
N_c	5,14		
s_c	1,04		
q_s	53,62	kPa	
γ_fill	18	kPa	*(Trafikverket, 2014)*
ϕ_fill	45	°	*(Trafikverket, 2014)*
δ	30	°	
δ/ϕ_fill	0,67		
K_p	17		*(Swedish Standards Institute, 2005)*
s_p	1,21		
H	0,55	m	
q_p	71,38	kPa	

Punching Shear Resistance - BR 470 with supplement by Miller

(Dobie et al. 2019, Miller 2013)

Ultimate bearing capacity of system

		Unit	*Comment*
q_u	125	kPa	
B	0,9	m	
L	4,2	m	
s_u	10	kPa	Evaluated from ground investigation
N_c	5,14		
s_c	1,04		
q_s	53,62	kPa	
γ_fill	18	kPa	*(Trafikverket, 2014)*
ϕ_fill	45	°	*(Trafikverket, 2014)*
δ	30	°	
δ/ϕ_fill	0,67		
K_p	17		*(Swedish Standards Institute, 2005)*
s_p	1,21		
q_u,clay	53,62	kPa	Calculated using the general bearing capacity equation
F(ϕ)	0,36		
N_γ	234,37		
ξ_γ	0,91		
q_u,fill	1735,68	kPa	Calculated using the general bearing capacity equation
q_u,clay/q_u,f	0,03		
γ	0,61		
H	0,70	m	
q_p	71,38	kPa	

General bearing capacity equation

Ultimate bearing capacity of clay

		Unit	*Comment*
c	10	kPa	Evaluated from ground investigation
σ'_b	0	kPa	
γ'	16	kN/m3	Evaluated from CPT and general test
ϕ	0		
B_ef	1	m	
L_ef	4,5	m	
A_ef	4,5	m2	
N_c	5,14		
N_q	0		
F(ϕ)	0,09		
N_γ	0		
s_c^0	1,04		
sq	1		
s_γ	0,91		
ξ_c	1,04		
ξ_q	1		
ξ_γ	0,91		
q_u,clay	53,70	kPa	

2:1 method - reality

(Bergdahl et al., 1993)

		Unit
B	1	m
L	4,5	m
q	108	kPa

z	Δσz (kPa)
0	108,00
0,2	86,17
0,4	70,85
0,6	59,56
0,8	50,94
1	44,18
1,2	38,76
1,4	34,32
1,6	30,64
1,8	27,55
2	24,92

C Geogrid Technical Data

Tensar. THE COMPANY YOU CAN BUILD ON™

Product Specification - TriAx® TX190L Geogrid

Tensar International Corporation reserves the right to change its product specifications at any time. It is the responsibility of the person specifying the use of this product and of the purchaser to ensure that product specifications relied upon for design or procurement purposes are current and that the product is suitable for its intended use in each instance.

Tensar TriAx® Geogrid

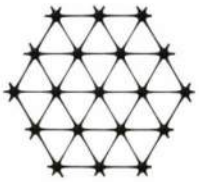

General

1. The geogrid is manufactured from a punched polypropylene sheet, which is then oriented in three substantially equilateral directions so that the resulting ribs shall have a high degree of molecular orientation, which continues at least in part through the mass of the integral node.
2. The properties contributing to the performance of a mechanically stabilized layer include the following:

Index Properties	Longitudinal[1]	Diagonal[1]	General[1]
▪ Rib pitch[2], mm (in)	60 (2.40)	60 (2.40)	
▪ Rib shape			Rectangular
▪ Aperture shape			Triangular

Structural Integrity	
▪ Junction efficiency[3], %	93
▪ Isotropic Stiffness Ratio[4]	0.6
▪ Overall Flexural Rigidity[5], mg-cm	1,500,000
▪ Radial stiffness at low strain[6], kN/m @ 0.5% strain	350
(lb/ft @ 0.5% strain)	(23,989)

Durability	
▪ Resistance to chemical degradation[7]	100%
▪ Resistance to ultra-violet light and weathering[8]	70%

Dimensions and Delivery

The TX geogrid shall be delivered to the jobsite in roll form with each roll individually identified and nominally measuring 4.0 meters (13.1 feet) in width and 50 meters (164 feet) in length and/or 3.8 meters (12.5 feet) in width and 50 meters (164 feet) in length.

Notes

1. Unless indicated otherwise, values shown are minimum average roll values determined in accordance with ASTM D4759-02. Brief descriptions of test procedures are given in the following notes.
2. Nominal dimensions.
3. Load transfer capability determined in accordance with ASTM D6637-10 and ASTM D7737-11 and expressed as a percentage of ultimate tensile strength.
4. The ratio between the minimum and maximum observed values of radial stiffness at 0.5% strain, measured on rib and midway between rib directions.
5. Determined in accordance with ASTM D7748/D7748M-14.
6. Radial stiffness is determined from tensile stiffness measured in any in-plane axis from testing in accordance with ASTM D6637-10.
7. Resistance to loss of load capacity or structural integrity when subjected to chemically aggressive environments in accordance with EPA 9090 immersion testing.
8. Resistance to loss of load capacity or structural integrity when subjected to 500 hours of ultraviolet light and aggressive weathering in accordance with ASTM D4355-05.

Tensar International Corporation
2500 Northwinds Pkwy.
Atlanta, Georgia 30009
Phone: 800-TENSAR-1
www.tensarcorp.com

D Measurement Instrumentation Specifications

Table D.1: *Specification of earth pressure cell (GEOKON, 2021).*

	Earth Pressure Cell Model 4800 (circular)
Range	1-2 MPa
Resolution	±0.025 % FSR
Accuracy	±0.5 % FSR
Linearity	±0.5 % FSR
Overrange	1.5 x Rated pressure
Operating Temperature	-20 to 80° C
Excitation Frequency Range	1400-3500 Hz
Outpout Frequency Range	2000-3000 Hz
Cell Dimensions (active area)	230 mm OD
Coil resistance	150 Ω
Material	316 Stainless Steel
Weight	2.3 kg

Table D.2: *Specification of crackmeter (GEOKON, 2020)*

	Crackmeter Model 4420
Range	50 mm
Resolution	±0.025 % FSR
Linearity	±0.25 % FSR
Thermal Zero Shift	<0.05 % FSR/C°
Stability	<0.2 %/yr (under static conditions)
Overrange	115 % FSR
Temperature Range	-20 to 80° C
Frequency Range	1400-3500 Hz
Coil resistance	180 Ω, + 10 Ω
Cable Type	Two twisted pair (four conductor) 22 AWG. For shield, PVC jacket, nominal OD=6.3 mm
Cable Wiring Code	Red and black are the VW sensor, white and green are the thermistor
Length (midrange, end to end)	415 mm
Coil Assembly Dim (length x OD)	31.75 mm/25.4 mm

E Field Trial Results

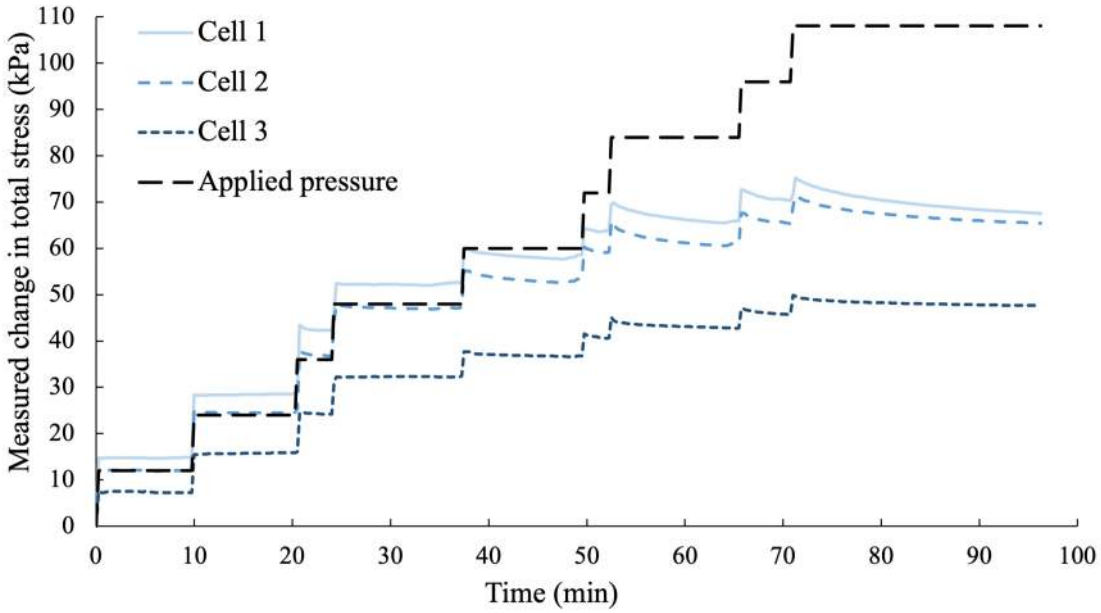

Figure E.1: *Measured change in total stress against time for test F.*

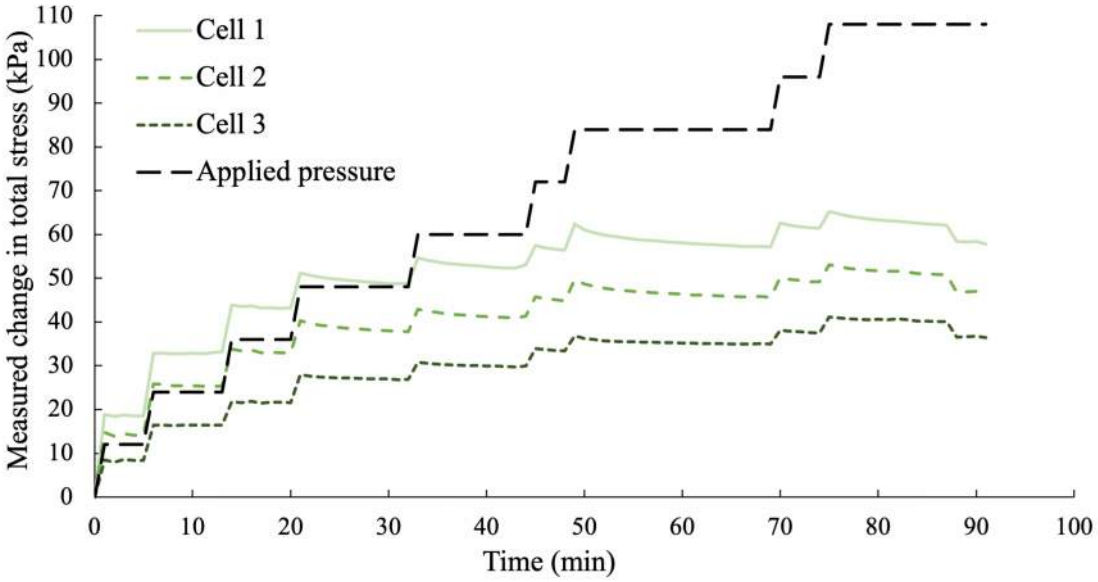

Figure E.2: *Measured change in total stress against time for test L.*

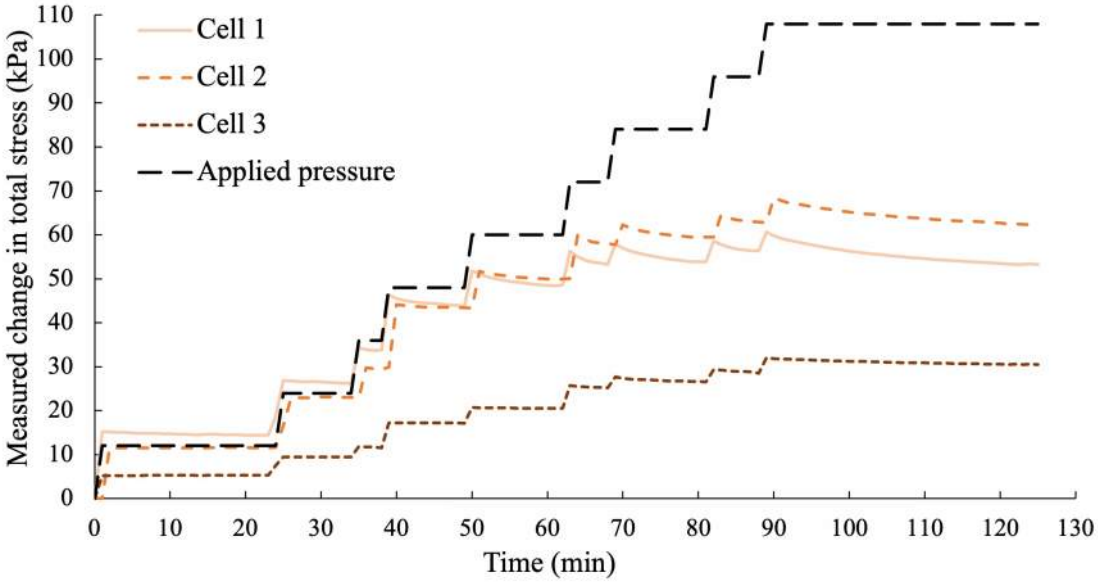

Figure E.3: *Measured change in total stress against time for test G.*

F Calculations for Final Analyses

Non-Cohesive Soil Overlaying Clay

Tcheng (1957)

Ultimate bearing capacity with platform h=0.8m

		Unit	*Comment*
B_ef	1	m	
L_ef	4,5	m	
H	0,8	m	
H/B_ef	0,8		
c_u	10	kPa	Evaluated from ground investigation
ξ_c	1,04		
N_c^*	6,13		
q_b	63,96	kPa	

Punching Shear Resistance
(Meyerhof, 1974)
H=0,8

		Unit	*Comment*
c_clay	10	kN/m2	Evaluated from ground investigation
γ_fill	18	kN/m3	*(Trafikverket, 2014)*
ϕ_fill	40	°	*(Trafikverket, 2014)*
B	1	m	
D	0	m	
N_c	5,14		
K_s	11,5		*(Meyerhof, 1974)*
H	0,80	m	
qu	162,58	kN/m2	

Punching Shear Resistance - BR 470

(Dobie et al. 2019)

Ultimate bearing capacity with platform H=0.8

		Unit	*Comment*
B	1	m	
L	4,5	m	
H	0,80	m	
s_u	10,00	kPa	Evaluated from ground investigation
N_c	5,14		
s_c	1,04		
q_s	53,62	kPa	
γ_fill	18	kPa	*(Trafikverket, 2014)*
ϕ_fill	40	°	*(Trafikverket, 2014)*
δ	26,67	°	
δ/ϕ_fill	0,67		
K_p	11		*(Swedish Standards Institute, 2005)*
s_p	1,22		
q_p	77,78	kPa	
q_u	131,40	kPa	

Punching Shear Resistance - BR 470 with supplement by Miller

(Dobie et al. 2019, Miller 2013)

Ultimate bearing capacity with platform h=0.8

		Unit	*Comment*
B	1	m	
L	4,5	m	
H	0,80	m	
s_u	10	kPa	Evaluated from ground investigation
N_c	5,14		
s_c	1,04		
q_s	53,62	kPa	
γ_fill	18	kPa	*(Trafikverket, 2014)*
ϕ_fill	40	°	*(Trafikverket, 2014)*
δ	26,67	°	
δ/ϕ_fill	0,67		
K_p	11		*(Swedish Standards Institute, 2005)*
s_p	1,22		
q_u,clay	53,62	kPa	Calculated using the general bearing capacity equation
F(ϕ)	0,36		
N_γ	85,59		
ξ_γ	0,91		
q_u,fill	701,81	kPa	Calculated using the general bearing capacity equation
q_u,clay/q_u,fill	0,08		
γ	0,76		
q_p	59,42	kPa	
q_u	113,04	kPa	

Burd and Frydman (1997)

Ultimate bearing capacity of system

		Unit	*Comment*
s_u	10	kPa	Evaluated from ground investigation
γ_fill	18	kPa	*(Trafikverket, 2014)*
H	0,8	m	
B	1	m	
B/H	1,25		
s_u/γ_fillH	0,69		
p/γ_fillB	5		
p	90,00	kPa	

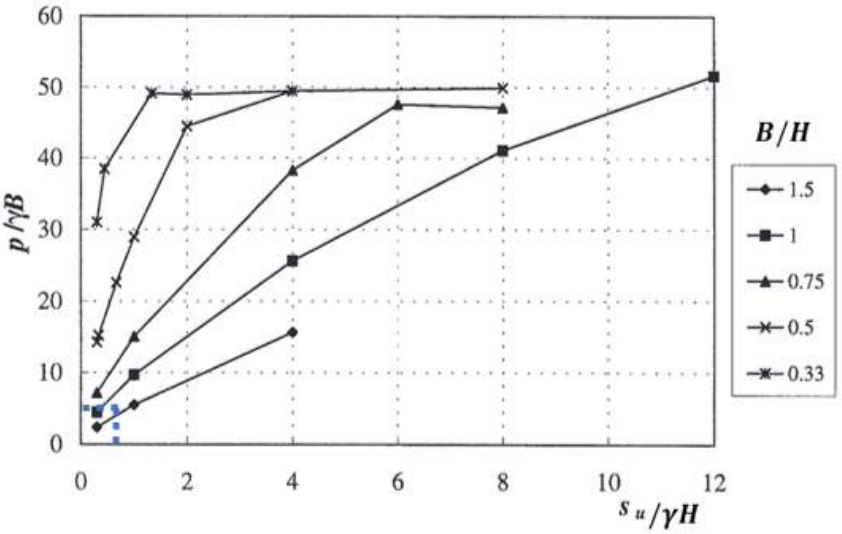

β-angle by Burd and Frydman (1997)

only fill

		Unit	*Comment*
B	1	m	
H	0,8	m	
s_u	10,00	kPa	Evaluated from ground investigation
N_c	5,14		

Method	*p (kN/m2)*	*β (°)*
Tcheng (1957)	63,96	8,67
Meyerhof (1974)	162,58	53,50
BR470	131,40	44,20
BR470+Miller (2013)	113,04	36,83
Burd & Frydman (1997	90,00	25,13
Plaxis	112,46	36,58

Non-Cohesive Soil Overlaying Clay with log mats

Ultimate bearing capacity with platform h=0.8m

		Unit	*Comment*
b_ef	5,5	m	
l_ef	5,4	m	
h	0,8	m	
h/b_ef	0,15		
c_u	10	kPa	Evaluated from ground investigation
ξ_c	1,04		
N_c^*	4,39		
qb	45,76	kPa	
Ultimate load	1359,05	kN	
Area_track	4,5	m2	
Pressure_track	302,01	kPa	

Punching Shear Resistance - Log mats

(Meyerhof, 1974)

Ultimate bearing capacity with platform H=0.8m

		Unit	*Comment*
c_clay	10	kPa	Evaluated from ground investigation
γ_fill	18	kN/m3	*(Trafikverket, 2014)*
ϕ_fill	40	°	*(Trafikverket, 2014)*
B	5,5	m	
D	0	m	
N_c	5,14		
K_s	4,5		*(Meyerhof, 1974)*
H	0,80	m	
q_u	59,32	kPa	
Ultimate loa	1761,95	kN	
Area_track	4,5	m2	
Pressure_tra	391,54	kPa	

Punching Shear Resistance - BR 470
Log mat
(Dobie et al. 2019)
Ultimate bearing capacity with platform h=0.8

		Unit	*Comment*
B	5,5	m	
L	5,4	m	
H	0,80	m	
s_u	10,00	kPa	Evaluated from ground investigation
N_c	5,14		
s_c	1,04		
q_s	53,62	kPa	
γ_fill	18	kPa	*(Trafikverket, 2014)*
ϕ_fill	40	°	*(Trafikverket, 2014)*
δ	26,67	°	
δ/ϕ_fill	0,67		
K_p	11		*(Swedish Standards Institute, 2005)*
s_p	2,02		
q_p	23,36	kPa	
q	76,98	kPa	
Ultimate load	2286,19	kN	
Area_track	4,5	m2	
Pressure_track	508,04	kPa	

Punching Shear Resistance - BR 470 with supplement by Miller

(Dobie et al. 2019, Miller 2013)

Log mat

Ultimate bearing capacity with platform H=0.8

		Unit	*Comment*
B	5,5	m	
L	5,4	m	
H	0,80	m	
s_u	10	kPa	Evaluated from ground investigation
N_c	5,14		
s_c	1,04		
q_s	53,62	kPa	
γ_fill	18	kPa	*(Trafikverket, 2014)*
ϕ_fill	40	°	*(Trafikverket, 2014)*
δ	26,67	°	
δ/ϕ_fill	0,67		
K_p	11		*(Swedish Standards Institute, 2005)*
s_p	2,02		
q_u,clay	53,62	kPa	Calculated using the general bearing capacity equation
F(ϕ)	0,36		
N_γ	85,59		
ξ_γ	0,59		
q_u,fill	2510,55	kPa	Calculated using the general bearing capacity equation
q_u,clay/q_u,	0,02		
γ	0,55		
q_p	12,77	kPa	
q_u	66,39	kPa	
Ultimate load	1971,73	kN	
Area_track	4,5	m2	
Pressure_trac	438,16	kPa	

β-angle by Burd and Frydman (1997)

Log mats

		Unit	*Comment*
B	5,5	m	
H	0,8	m	
s_u	10,00	kPa	Evaluated from ground investigation
N_c	5,14		

Method	*p (kN/m2)*	*β (°)*
Tcheng (1957)	45,76	-20,72
Meyerhof (1974)	59,32	27,87
BR470	76,98	59,66
BR470+Miller (201	66,39	45,03

BR470 with geogrid approach
(Dobie et al., 2019)

		Unit	*Comment*
q_u	131,40	kPa	Calculated from BR470
T_ult	350	kN/m	Specification of geogrid
B	1	m	
q_g	350	kPa	
q_u,geogrid	481,40	kPa	

T-method geogrid

		Unit	*Comment*
q_b	61,89	kPa	Calculated by general bearing capacity equation
s_u	10	kPa	Evaluated from ground investigation
γ'	18	kN/m3	*(Trafikverket, 2014)*
H	0,8	m	
B	1	m	
σ'_0	14,4	kPa	
T	2,66		
s_u/σ'_0	0,69		
T_corr	2,39		
q_u	180,37	kPa	

β-angle by Burd and Frydman (1997)

Geogrid

		Unit	*Comment*
B	1	m	
H	0,8	m	
s_u	10,00	kPa	Evaluated from ground investigation
N_c	5,14		

Method	*p (kN/m2)*	*β (°)*
BR470	481,40	79,17
T-method	180,37	57,46
Plaxis	109,18	35,08